Design and Application of Compliant Quasi-Kinematic Couplings

by

Martin L. Culpepper

B. S. Mechanical Engineering
Iowa State University, 1995

M. S.
Massachusetts Institute of Technology, 1997

Submitted to the Department of Mechanical Engineering
in Partial Fulfillment of the Requirements for the Degree of

Doctor of Philosophy in Mechanical Engineering
at the
Massachusetts Institute of Technology

February 2000

© 2000 Massachusetts Institute of Technology
All rights reserved

Signature of Author . . . . . .
Department of Mechanical Engineering
January 07, 2000

Certified by . . . . . .
Alexander H. Slocum
Professor of Mechancial Engineering
Thesis Supervisor

Accepted by . . . . . .
Professor Ain A. Sonin
Chairman, Department Committee on Graduate Studies

Design and Application of Compliant Quasi-Kinematic Couplings

by

MARTIN L. CULPEPPER

Submitted to the Department of Mechanical Engineering
on January 07, 2000 in Partial Fulfillment of the
Requirements for the Degree of Doctorate of Philosophy in
Mechanical Engineering

ABSTRACT

Better precision at lower costs is a major force in design and manufacturing. However, this is becoming increasingly difficult to achieve as the demands of many location applications are surpassing the practical performance limit (~ five microns) of low-cost couplings. The absence of a means to meet these requirement has motivated the development of the Quasi-Kinematic Coupling (QKC). This thesis covers the theoretical and practical considerations needed to model and design QKCs.

In a QKC, one component is equipped with three spherical protrusions while the other contains three corresponding conical grooves. Whereas Kinematic Couplings rely on six points of contact, the six arcs of contact between the mated protrusions and grooves of QKCs result in a weakly over-constrained coupling, thus the name Quasi-Kinematic. QKCs are capable of sub-micron repeatability, permit sealing contact as needed in casting, and can be economically mass produced.

The design and application of a QKC is demonstrated via a case study on the location of two engine components. Integration of the QKC has improved coupling precision from 5 to 0.7 microns. In addition, this QKC uses 60% fewer precision features, 60% fewer pieces, costs 40% less per engine, and allows feature placement tolerances which are twice as wide as those of the previous dowel-pin-type coupling.

Thesis Supervisor: Prof. Alexander H. Slocum
Title: Professor of Mechanical Engineering

ACKNOWLEDGMENTS

I would like to thank my wife for putting up with my long hours of work. She is most precious to me. I thank her for all her support, love, and patience.

To my Dad, who taught me perseverance and my mom who taught me patience, I thank them for helping me walk the straight and narrow. I once asked, "Could they have guessed that their rowdy five-year-old "tinkerer" would one day grow up to be an engineer?" They replied, "Yes, you had so much practice breaking things, something had to go right for you."

I would also like to thank Professor Alexander Slocum for his help and inspiration. Without his guidance I would not have achieved this level of success.

To Profs. Hardt, Sarma, Suh, and Trumper I give thanks for advising me on conducting and publishing research. I would also like to thank them for their guidance on preparing for an academic career.

To Profs. Sarma and Anand I give my gratitude for serving as members of my thesis committee. Their advice and critiques were very helpful.

I would also like to thank F. Z. Shaikh, J. Schim, G. Vrsek, R. Tabaczynski, V. B. Shah, Greg Minch, and Kevin Heck for their financial and technical support during this project.

Finally, I would like to thank God, the ultimate designer in the universe. As a fellow designer, I look at this world and wonder how frustrated He must get with us..... Thank God for His patience.

TABLE OF CONTENTS

ACKNOWLEDGMENTS **5**

TABLE OF CONTENTS **7**

LIST OF FIGURES **11**

LIST OF TABLES **15**

NOMENCLATURE **17**

CHAPTER 1. INTRODUCTION **21**

1.1 Motivation 21

1.2 Precision Coupling Systems 23

1.3 Thesis Scope and Organization 25

1.4 Types of Passive Mechanical Couplings 26

1.4.1 Elastic Averaging Methods 26

1.4.2 Pinned Joints 27

1.4.3 Kinematic Couplings 28

1.4.4 Compliant Kinematic Couplings 29

1.4.5 Quasi-Kinematic Couplings (QKCs) 30

1.4.6 Comparison of Mechanical Coupling Types 31

CHAPTER 2. QUASI-KINEMATIC GEOMETRY AND FUNCTION **33**

2.1 Physical Components of QKCs 33

2.2 Analytic Components of QKCs 34

2.2.1 Joint Coordinate Systems 35

2.2.2 Analytic Components of Couplings 36

2.2.3 Contact Angle 37

2.3 Function of Quasi-Kinematic Couplings 38

CHAPTER 3. MODELING AND ANALYSIS OF QKCS **39**

3.1 Modeling of Quasi-Kinematic Couplings 39

3.1.1 Kinematic Coupling Solution 39

3.1.2 Solving the QKC Over Constraint Problem 41

3.2 Quasi-Kinematic Coupling Contact Mechanics 42

3.2.1 Contact Analysis Using a Rotating Coordinate System 42
3.2.2 Relationship Between Surface Stresses and Force Per Unit Length . . 45
3.2.3 Far Field Distance of Approach 46
3.2.4 Relationship Between fn and dn 50
3.3 Using the Quasi-Kinematic Coupling Model/Analysis 51
3.3.1 Quasi-Kinematic Coupling Reaction Forces 51
3.3.2 Stiffness of QKCs 54
3.3.3 Limits on the Estimation of QKC Stiffness 54

CHAPTER 4. DESIGN AND MANUFACTURE OF QUASI-KINEMATIC COUPLINGS . 57

4.1 Overview of the Quasi-Kinematic Coupling Design Process 57
4.2 Problem Definition 58
4.2.1 Constraints 59
4.2.2 Functional Requirements 59
4.2.3 Design Parameters 60
4.3 Geometry Generation 60
4.3.1 Quasi-Kinematic Coupling Gap 61
4.4 Design Check 69
4.5 Iteration If Needed 70
4.6 Design Specific Quasi-Kinematic Coupling Constraints 70
4.6.1 Enhancing QKC Performance Via Moderate Plastic Deformation . . 70
4.6.2 Affects of Localized Plastic Deformation on QKC Performance . . . 76
4.6.3 Load and Displacement Behavior of QKC Joints 82
4.6.4 Ratio of Contactor to Target Hardness 83
4.7 Manufacturing of Quasi-Kinematic Coupling Elements 84
4.7.1 Manufacture of Target Surfaces 84
4.7.2 Manufacture of Contactors 85
4.7.3 Feature Size and Placement Tolerances 86
4.8 To QKC or Not To QKC? 87

CHAPTER 5. CASE STUDY: ASSEMBLY OF A SIX CYLINDER AUTOMOTIVE ENGINE 89

5.1 Problem Definition 89
5.1.1 Application: The Six Cylinder Engine. 89
5.1.2 Main Journal Bearing Assembly 90
5.1.3 The Need For Repeatability 91
5.1.4 Rough Repeatability Error Budget 93
5.2 Constraints 94

5.3 Functional Requirements 95
5.4 Gap 96
5.5 Joint Location and Orientation 97
5.5.1 Review of Sensitive Directions 97
5.5.2 Error Loads 97
5.5.3 Joint Location/Orientation 98
5.5.4 Coupling Stiffness 98
5.6 Functional Requirement Tests 99
5.7 Verification of Plastic Deformation Range 101
5.8 Testing and Performance Verification 102
5.8.1 Coupling Repeatability 102
5.8.2 The Affect of Contact Angle on Repeatability 105
5.8.3 The Effect of Joint Misalignment on Repeatability 106
5.9 Comparison of QKC and Pinned Joint Methods 107
5.9.1 Manufacturing Comparison 107
5.9.2 Design Comparison 107

CHAPTER 6. SUMMARY AND FUTURE WORK 109
6.1 Implications of the QKC 109
6.1.1 Manufacturing 109
6.1.2 Economic and Technological (Other Applications) 109
6.2 Future Work 110
6.2.1 Plastic Line Contact 110
6.2.2 Displacement and Coupling Disturbances 110
6.2.3 Metric For Degree of Over-Constraint 111

REFERENCES 113

Appendix A. Excel Spreadsheet Used To Iterate Best Solution 117

Appendix B. MathCad Worksheet For Finding Coupling Stiffness 121

Appendix C. Non-Linear Finite Element Analysis 133
C.1 About the FEA Code 133
C.2 What the Code Does 134
C.3 Complete Cosmos/M 2.5 Non-linear FEA Code 136

Appendix D. General Quasi-Kinematic Coupling Patent 141

Appendix E. Automotive Quasi-Kinematic Coupling Patent 157

Appendix F. Derivation of Sinusoidal Normal Displacements 183

F.1 Review of Distances of Approach 183

F.2 Components Due to drcc 185

F.2.1 Magnitude 185

F.2.2 Direction 186

F.3 Components Due to exy 186

F.3.1 Calculating Errors Due To Rotation 186

F.3.2 Decomposition of Rotational Errors 187

F.3.3 Applying Decomposition of Rotational Errors to QKCs 189

F.4 Components Due to ez 190

F.5 General Distance of Approach Equation 191

Appendix G. Proof For Constant Plane Strain Assumption 193

G.1 Introduction to the Analysis 193

G.2 Goal and Reasoning Behind the Analysis 193

G.3 Analysis For Estimating the Angular Strain Ratio 195

LIST OF FIGURES

Figure 1.1 2.5 Liter Six Cylinder Engine 22
Figure 1.2 Six Cylinder Engine Assembly Partially Assembled 23
Figure 1.3 Kinematic Coupling Fixture Shown With Six Degrees of Freedom . . 23
Figure 1.4 Model of a Mechanical Coupling System 24
Figure 1.5 Types of Elastically Averaged Couplings 26
Figure 1.6 Example of Casting Mold Located With Pinned Joints 27
Figure 1.7 Traditional Kinematic Coupling 29
Figure 1.8 Mold Halves With Flexural Kinematic Coupling Elements 30
Figure 1.9 Generic Quasi-Kinematic Coupling 31
Figure 1.10 Practical Performance Limits of Common Low-Cost Couplings 32
Figure 2.1 Physical Components of a Generic QKC 34
Figure 2.2 Two Targets Combined Into a Conical Groove 34
Figure 2.3 Placement of Joint Coordinate System and Variables For Joint i 35
Figure 2.4 Analytic Components of A Quasi-Kinematic Coupling 37
Figure 2.5 Quasi-Kinematic Coupling Contact Angle, θCT, Note View Is Into Conical Groove From Top 37
Figure 2.6 Mating Cycle of Quasi-Kinematic Couplings 38
Figure 3.1 Solution Procedure For Kinematic Couplings 40
Figure 3.2 Traditional Hard Mount Kinematic Coupling 40
Figure 3.3 Solution Procedure For Quasi-Kinematic Couplings In Context of Traditional Approach 41
Figure 3.4 Stiffness Solution Model For Quasi-Kinematic Couplings 42
Figure 3.5 Conical Coordinate System and Contact Stress Profile 43
Figure 3.6 Cone Cross Section Showing Placement of Conical Coordinate System in Symmetric Profile 43
Figure 3.7 Rotating Conical Coordinate System At Joint i 45
Figure 3.8 Normal Distance of Approach of Two Far Field Points In Mated Contactor and Target 47
Figure 3.9 View Into Cone During Radial Displacement of Axisphere Center . . 48

Figure 3.10 Decomposition of Radial and Axial Movements to Conical Coordinates 49
Figure 3.11 Example Comparison Between Elastic Hertz Analysis and FEA Results 50
Figure 3.12 Example Curve Fits For Quasi-Kinematic Coupling Analysis 51
Figure 3.13 qrf and qri For a Target Mated With A Full Axisymmetric Contactor . 52
Figure 4.1 Design Procedure For Quasi-Kinematic Couplings 58
Figure 4.2 QKC Joint Showing Gap (G) and Related Variables 61
Figure 4.3 Model for Iterative Solution To Joint Geometry 64
Figure 4.4 Sensitivity of Nominal Gap to qc For the QKC Described in the Case Study 66
Figure 4.5 Comparison of Two Coupling Triangles 67
Figure 4.6 Comparison of Groove Orientations in Traditional and Aligned Kinematic Couplings 68
Figure 4.7 Aligned Grooves in Quasi-Kinematic Couplings 68
Figure 4.8 Stiffness Plot of Aligned Kinematic Coupling 69
Figure 4.9 Rough Model Of Surface Finish Affects on Couplings 71
Figure 4.10 Profile Trace of Burnished Quasi-Kinematic Coupling Groove Surface 72
Figure 4.11 Model For Analyzing Surface Asperity Deformation Due To Normal Loads 73
Figure 4.12 Simple Model of Asperity Before and After Deformation 73
Figure 4.13 Plastic Deformation From Normal and Tangential Traction 74
Figure 4.14 Simple Model of Edge Contact in Quasi-Kinematic Couplings 76
Figure 4.15 Deformed Contactor Surface, Cleaned For Viewing 77
Figure 4.16 Location For Wear Particle Generation in QKCs 78
Figure 4.17 Side View of 3D FEA Mesh, Shows Examples of Mesh Densities Used in Finite Element Analysis, Symmetry of Model Allowed Use of 1/4 of Joint Geometry 79
Figure 4.18 Quasi-Kinematic Coupling Plastic Deformation Test Fixture 80
Figure 4.19 Axial View of Contactor, Effect of Contact Angle on Ovaling On Similarly Loaded Pegs 81
Figure 4.20 Axial Load-Displacement Plot for Engine QKC Joint 82
Figure 4.21 Method For Inexpensive Manufacture of Target Surfaces 85
Figure 4.22 Spherical Peg For Press Fit in Quasi-Kinematic Couplings 85
Figure 4.23 Practical Performance Ranges For Common Couplings 87

Figure 5.1 2.5 Liter Six Cylinder Engine 89
Figure 5.2 Cross Section of Typical Journal Bearing Assembly 90
Figure 5.3 Block and Bedplate Components 92
Figure 5.4 Six Cylinder Block - Bedplate Assembly 92
Figure 5.5 Block and Bedplate Assembled With Crankshaft and Main Bearings In Place 93
Figure 5.6 Center Line Error Between Block and Bedplate 93
Figure 5.7 Sensitivity of Nominal Six Cylinder Engine QKC Gap to qc 97
Figure 5.8 Position of QKC Joint in Six Cylinder Engine 99
Figure 5.9 Orientation of QKC Coupling Joints To Maximize Repeatability In Sensitive Direction 99
Figure 5.10 Profile Trace of Burnished Quasi-Kinematic Coupling Groove Surface 102
Figure 5.11 Top View of Test Setup For Six Cylinder Engine QKC 103
Figure 5.12 Front View For Six Cylinder Engine Quasi-Kinematic Coupling . . . 103
Figure 5.13 Repeatability Measurements For Six Engine QKC 104
Figure 5.14 Effect of qc (shown as qcon) on Coupling Repeatability 105
Figure 5.15 Affect of Joint Misalignment on Repeatability 106
Figure 5.16 ComparisonofManufacturingProcessesForDifferentPinnedandQKCCouplings 107
Figure 6.1 Model of a Mechanical Coupling System 111
Figure C.1 Axisymmetric Mesh For FEA Model of QKC Joint, Note: Mesh Shown to Illustrate FEA Geometry, Actual Mesh Was Much Finer (Considerably More Cluttered) 134
Figure C.2 Elastoplastic Model For Material Properties of 12L14 Steel 135
Figure F.1 Decomposition of Radial and Axial Movements to Conical Coordinates 184
Figure F.2 Radial Displacement of Axisphere Center Relative To Cone Axis of Symmetry 185
Figure F.3 Abbe Error Due To Rotation. (Rotation Vector Points Out Of Page) . 187
Figure F.4 Model For Decomposition of Rotation Abbe Error 187
Figure F.5 Model For Calculating the Affects of exy 189
Figure F.6 Model For Calculating the Affects of ez 190
Figure G.1 Relation of Angular Strain and Radial Distance of Approach Ratios . . 196

LIST OF TABLES

TABLE 4.1 Example Quasi-Kinematic Coupling Functional Requirements and Design Parameters 60

TABLE 4.2 Affect of Minimizing qcon Important QKC Constraints/Functional Requirements 65

TABLE 5.1 Qualitative Effect of Bearing Centerline Misalignment 91

TABLE 5.2 Nominal Dimension and Associated Tolerances for QKC Kinematic Elements 96

TABLE 5.3 Quasi-Kinematic Coupling Gap 96

TABLE 5.4 Error Loads on Six Cylinder Assembly 98

TABLE 5.5 Comparison of Six Cylinder Pinned and Quasi-Kinematic Coupling Designs 108

TABLE 6.1 Steps in MathCad™ Worksheet for QKC Stiffness Determination . . 122

TABLE F.1 Error Motion Affects on Normal and Lateral Distances of Approach . 184

TABLE F.2 Tabulated Relation Between qr and dr(qr) 186

TABLE G.1 Order of Magnitude Scaling Quantities 194

NOMENCLATURE

UPPER CASE:

A	Engine contactor (peg) radius at mating surface [m, inches]
B	Cone radius at mating surface [m, inches]
COD	Alternate name for A [m, inches]
DBH	QKC bolt hole diameter [m, inches]
DH	Diameter of bolt hole through contactor [m, inches]
DP	Diameter of contactor insert shank [m, inches]
DR	Radius of six cylinder dowel pin [m, inches]
F	Resultant force between contactor and target [N, lbf]
G	Gap [m, inches]
INT	Interference of contactor-bedplate fit [m, inches]
K	Unit force - normal displacement power line fit coefficient [units of 1/b]
L	Length of indentor which plastically deforms surface asperities [m, inches]
LPEG	Length of QKC contactor shank [m, inches]
P	Load per unit length normal to asperity surface [N/m, lbf/in]
PID	Alternate name for DH [m, inches]
POD	Alternate name for DP [m, inches]
VD	Position of contact cone apex in z direction [m, inches]

LOWER CASE:

a	Width of contact stress profile in positive *l* direction [m, inches]
b	Unit force - normal displacement power line fit exponent [units of 1/b]
k	Material yield stress in simple shear [MPa, psi]
t	Thickness of contactor insert shank [m, inches]
w	Width of smashed asperity surface [m, inches]

GREEK:

α	Half included angle of asperity [radians]
δ_e	Error between engine half bore center lines [m, inches]
δ_{final}	Final generic QKC gap [m, inches]
δ_{GMS}	Margin of safety [m, inches]
$\delta_{initial}$	Initial generic QKC gap [m, inches]
δ_l	Displacement component of far field point in contactor along l direction [m, inches]
δ_n	Displacement component of far field point in contactor along n direction [m, inches]
δO_{SRr}	Variation in offset of sphere center in r direction [m, inches]
δO_{SRz}	Variation in offset of axisphere center in z direction [m, inches]
$\delta\theta_{ctool}$	Variation in included angle of new cone tooling [radians]
$\delta\theta_{cwear}$	Variation in included angle due to tool wear [radians]
δ_r	Displacement component of far field point in contactor along r direction [m, inches]
δR_S	Variation in axisphere radius [m, inches]
δ_{VD}	Variation in contact cone apex depth [m, inches]

δ_{xcc}	Relative movement of coupled components in x direction [m, inches]
δ_{xi}	Incremental movement in x direction [m, inches]
δ_{ycc}	Relative movement of coupled components in y direction [m, inches]
δ_{yi}	Incremental movement in y direction [m, inches]
δ_{z}	Displacement component of far field point in contactor along z direction [m, inches]
δ_{zBF}	Variation in location of mating surface on bottom coupling component in z direction (flatness) [m, inches]
δ_{zi}	Incremental movement in z direction [m, inches]
δ_{zcc}	Relative movement of coupled components in z direction [m, inches]
Δ_{r}	Coupling error [m, inches]
ΔG	Variation (+/-) in joint gap [m, inches]
ε_{xi}	Incremental rotation about x axis [radians]
ε_{yi}	Incremental rotation about y axis [radians]
ε_{zi}	Incremental rotation about z axis [radians]
ϕ	Dummy variable for $\theta_{\delta rmax}$ [radians]
γ_{b}	Chamfer angle on end of contactor insert shank [m, inches]
λ	Waviness spacing of surface irregularities [m, inches]
μ_{f}	Coefficient of friction between clamping means and coupling [---]
μ_{Ti}	Total coefficient of friction in i direction [---]
ν_{i}	Poison's ratio [---]
θ_{c}	Half included cone angle [radians]
θ_{con}	Alternate name for θ_{CT} [radians]
θ_{CT}	Contact angle, [radians]
θ_{r}	Conical integration angle [radians]
θ_{ri}	Integration angle at beginning of contact arc [radians]
θ_{rf}	Integration angle at end of contact arc [radians]
ρ	Density [kg/m^3, lbf/in^3]
σ_{n}	Normal surface contact stress [MPa, psi]
σ_{y}	Yield stress [MPa, psi]
τ_{f}	Friction contact stress [MPa, psi]

SUBSCRIPTS:

$CH_{x\text{-}b}$	Width of chamfer on end of contactor insert shank [m, inches]
E_{e}	Equivalent modulus of elasticity [MPa, psi]
E_{i}	Modulus of component/part i [m, inches]
F_{f}	Amonton's friction force [N, lbf]
F_{i}	i^{th} contact force in quasi-kinematic coupling [N, lbf]
f_{n}	Force per unit arc/line length [N/m, lbf/in]
f_{nYIELD}	Force per unit contact length require to initiate yield [N/m, lbf/in]
F_{N}	Amonton's normal force [N, lbf]
F_{p}	Coupling preload force [N, lbf]
G_{Cr}	Groove center offset in r direction [m, inches]
G_{Cz}	Groove center offset in z direction [m, inches]
G_{MAX}	Maximum gap [m, inches]
G_{MIN}	Minimum gap [m, inches]

h_{nf}	Final height of asperity smashed by normal load [m, inches]
h_o	Initial peak-to-valley height of asperity [m, inches]
K_r	Stiffness in radial (r) direction, also called in-plane stiffness [m, inches]
K_z	Stiffness in mating (-z) direction [m, inches]
M_p	Coupling preload moment [Nm, in-lbf]
O_{GR}	Absolute groove offset in r direction [m, inches]
O_{SRr}	Offset of axisphere center in r direction [m, inches]
O_{SRz}	Offset of axisphere sphere center in z direction [m, inches]
R_C	Contact radius from z axis [m, inches]
R_e	Equivalent radius of contact [m, inches]
R_G	Groove radius [m, inches]
R_i	Radius of component/part i [m, inches]
R_s	Axi-sphere Radius [m, inches]
S_{Cr}	Radial position of Axi-sphere center in the r direction [m, inches]
S_{Cz}	Position of Z Axi-sphere center in z direction [m, inches]
s_i	Beginning of contact arc [m, inches]
s_f	End of contact arc [m, inches]
w_{nf}	Width of smashed asperity surface due to normal load [m, inches]
Xcp	X location of contact point (in plane cross section) between target and contactor surface [m, inches]
Ycp	Y location of contact point (in plane cross section) between target and contactor surface [m, inches]
z_{TF}	Location of mating surface on top coupling component in z direction [m, inches]
z_{BF}	Location of mating surface on bottom coupling component in z direction [m, inches]

SUPERSCRIPTS:

$\underline{a}'$	Width of contact stress profile in negative *l* direction [m, inches]
$\overline{p}$	Average pressure on indentor which flattens asperities [MPa, psi]

Chapter 1

INTRODUCTION

1.1 Motivation

The manufacture of quality products is dependent upon the ability of manufacturing and assembly processes to repeatably align and maintain the position of objects. As a result, better precision at lower cost is a major driving force in design and manufacturing. Often the two are seen as mutually exclusive, but in order for manufacturers to survive, they must find low-cost means which will increase their precision and thus the quality of their goods.

This can be difficult, as most manufacturing processes require their alignment and fixturing methods to withstand brute force and/or high impact loads. As a result, the most common class of couplings used in manufacturing rely on elastic averaging or forced geometric congruence. For example, pinned joints, tapers, V-flat, and other elastic averaging methods have been widely used for their high load carrying capacity and their ability to form sealing interfaces.

Designers and manufacturers have pushed the practical performance of these methods to their limit of approximately five microns. Below this level, the use of conventional couplings becomes impractical, either because manufacturers can not hold the restrictive tolerances required to make them, or the cost for them to do so becomes too high. Many current and certainly next generation assemblies require better coupling performance at a

lower cost. The absence of a low-cost means of precision location has motivated the development of a fundamentally new machine element, the quasi-kinematic coupling.

Quasi-Kinematic Couplings (QKCs) are a passive means for precision location which combine elastically averaged and kinematic design principles. The result is a stiff coupling which delivers sub-micron repeatability and permits sealing between mated surfaces. It is particularly well suited for high volume manufacturing applications such as product assembly, fixtures, molds, and other processes.

A good example of the need for low-cost precision is the automotive engine shown in Fig.1.1. In manufacturing this engine (see section 5.1 for details), the components are bolted together as shown in Fig.1.2. Then the crank bore is simultaneously machined into each component, with a half bore in each. Afterwards, the two components are disassembled, the main bearings and crank shaft are installed between them, and the components are reassembled. Maintaining the same alignment of the block and bedplate half bores before and after assembly is critical as mismatch between them will adversely affect the performance of the engine's bearings (see Section 5.1.3 on page 91).



Figure 1.1 2.5 Liter Six Cylinder Engine

This had been accomplished using 8 pinned joints which were capable of only five microns repeatability. This design required tight feature size and placement tolerances which resulted in high rework and scrap costs. Replacement of this coupling with a Quasi-Kinematic Coupling (QKC) has enabled the manufacturer to improve their preci-

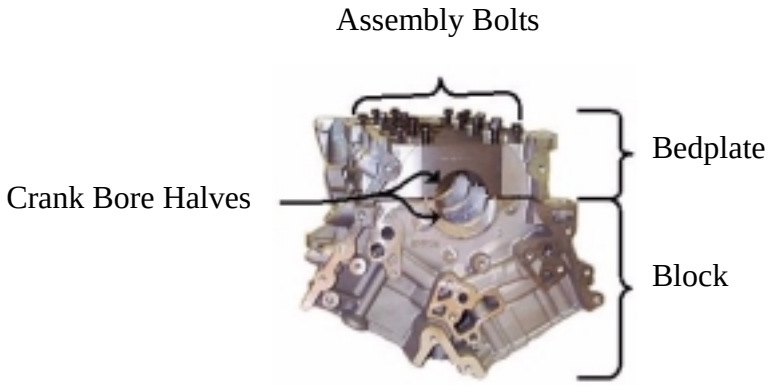


Figure 1.2 Six Cylinder Engine Assembly Partially Assembled

sion from 5 microns to 0.7 microns, reduce cost, and simplify their manufacturing process and tooling.

1.2 Precision Coupling Systems

The position and orientation of one object with respect to another can be described by six relative degrees of freedom shown in Fig.1.3 as δ_{xi}, δ_{yi}, δ_{zi}, ε_{xi}, ε_{yi}, and ε_{zi}. The requirements of precision location are to constrain N of these degrees of freedom. The design parameters are the means, usually contacting elements, which maintain position and orientation by providing resistance to motion in the N degrees of freedom.

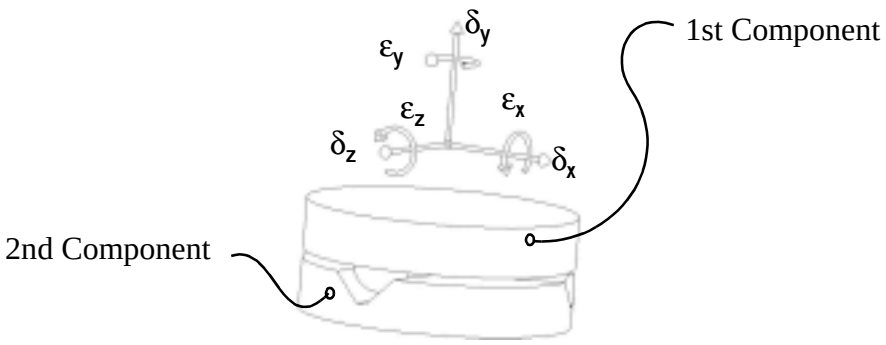


Figure 1.3 Kinematic Coupling Fixture Shown With Six Degrees of Freedom

If one treats a coupling as a system with behavior determined by geometric, material, kinematic and thermodynamic properties, the coupling system can be modeled as shown in Fig.1.4. Given a coupling system where the inputs are uniquely matched to the outputs, one can expect repeatable outputs from repeatable inputs. Practically, there are variations in the inputs and system characteristics. The resulting outputs differ from the expected output by an amount described as the error or repeatability

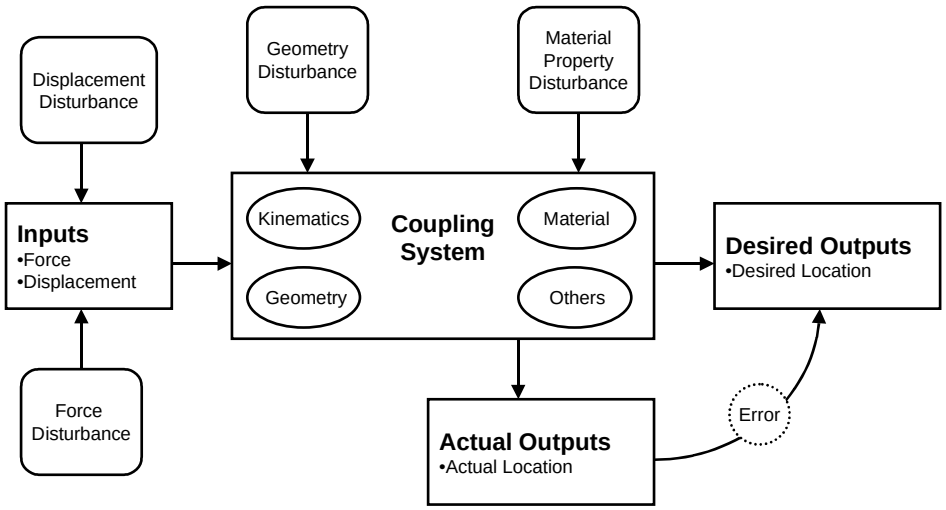


Figure 1.4 Model of a Mechanical Coupling System

Designing components to maintain precision location requires consideration of the effects of applied disruptions, i.e. variations from nominal, on the interacting kinematic and continuum characteristics of the components/systems. These disruptions, shown acting on a coupling system in Fig.1.4, may be grouped into four categories:

- **Force (momentum)** - A momentum transfer to, or between the coupled components. These can include forces due to coupling acceleration, error loads, friction forces, etc...
- **Geometry** - Geometry disruptions are variations in the geometry of the coupling or other structures which interact with the coupling. These can include geometric such as surface finish irregularities.

- **Displacement** - A displacement disruption is a relative motion between the coupled components. Generally, it is not desirable for these displacements to be parallel to sensitive directions. Sensitive directions are those in which we wish to minimize error. Examples of this type of disturbance include the stroke of compliant members or undesirable displacements due to creep.
- **Coupling Properties** - These disruptions result from variations of the coupling's constitutive, thermal, or other properties. Note, care has been taken not to specify this as a continuum disruption as on a small scale, for example in MEMs devices, the physics which describe the behavior of some phenomena no longer follows a continuum model.

1.3 Thesis Scope and Organization

The pursuit of scientific knowledge is a series of steps from one level of knowledge to the next. When beginning research in a fundamentally new area, the best course of action is to choose those issues which have the largest affect on the practical use of the scientific knowledge. This is particularly important in this application as defining the effects off each type of disruption on any coupling is an enormous task. Therefore, this thesis will cover the practical and theoretical considerations needed to model, design, and manufacture QKCs with emphasis on the affects of momentum and geometry disturbances. These disturbances are generally the most common disturbance. Displacement and coupling property disturbances usually are limited to a small number of specialized applications and will be left as subjects of future research.

Thesis Organization

The first chapter in this thesis provides the reader with a short background on common mechanical couplings. This knowledge is needed to understand the application of QKCs and to appreciate their importance. The second chapter covers basics Quasi-Kinematic Coupling geometry and function. It includes the terminology and variables which will be used to describe the geometric components, analytic components, and their interaction. Chapter three describes the methods for modeling and designing QKCs. The author has chosen to incorporate a fair bit of analytical content in this chapter, but has taken care to present it so that it does not read like an Appendix. The fifth chapter covers the details of

the tools and procedures for designing QKCs. This is followed by a case study on the design and integration of a QKC into an automotive engine. The thesis then closes with a brief discussion of future work and future target applications.

1.4 Types of Passive Mechanical Couplings

There are many types of mechanical couplings. Instead of attempting to cover all of these couplings in detail, they have been grouped into categories. The following discusses the virtues, shortcomings, and general principles behind the operation of each category.

1.4.1 Elastic Averaging Methods

Methods of alignment based on elastic averaging such as tapers, rail and slots, dove tail joints, V and flats, and press fits result in forced geometric congruence, or over-constraint. Example of these are shown in Fig.1.5. Though they can be used to define location, by their nature they are grossly over-constrained, resulting in poor performance and cost/ quality problems. Common problems include geometric disruptions such as the effects of surface finish and contaminants. These effects often require a long wear in period during which the surface irregularities are burnished. Thus good repeatability is not achieved until after a substantial "wear-in" period.

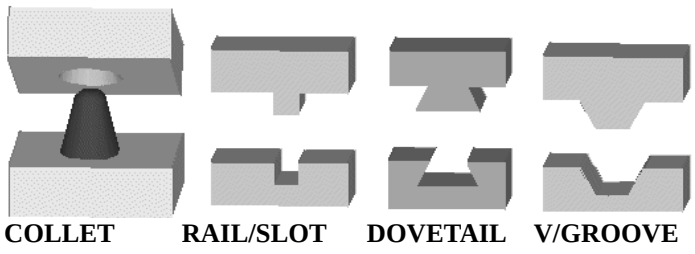


Figure 1.5 Types of Elastically Averaged Couplings

Despite their problems, elastically averaged couplings have several desirable characteristics. When high load capacity is required, the coupling interfaces can be designed with the

appropriate contact area to make a stiff joint. They can also be designed to provide sealing interfaces between the coupled components.

1.4.2 Pinned Joints

The pin-hole and pin-slot alignment methods have long been considered the easiest and least costly method for aligning components. They operate by constraining relative movement between components via pins which mate into corresponding holes or slots. An example using holes is shown in Fig.1.6. If there is no clearance, i.e. a press fit, between the pin and hole these couplings can be grouped with elastically averaged couplings.

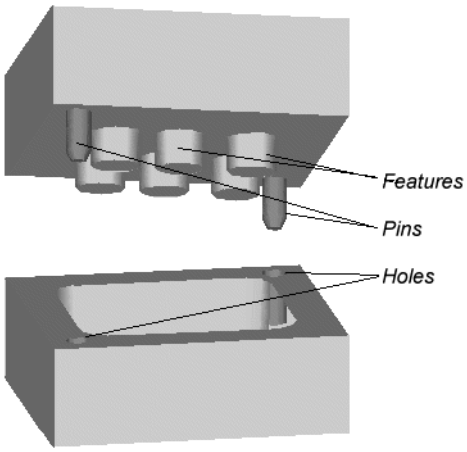


Figure 1.6 Example of Casting Mold Located With Pinned Joints

When a finite clearance exists between the pin and hole, the relative location of the two coupled components is not uniquely defined. To a point this may be acceptable if the clearance or "slop" between the pins and holes is small compared to the required repeatability. However, increased precision requires smaller clearances. Maintaining these clearances forces trade-offs between repeatability and two important factors, ease of assembly and manufacturing cost.

In most pinned joint assemblies which are roughly the size of a bread box or larger, achieving better than 0.08 mm (0.003 inches) is problematic due to jamming and wedging. This is an approximate number and depends upon the size of the system. For instance, a clearance of 0.08 mm (0.003 inches) in MEMs devices is much different than the same clearance between the large components of an airplane frame.

Wedging and jamming are especially troublesome in applications where manual assembly of large and/or heavy components is required. During a wedge or jam, most precision assemblies require gentle handling, i.e. they can not be "hit with a hammer". Once cleared, there is an instantaneous need to switch from low-force finesse motion, to the high-force motion needed to support the weight of the freed component. Often, in the above switch, fingers get pinched or parts of the coupling or components can be damaged. The time and care needed to avoid this situation, translates into lower productivity and higher costs.

Another problem is that manufacturing of precision pinned joints is expensive as the location of hole/slot centers (4 per joint), hole/slot sizes (4 per joint), and peg diameters (2 per joint), must be held to tolerances which are more restrictive than the required repeatability of the joint.

1.4.3 Kinematic Couplings

A kinematic coupling, as shown in Fig.1.7, can provide economical, sub-micron repeatability. They are relatively insensitive to contaminants, and for most designs, do not require an extensive wear in period. However, because these types of couplings transmit force through near point contact, care must be taken to design the coupling elements such that they can withstand the high contact stresses at these points (Slocum, 1988a) and maintain surface integrity after repeated cycles (Slocum and Donmez, 1988b). Though they can be designed for moderate stiffness, their ability to resist error causing loads is still limited by the mechanics which dominate the stiffness of the point contacts. In addition, due



Figure 1.7 Traditional Kinematic Coupling

to their kinematic nature, they do not allow intimate contact between mating surfaces as is needed to form sealing joints (Culpepper et. al., 1998).

1.4.4 Compliant Kinematic Couplings

In compliant kinematic couplings, one or more mechanical members are designed to have certain compliance characteristics. For instance, the flexural kinematic coupling in Fig.1.8 uses a multiplicity of cantilevers in series to provide compliance. This enables the coupling to locate components in N degrees of freedom while permitting 6-N degrees to remain free (Slocum et. al., 1997). This may be desired for instance in molding applications where the location of the mold surfaces could be initially constrained, but with some distance separating them (Slocum, 1998b). Then a prescribed force is applied such that the compliant member(s) displace perpendicular to the plane of mating, and allow the mold halves to come into contact (Culpepper et. al., 1998).

When designed properly, these couplings can deliver 5 micron repeatability (Culpepper et. al., 1998). In addition, because they allow contact between the mated components, the location of molds, engine components, and other applications which require sealing con-

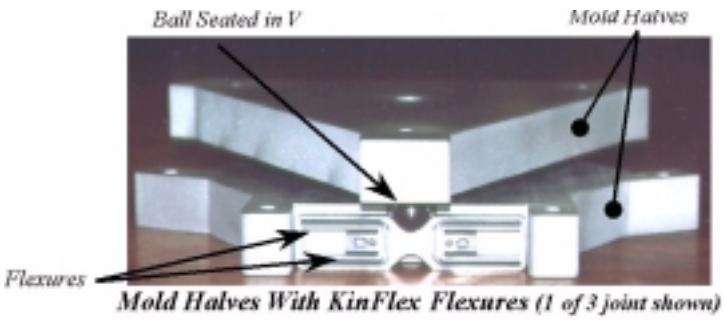


Figure 1.8 Mold Halves With Flexural Kinematic Coupling Elements

tact can benefit from their use. The ability of these couplings to permit contact gives them a unique characteristic, the ability to decouple the location and stiffness requirements of the coupling system. For instance, when the coupling shown in Fig.1.8 is mated, location is provided by the kinematic elements attached to the flexures. Resistance to error causing loads in the direction of mating is provided by the contact between the opposed faces of the mated components. Resistance in the plane of mating is provided by the friction at the interface between the coupled components (Culpepper et. al., 1998).

The use of these couplings is primarily determined by the economics of the application. Generally, they are affordable in precision fixtures or low to medium product integrated applications. They are usually not affordable in high volume applications due to the cost of making and assembling the flexural elements.

1.4.5 Quasi-Kinematic Couplings (QKCs)

A Quasi-Kinematic Coupling is a fundamentally new type of coupling which operates on elastic and kinematic design principles. In their generic form, they consist of convex solids of revolution attached to one component which mate with corresponding concave or "grooved" recesses of revolution in the second component. The coupling is assembled by placing the convex members into the corresponding grooves. These mates result in 6 arcs of contact as shown in Fig.1.9; and not points of contacts as in a true kinematic coupling. The resulting coupling is not as grossly over-constrained as many elastically averaged

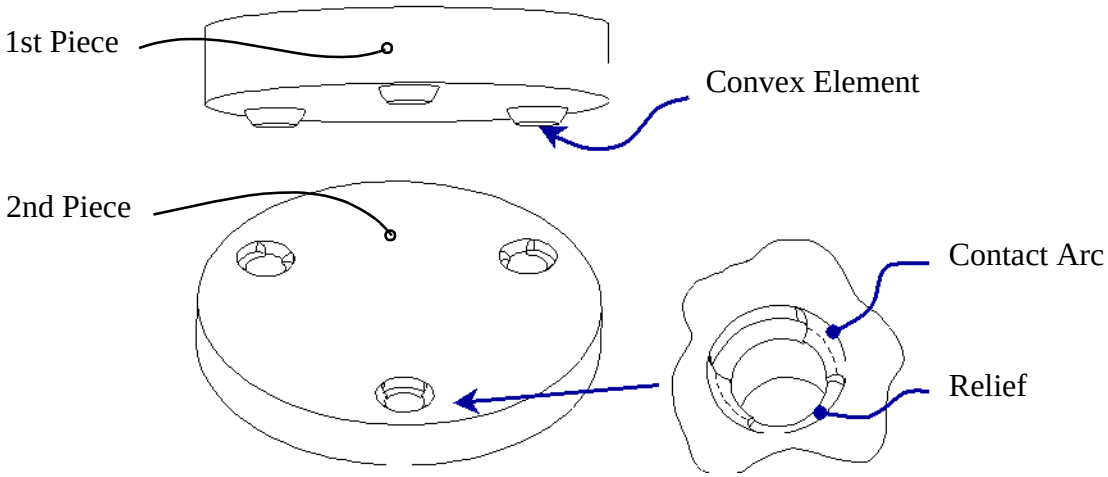


Figure 1.9 Generic Quasi-Kinematic Coupling

couplings such as collets and tapers, but not truly kinematic, thus the names quasi-kinematic or "near kinematic."

As will be shown, the Quasi-Kinematic Coupling can be designed to allows sealing between faces of mated components. They are less sensitive to errors in the placement of their locating features than current methods, require fewer precision features, and can be manufactured economically in large volumes. Its use can be extended into other manufacturing and assembly applications such as molding, tooling, and fixture location.

1.4.6 Comparison of Mechanical Coupling Types

Figure 1.10 provides a comparison of the typical performance limits of common low-cost couplings. Note that the QKC will enable manufactures to achieve approximately one order of magnitude better precision than traditional methods. In many cases, this can be done for substantially lower cost.

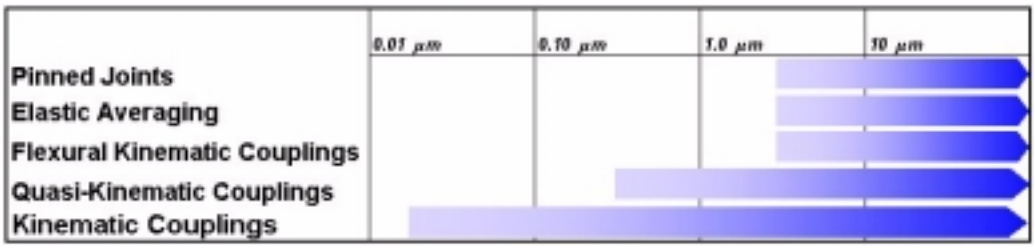


Figure 1.10 Practical Performance Limits of Common Low-Cost Couplings

Chapter 2

QUASI-KINEMATIC GEOMETRY AND FUNCTION

This chapter describes the components of a QKC system and the reference systems used to define their location. In line with the definitions in Chapter 1, we will examine a QKC as a coupling system which consists of physical and analytic components. The physical components are the coupled components to which contactors and targets, the kinematic elements, are physically attached to or machine into. The analytic components are those parts of the system used to mathematically describe and analyze the coupling.

2.1 Physical Components of QKCs

Contactors and targets are the features which establish intimate contact between the two coupled components. Figure 2.1 shows the physical components of a generic QKC system. In brief, contactors have convex surfaces of revolution while targets have either convex or concave surfaces of revolution. This terminology is different from traditional kinematic coupling terminology which refers to these members as balls and v-grooves. The difference is used as QKC contactors and targets are surfaces of revolution, which need not be spherical, straight v-grooves, or gothic arches.

Three drivers in reducing high volume precision manufacturing costs are the reduction of the number of precision machining tasks, precision tolerances, and precision features. As the QKC is geared toward use in high volume precision applications, one simplification will be made to its design. Pairs of contactors and targets can be incorporated into com-

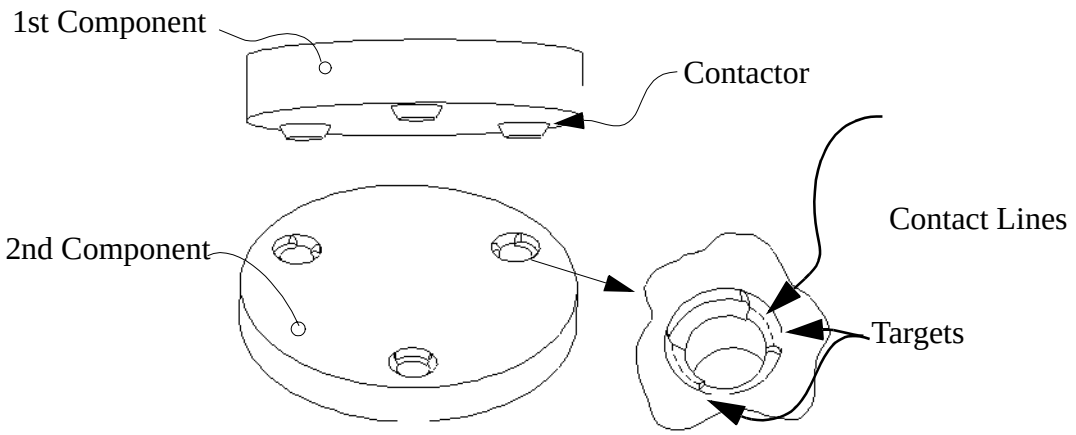


Figure 2.1 Physical Components of a Generic QKC

mon pieces or features. In effect, this allows the simultaneous machining of pairs of contactors or targets, halving the number of feature fabrication tasks. In turn, this reduces the number of precision tolerances by coupling feature location and feature size tolerances between pairs. For example, the tolerances on the location and orientation of the targets in the conical groove of Fig.2.2 can be considered the same as long as geometry variations due to spindle run out and perpendicularity errors are an order of magnitude less than the tolerances on the placement and feature size of the QKC elements. This is usually the case with modern machine tools and spindles.

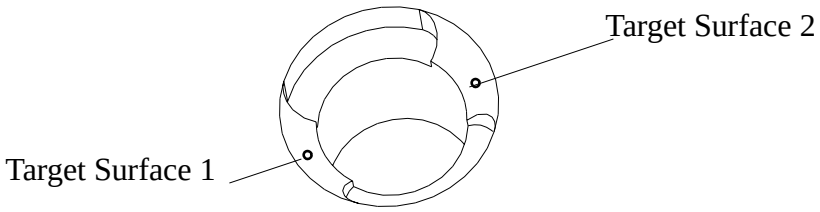


Figure 2.2 Two Targets Combined Into a Conical Groove

2.2 Analytic Components of QKCs

The analytic components of the coupling system are the joint coordinate systems, coupling triangle, coupling centroid, and coupling centroid coordinate system. These components

are used to define the location of the physical components of the coupling and provide the means to analyze and describe the errors in the coupling system.

2.2.1 Joint Coordinate Systems

A cross section of a QKC joint is shown in Figure 2.3. Each joint has a coordinate system in which the axis of symmetry for the contactors and targets is co-linear with the z axis of the joint coordinate system. The x and y axes of every joint coordinate system is placed in the coupling plane of the triangle which is defined by the plane through the nominal location of the contact arcs. Though this constrains the applicability of the coming analysis to planar couplings, this still encompass the majority of coupling applications.

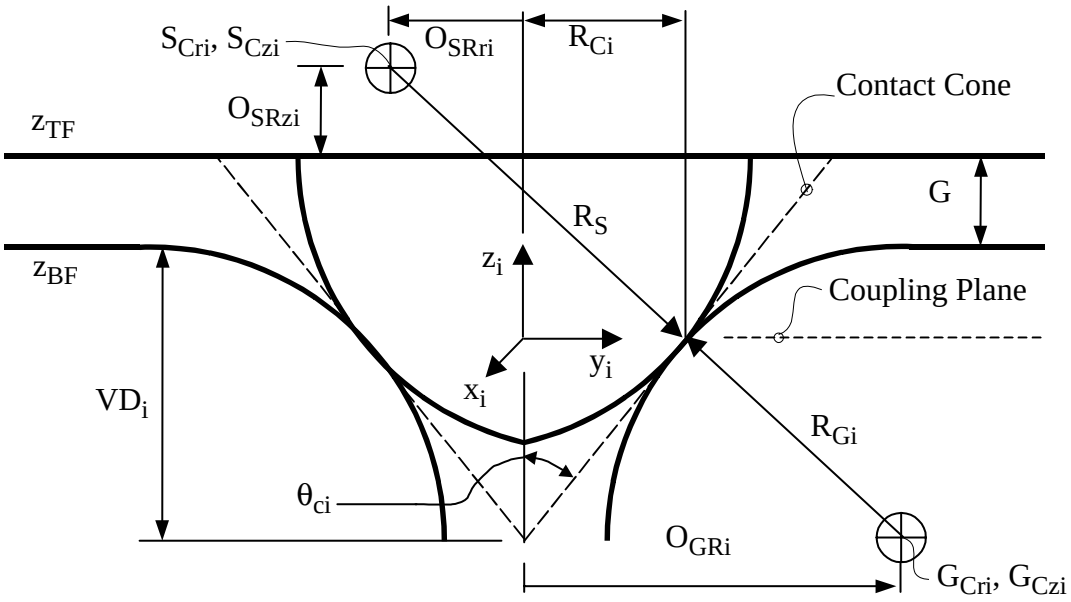


Figure 2.3 Placement of Joint Coordinate System and Variables For Joint i

Each joint has a contact cone. This is the surface defined by the tangents to the contactors and targets at cross sections through the axis of symmetry. In the 2D case shown in Fig.2.3, it appears as a "V", but since the elements contact over an arc in three dimensional

space, the actual shape is a cone. This cone is very important as half its included angle (θ_c) is used extensively in the calculation of QKC stiffness. We shall cover this in more detail in Chapter 3.

Several variables which describe characteristics of QKC joints are defined via Figure 2.3. The most important are:

- VD - Depth of the contact cone
- G - Gap, or distance between opposing faces of coupled components
- R_G - Groove radius at contact point
- R_S - Sphere radius at contact point
- O_{SR} - Offset of groove radius from center line
- O_{GR} - Offset of groove radius from center line

Note that some variables appearing with the subscript r, i.e. S_{Cr} and G_{Cr}, would seem to be redundant. The r subscript signifies that these values are invariant with respect to x and y and have been defined using a radial coordinate within the x-y plane specified from the joint coordinate system. This is in contrast to their "redundant" counterparts, O_{SR} and O_{GR}, which must retain their sign for use in some calculations. Note that variables which can either be positive or negative are shown using one sided arrows. The direction of the arrow with respect to left or right of the axis of symmetry provides the sign of the quantity, left is negative. For example, in Figure 2.3, O_{SR} is shown as negative, while O_{GR} is shown as positive. For a convex groove, O_{GR} would be negative.

2.2.2 Analytic Components of Couplings

The coupling triangle is defined by lines which connect the joint coordinate systems as shown in Fig.2.4. The coupling centroid is defined as the intersection of the angle bisectors of the included angles of the coupling triangle. A coordinate system, the centroid coordinate system, is placed at this location. Note that these analytic components exist for each of the coupled components and are initially coincident. After geometric or force dis-

turbances, these coordinate systems will separate. The linear and angular movements between these coordinate systems are used to describe the error between the components.

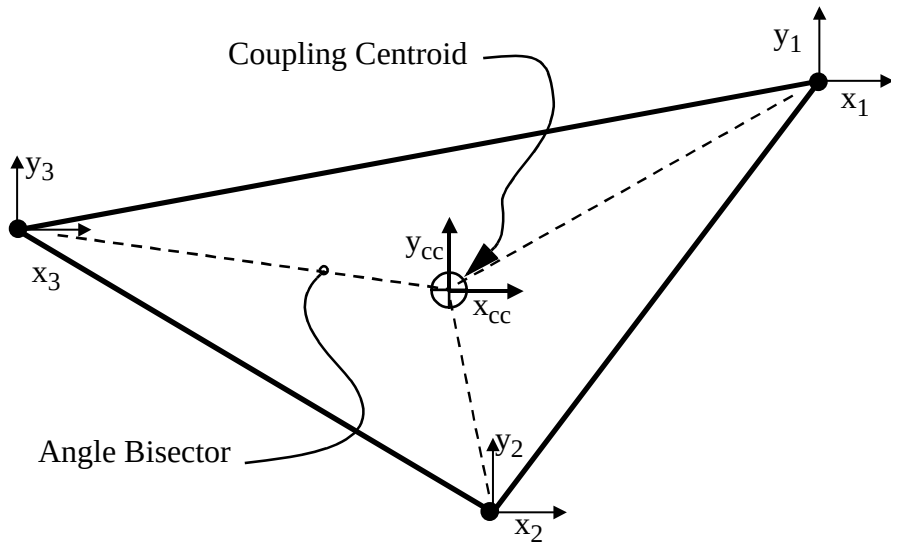


Figure 2.4 Analytic Components of A Quasi-Kinematic Coupling

2.2.3 Contact Angle

Each contactor-target contact arc sub-tends an angle called the contact angle, θ_{CT}, as shown in Fig.2.5. As the contact angle decreases, the arcs of contact become smaller, approaching point contact in the limit as θ_{CT} goes to zero.

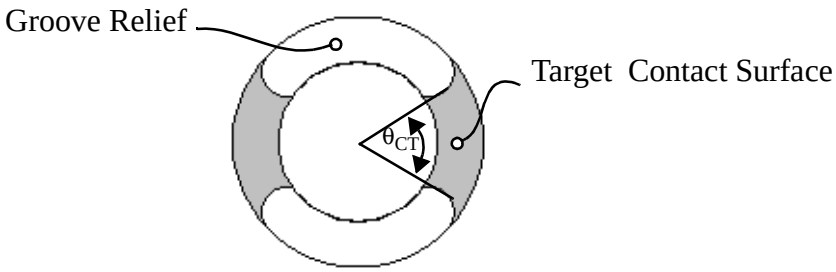


Figure 2.5 Quasi-Kinematic Coupling Contact Angle, θ_{CT}, Note View Is Into Conical Groove From Top

2.3 Function of Quasi-Kinematic Couplings

Due to friction and surface irregularities (Slocum, 1992a), when the coupling components are first mated as in Figure 2.6-A, the components will not occupy the most stable equilibrium. Proper seating can be achieved by a preload that overcomes the contact friction and causes the spherical elements to brinell out surface irregularities at the contacts (Culpepper et. al., 1999a).

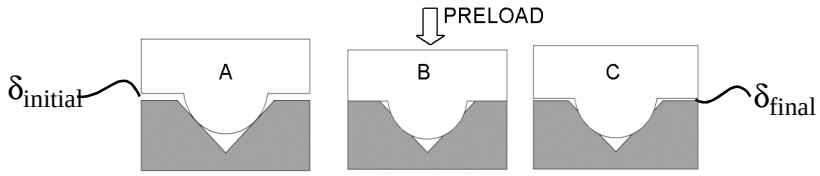


Figure 2.6 Mating Cycle of Quasi-Kinematic Couplings

If mating of opposed faces is desired, i.e. for sealing or stiffness, the gap between components and the compliance of the kinematic elements can be chosen such that the preload will close the initial gap, $\delta_{initial}$ as shown in Fig.2.6-B. On removal of the load, all or part of the gap is restored through elastic recovery of the kinematic elements, thereby preserving the kinematic nature of the joint for subsequent mates. If the initial deformation is elastic, the whole gap will be restored. If elastic and plastic, only a portion of the gap will be recovered.

With the gap closed, high stiffness can be achieved. This is due to the fact that the coupling stiffness becomes dependent on the interaction of the opposing surfaces, not the quasi-kinematic interfaces. As such, the stiffness in the direction perpendicular to the plane of the mated surfaces depends primarily on the stiffness of the clamping method. The stiffness in directions contained in the plane of the mated surfaces, i.e. the plane of mating, depends on the contact friction between the components and the load used to press them into contact (Culpepper et. al., 1998).

Chapter 3

MODELING AND ANALYSIS OF QKCS

3.1 Modeling of Quasi-Kinematic Couplings

As explained in Section 2.3, these couplings operate on principles which are fundamentally different from those which govern the behavior of traditional kinematic couplings. As such they exhibit unique characteristics, some of which contradict classical kinematic coupling theory. For instance the posses the ability to align the grooves to provide maximum stiffness in one direction. The following sections review the traditional kinematic coupling solution process, explains why a new process is needed, then presents a means to model and analyze the behavior of QKCs.

3.1.1 Kinematic Coupling Solution

It is beneficial to understand how one analyzes a traditional hard mount kinematic coupling before attempting to analyze a QKC. Given the geometry, material, and applied loads, one can model these couplings and find a closed form solution (Slocum, 1992a). Figure 3.1 shows the general solution procedure. It is not possible to determine relative movement between the components without considering the interaction at the contacts. Therefore, the determination of the contact forces and displacements is necessary.

Consider the Kinematic Coupling of Fig.3.2 in static equilibrium. Were a combination of forces and torques applied to the top component, reaction forces would the develop at the

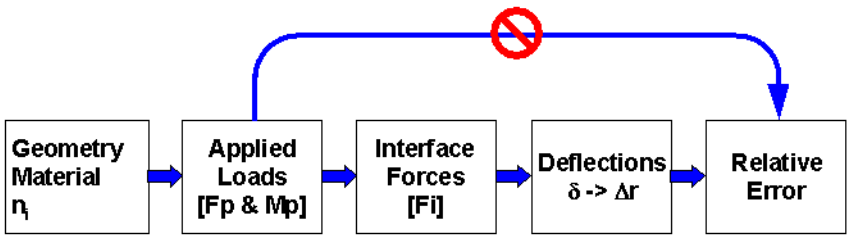


Figure 3.1 Solution Procedure For Kinematic Couplings

point contacts. A solution to the problem consists of the direction and magnitude of the individual contact force vectors. For each contact force vector, the direction of the vector is described by three independent quantities and the magnitude of the vector by one. This yields 24 (6 x 4) quantities which must be solved for.



Figure 3.2 Traditional Hard Mount Kinematic Coupling

Basic free body diagram analysis tells us that the contact forces will be perpendicular to the groove surfaces if one can assume the coefficient of friction at the contact interfaces is small. As we know the geometry of the grooves, we can determine the direction of the contact forces. ***This is an important characteristic of kinematic couplings, which quasi-kinematic couplings do not posses.***

With the directions of the forces known, only the magnitude of the six contact forces need be determined. The six force and moment equilibrium equations can be used to determine these forces, which are then used to calculate the hertzian deflections between the balls and grooves. Knowing these deflections, one can estimate the relative movement of the mated components (see Slocum, 1992a for further detail).

3.1.2 Solving the QKC Over Constraint Problem

Since QKCs rely on arc, not line or point contact, it is not possible to know a priori the direction of the reaction forces between the contactors and targets. This leaves 24 unknowns, six equilibrium equations, and one equation for the minimization of stored energy. There are more unknowns than equations, making solution in closed form impossible. However, one can reverse part of the process used by kinematic coupling to estimate the stiffness of the coupling. This is shown in the context of the kinematic coupling solution procedure of Fig.3.3 and represented by the formal QKC solution process shown in Fig.3.4

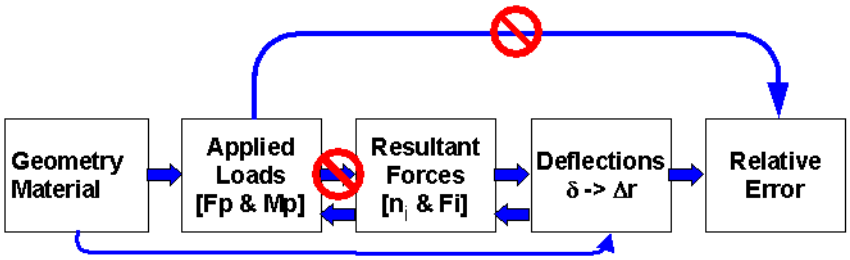


Figure 3.3 Solution Procedure For Quasi-Kinematic Couplings In Context of Traditional Approach

Given the geometry, material properties of the coupling components, and contact stiffness, one can impose a displacement between the coupled components and use the contact stiffness (as a function of displacement) to determine the resultant forces between the contactors and targets. The applied loads are then calculated and used to determine the stiffness in the direction of the imposed displacement. Though this method is less desirable than a

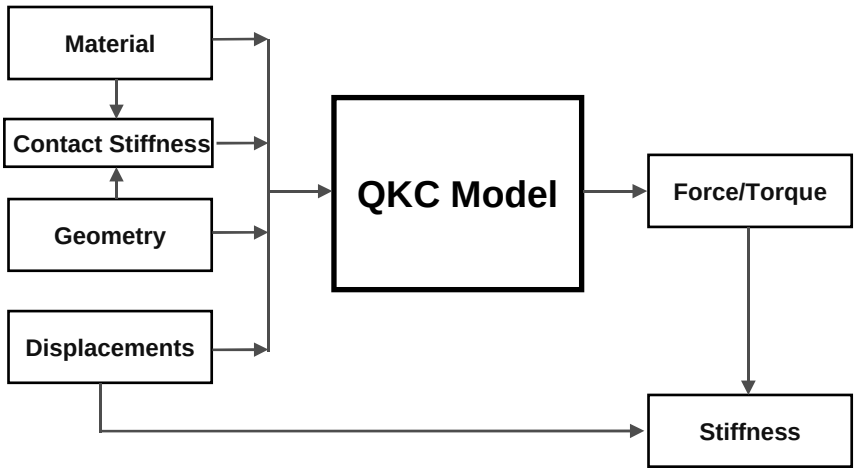


Figure 3.4 Stiffness Solution Model For Quasi-Kinematic Couplings

closed form solution, it provides enough information to make practical use of these couplings.

3.2 Quasi-Kinematic Coupling Contact Mechanics

No solutions for non-conforming axisymmetric arc contacts were found in the literature or through consultations with leading researchers in the field. The only reference of some help covered an iterative stiffness estimation for contact between a ball and a cone (Hale, 1999). This method is limited to applications with concentric contact of spheres and cones. It is not suitable for our analysis as one must be able to calculate the stiffness of the contactor-target interface when the axes of the contactor and target are misplaced by a small amount. Furthermore this method can not take into account interrupted contact between a contactor and target which occurs at the edge of the contactor/target surfaces, i.e. where the reliefs begin. This has led to the following analysis for determining the resultant force due to arc contact between non-conforming axisymmetric solids.

3.2.1 Contact Analysis Using a Rotating Coordinate System

The purpose of this section is to introduce the concept of a rotating coordinate system and explain why it is useful to our analysis. This is done in the context of an axisphere mated in a cone. This method can be

extended to arc contact between general solids of revolution by replacing the cone in the following discussion with the contact cone (see Figure 2.3 on page 35).

Consider the cross section of the cone shown in Fig.3.5. Were we to press a sphere or axisphere into a full cone, the arc of contact would be a circle. A conical coordinate system

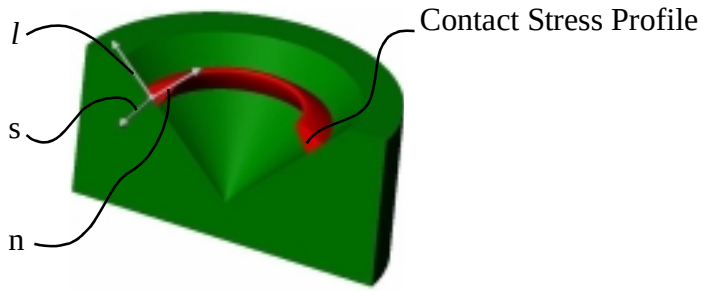


Figure 3.5 Conical Coordinate System and Contact Stress Profile

consisting of unit vectors n, *l*, and s, is placed coincident with the arc of contact and orientated such that the n vector is normal to the cone surface and point toward the cone's axis of symmetry. The *l* vector points along the cone surface and away from the cone's vertex. The s vector is perpendicular to the s and *l* vectors and points in the direction of increasing θ_r (θ_r is introduced below). The origin of the coordinate system is placed in the approximate center of the contact stress profile as shown in Fig.3.6. The shortest distance from

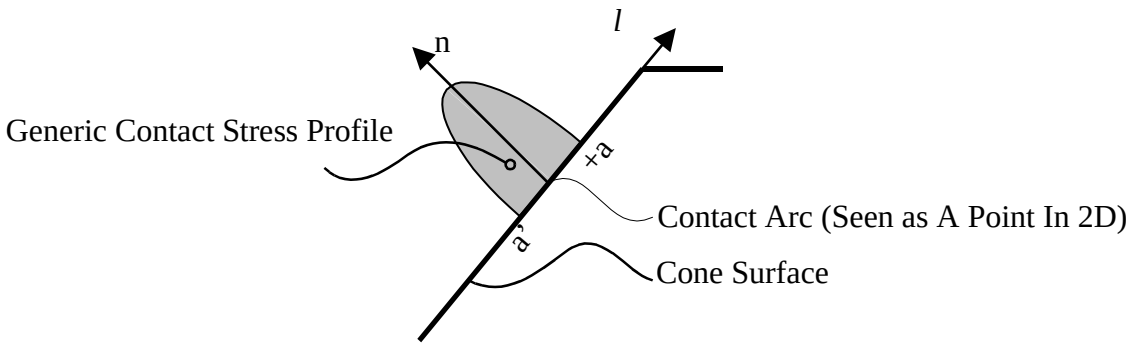


Figure 3.6 Cone Cross Section Showing Placement of Conical Coordinate System in Symmetric Profile

the cones axis of symmetry to the center of the contact arc is called the contact radius, Rc. It will be used to calculate the resultant force between the contactor and target.

A symmetric contact profile is attained if friction is negligible and the material properties and the geometry of the contacting elements do not change much over the area of contact. Practically, the effects of friction will skew this profile to one side, however, it has been shown that in 2D line contact problems subjected to extreme engineering values, the effect of friction will be to skew the maximum of the contact stress profile by approximately six percent of the width of the contact zone (Johnson, 1985). In the case of large coefficients of friction, the profile may not be symmetric, but positioning it about the "frictionless line of symmetry" will introduce little error in the value of Rc. Typically the shift is on the order of 6 - 10 % of the profile width, which is much smaller than the contact radius, Rc.

We plan to integrate the stress profile to obtain the force between the cone and groove. To capture the contribution of all points along the arc, the n-l-s coordinate system is allowed to rotate around the axis of symmetry of the cone during an integration. This will be explained later in Section 3.3.1, but for now it is enough to know that the coordinate system rotates. This rotation is defined by the angle θ_r which is the angle between the vector n' and the x axis of a Cartesian coordinate system whose z axis is co-linear with the axis of symmetry of the cone. This is illustrated in Fig.3.7. Note that the n' vector is the component of the n vector in the x-y plane.

If given the stress profile in Conical coordinates, i.e. as a function of θ_r, one can obtain the resultant force relative to the joint's frame of reference (Cartesian) by transforming the Conical coordinates to Cartesian coordinates, then integrating the modified function over θ_r. The transformation, the Culpepper Transformation, required to do this is provided in Equation 3.1. The use of this equation will be further explored in Section 3.2.2.

$$\begin{bmatrix} \hat{n} \\ \hat{s} \\ \hat{l} \end{bmatrix} = \begin{bmatrix} -\cos(\theta_r)\cos(\theta_c) & -\sin(\theta_r)\cos(\theta_c) & \sin(\theta_c) \\ -\sin(\theta_r) & \cos(\theta_r) & 0 \\ \cos(\theta_r)\sin(\theta_c) & \sin(\theta_r)\sin(\theta_c) & \cos(\theta_c) \end{bmatrix} \begin{bmatrix} \hat{i} \\ \hat{j} \\ \hat{k} \end{bmatrix} \tag{3.1}$$

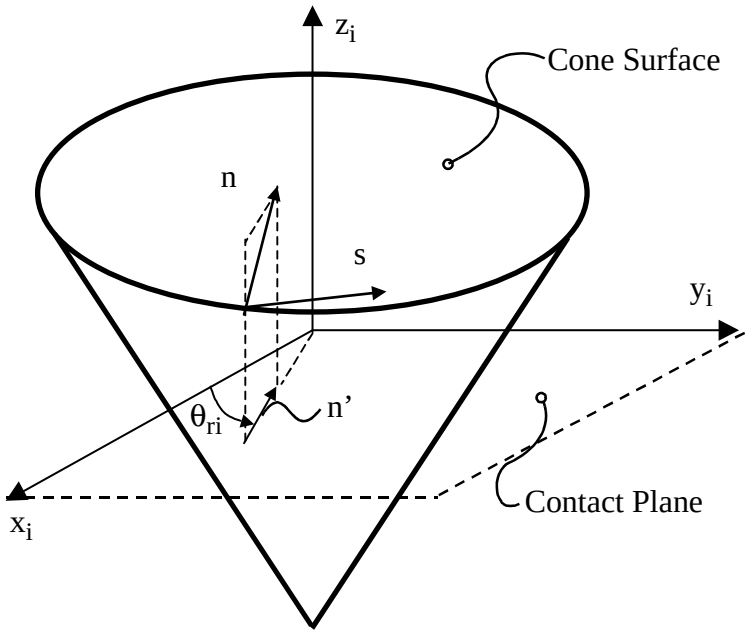


Figure 3.7 Rotating Conical Coordinate System At Joint i

3.2.2 Relationship Between Surface Stresses and Force Per Unit Length

The goal of this section is to discuss how the contact stress profile, force per unit length, and friction are related analytically. These relations will be used in section 3.3.1 to calculate the resultant force between the contactor and targets.

Contact Stress

The contact stress profile can be integrated to determine the force per unit length of contact. This can be done for any surface contact profile, elastic or plastic. As an example, we will use an elastic Hertzian contact profile of the form:

$$\sigma_n(l, \theta_r) = \frac{2f_n(\theta_r)}{\pi a}\left(1 - \frac{l^2}{a^2}\right)^{1/2}\hat{n} \tag{3.2}$$

Integrating Equation 3.2 gives the expected result:

$$\int_{-a}^{a} \frac{2f_n(\theta_r)}{\pi a}\left(1 - \frac{x^2}{a^2}\right)^{1/2} dl = f_n(\theta_r)\hat{n} \tag{3.3}$$

Friction Induced Traction

Friction is a complicated phenomena. It is the analytic embodiment of energy dissipation through (Suh, 1993):

- Adhesion of contacting materials
- Plowing by wear particles and asperities
- Plastic working of the asperities, contacting surfaces, and trapped particles

In our analysis, we will consider friction caused by plowing of wear particles and plastic working of asperities, contacting surfaces, and trapped particles. Adhesion typically plays a minor role, especially where contaminants, i.e. oil, cutting fluid, and oxide layers prevent adhesion and low temperatures do not act to breakdown surface oxide layers.

Following the approach of Section 3.2.1, we assume friction has little affect on the contact stress profile. Note, if this were not the case, one could change the limits of the following integral to adjust. It is then possible to describe the friction forces in the s and *l* directions using Amonton's Law of Friction. In our case it is:

$$f_i(\theta_r) = \int_{-a}^{a} \mu_{Ti}\, \sigma_n(l, \theta_r)\, dl = \mu_{Ti} f_n(\theta_r)\hat{i} \tag{3.4}$$

Note the subscript i denotes the friction force per unit length in either the s or *l* direction.

3.2.3 Far Field Distance of Approach

The goal of this section is to develop the equations for transforming imposed displacements (supplied by the user) in cartesian coordinates to a form which can be used in the next section to calculate the resultant forces from these displacements.

Far field distance of approach or distance of approach is a term frequently used in contact analysis. It is the change in distance between two far field points in contacting elements. Far field implies that the points are far from the contact region, meaning far from any points experiencing significant strain, say approximately 5% of the strain due to the contact. The intersection of our axisphere's radius with the z axis will serve as one point, the

other must be chosen along the line from the sphere center to the contact area. This point is subject to the strain constraint discussed above. Note that the distance of approach is not the compression of the surfaces at the contact interface. Determining this can be a complicated task and it does not take into account the strain away from the contact zone. For our purposes, working with the distance of approach is much simpler and still provides a general solution.

In learning how to make use of supplied displacements, we will first seek understanding through a qualitative description. Consider a sphere which is seated in a cone. Due to the axisymmetric nature of the problem, we can think of this as a series of 2D problems of cross sections of the axisphere-cone joint. When we press the axisphere into the cone, or in the -z direction, the distance of approach between the center of the sphere and far field points in a particular cross section will be equal for every cross section through the cone's axis of revolution. In other words, the distance of approach will be constant with θ_r. This is shown in Fig.3.8 as $\delta_n(\delta_z)$.

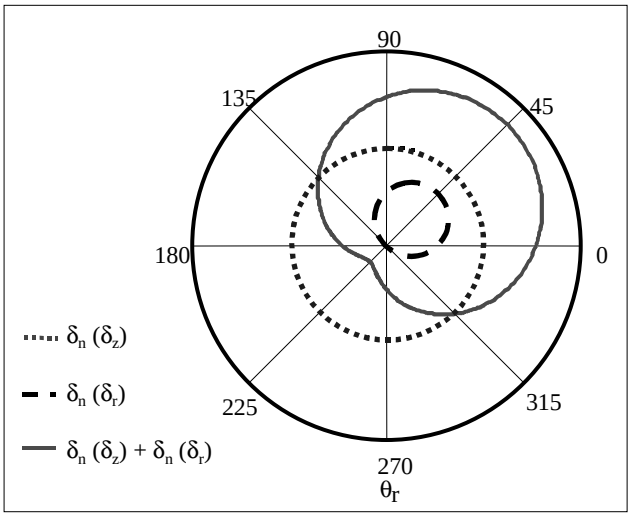


Figure 3.8 Normal Distance of Approach of Two Far Field Points In Mated Contactor and Target

Now consider imposing a displacement on the center of the sphere in a direction which is perpendicular to the cone's axis of symmetry. This is shown in Fig.3.9. Initially, the cen-

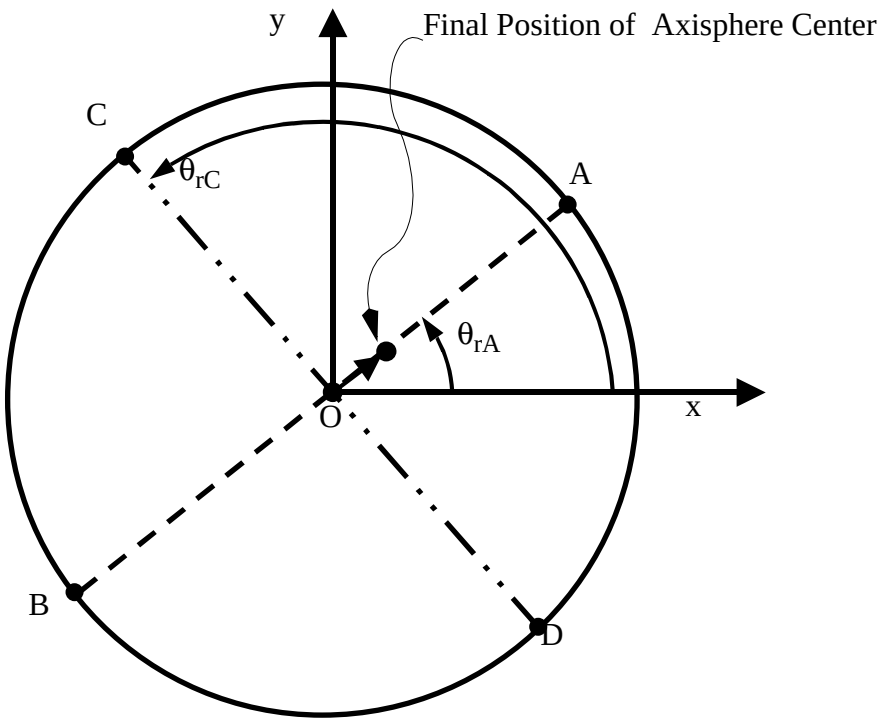


Figure 3.9 View Into Cone During Radial Displacement of Axisphere Center

ter of the sphere will be coincident with the cones axis of symmetry. After a finite motion parallel to the x-y plane is imposed, the distance of approach will vary sinusoidally about the cone, with θ_r. The maximum distance of approach will occur along the line $\overline{0A}$ (at θ_{rA}), the minimum along $\overline{0B}$ (at θ_{rB}) and zero distance of approach will occur along lines $\overline{0C}$ (at θ_{rC}) and $\overline{0D}$ (at θ_{rD}). This is shown if Fig.3.8 as $\delta_n(\delta_r)$. Note the superimposed displacements, $\delta_n(\delta_z) + \delta_n(\delta_z)$. The resulting curve is a cardoid (Swokowski, 1988).

Now we will look at this from a quantitative perspective. To perform the analysis, it is necessary to decompose the radial and axial components into the Conical coordinate system. Equations 3.5 and 3.6 provide the transformations for the generalized cross section

of a cone shown in Fig.3.10. When considering geometries other than cones, one should use the contact cone in place of the actual surface in Fig.3.10.

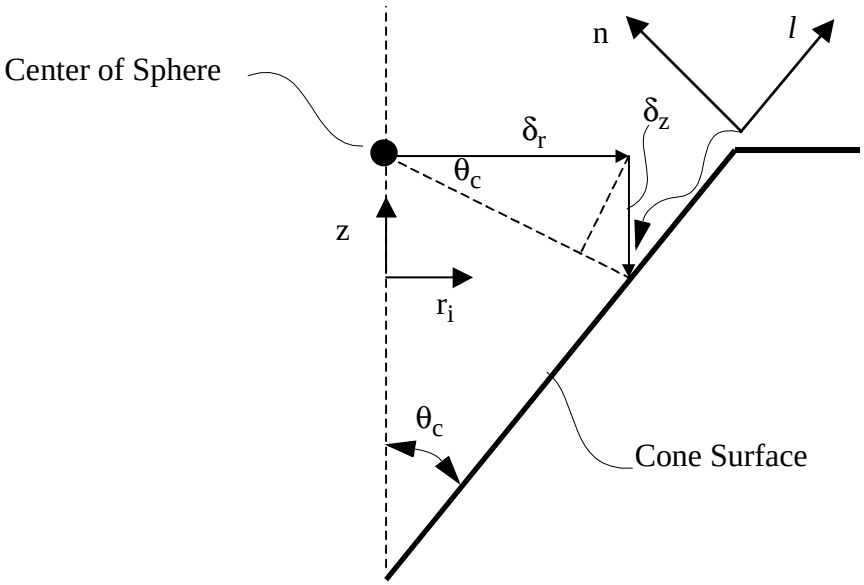


Figure 3.10 Decomposition of Radial and Axial Movements to Conical Coordinates

$$\delta_n(\theta_r) = -\delta_r(\theta_r)\cos(\theta_c) + \delta_z(\theta_r)\sin(\theta_c) \tag{3.5}$$

$$\delta_l(\theta_r) = \delta_r(\theta_r)\sin(\theta_c) + \delta_z(\theta_r)\cos(\theta_c) \tag{3.6}$$

One should note that a difficulty can arise if $\delta_l(\theta_r)$ becomes greater than zero. When a contactor and target are first mated, $\delta_l(\theta_r) = 0$. If the contactor is pressed down into the cone $\delta_l(\theta_r)$ becomes negative. If $\delta_l(\theta_r)$ becomes positive at any θ_r, this means that the contact has traveled up the side of the cone past the initial seating point. When this happens, a point at $\theta_r + \pi$ looses contact with the cone.

This is undesirable in practice as it will adversely affect the stiffness of the coupling. Analytically, the model may calculate a tensile or imaginary contact force per unit length (f_n), thereby providing erroneous results. Upon rearrangement, equation 3.6 gives the following criteria to avoid this situation.

$$\frac{-\delta_z(\theta_r)}{\delta_r(\theta_r)} \geq \tan(\theta_c) \quad \text{This must be satisfied for all } \theta_r! \tag{3.7}$$

Usually this is not difficult to achieve since $\delta_z(\theta_r)$ depends primarily on the preload displacement δ_z. This is typically 75 - 300 microns as opposed to the small error movements $\delta_r(\theta_r)$ whose maximum value δ_r is on the order of microns.

Note: The above is a worst case estimate for the situation where the coefficient of friction is zero. With finite friction, the distance of approach along the l direction may occur without relative movement (slipping) of the contact points. Equation 3.7 then becomes a conservative estimate for loss of contact between the target surface and the contactor.

3.2.4 Relationship Between f_n and δ_n

The purpose of this section is to develop a relationship between f_n and δ_n. This is the last step required before solving for the reaction forces between contactors and targets.

The task of finding the load per unit length vs. normal deflection, f_n vs. δ_n, behavior of arc contact becomes difficult as the problem is non-linear due to plastic flow. With no analytic solutions to this problem, one must use experimental or finite element methods. Figure Fig.3.11 shows good agreement between an analytic Hertzian contact analysis and an FEA based on the same geometry and loads. Though this plot is for elastic deformation, it

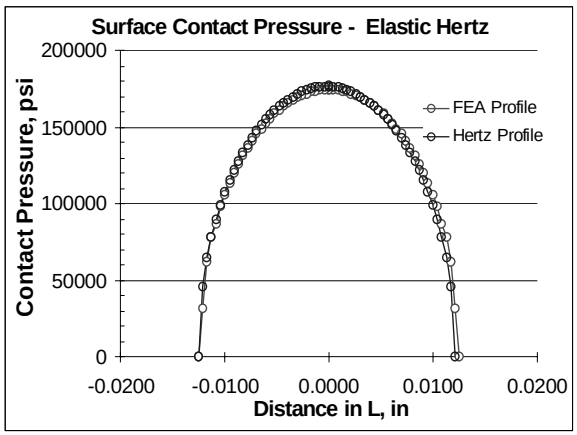


Figure 3.11 Example Comparison Between Elastic Hertz Analysis and FEA Results

is reasonable to expect that the FEA would provide good results for elasto-plastic problems. A general rule of thumb learned during this research, is that the mesh size of the contacting elements near the point of contact should be less than 5 % of the width of the contact region to obtain good agreement with classical Hertz theory. Using this rule of thumb in plastic contact has shown to provide results which are near convergence.

The next section will show how to use the results of these analysis. For now, it is enough to know that a curve must be fit to the FEA results for use in the QKC model. In many cases, one can accurately express the results by a power law relationship. Examples are shown through Fig.3.12 and equation 3.8.

$$f_n = K(\delta_n)^b \tag{3.8}$$

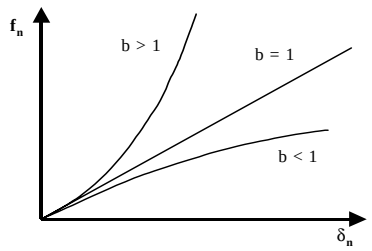


Figure 3.12 Example Curve Fits For Quasi-Kinematic Coupling Analysis

3.3 Using the Quasi-Kinematic Coupling Model/Analysis

This section describes how to make practical use of the analysis just presented. The ultimate goal is to get an estimate of the coupling's stiffness. We start by calculating the resultant reaction forces between the contactors and targets.

3.3.1 Quasi-Kinematic Coupling Reaction Forces

The total reaction force is found by integrating the surface stress over the contact arc.

$$F = \int_{si}^{sf}\int_{-a}^{a} [\sigma_n(l,s)\hat{n} + \mu_{Tl}\sigma_n(l,s)\hat{l} + \mu_{Ts}\sigma_n(l,s)\hat{s}]\,dl\,ds \tag{3.9}$$

Where s_i and s_f describe the start and finish points on the contact arc respectively.

Upon integration and substitution of $ds = R_c\, d\theta_r$, and using equation 3.4, we obtain:

$$F = \int_{\theta ri}^{\theta rf} R_c[f_n(\theta_r)\hat{n} + \mu_{Tl} f_n(\theta_r)\hat{l} + \mu_{Ts} f_n(\theta_r)\hat{s}]d\theta_r \tag{3.10}$$

The limits of the integrand, θ_{rf} and θ_{ri}, are the angular limits of θ_r to which contact exists on a given contactor-target contact arc. Note that $\theta_{rf} - \theta_{ri}$ will equal the contact angle, θ_{CT}. The value of θ_{ri} is the start of the contact arc. It is distinguished from θ_{rf} in that its value relative to the x axis is always less than θ_{rf}. . This is illustrated in Fig.3.13.

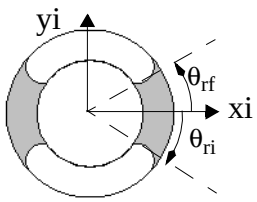


Figure 3.13 θ_{rf} and θ_{ri} For a Target Mated With A Full Axisymmetric Contactor

The last step is to change from Conical to Cartesian coordinates using Equation 3.1. The result is a vector with i, j, and k components.

$$F = \int_{\theta ri}^{\theta rf}\int_{-a}^{a}\left(R_C\sigma_n(l,\theta_r)\begin{bmatrix} -\cos(\theta_r)\cos(\theta_c) - \mu_{Ts}\sin(\theta_r) + \mu_{Tl}\cos(\theta_r)\sin(\theta_c) \\ -\sin(\theta_r)\cos(\theta_c) + \mu_{Ts}\cos(\theta_r) + \mu_{Tl}\sin(\theta_r)\sin(\theta_c) \\ \sin(\theta_c) + \mu_{Tl}\cos(\theta_c)\end{bmatrix}\begin{bmatrix}\hat{i}\ \hat{j}\ \hat{k}\end{bmatrix}\right)dl\,d\theta_r \tag{3.11}$$

This solution is for any contact stress profile, elastic or plastic. It assumes the contact stress profile shape and magnitude is not significantly affected by friction and that the friction shear stress at the interfaces obeys Amonton's Law. Amonton's Law states that the friction force is related to the normal force by the following relation:

$$F_f = \mu F_N \tag{3.12}$$

Where F_f is the friction force and F_N is the normal force. When taking the differential with respect to contact area, equation 3.12 can be expressed in terms of contact stress:

$$\tau_f(l, \theta_r) = \mu\sigma_n(l, \theta_r) \tag{3.13}$$

Where τ_f is the friction stress and σ_n is the normal stress.

$$F = \int_{\theta ri}^{\theta rf} \left(R_C f_n(\theta_r) \begin{bmatrix} -\cos(\theta_r)\cos(\theta_c) - \mu_{Ts}\sin(\theta_r) + \mu_{Tl}\cos(\theta_r)\sin(\theta_c) \\ -\sin(\theta_r)\cos(\theta_c) + \mu_{Ts}\cos(\theta_r) + \mu_{Tl}\sin(\theta_r)\sin(\theta_c) \\ \sin(\theta_c) + \mu_{Tl}\cos(\theta_c) \end{bmatrix} \begin{bmatrix} \hat{i} & \hat{j} & \hat{k} \end{bmatrix} \right) d\theta_r \tag{3.14}$$

We now substitute the curve fit for f_n vs. δ_n from Section 3.2.4. The type of fit does not matter. For demonstration, we will use the power fit. Substituting Equation 3.8 into 3.14 yields:

$$F = \int_{\theta ri}^{\theta rf} \left(R_C K(\delta_n(\theta_r))^b \begin{bmatrix} -\cos(\theta_r)\cos(\theta_c) - \mu_{Ts}\sin(\theta_r) + \mu_{Tl}\cos(\theta_r)\sin(\theta_c) \\ -\sin(\theta_r)\cos(\theta_c) + \mu_{Ts}\cos(\theta_r) + \mu_{Tl}\sin(\theta_r)\sin(\theta_c) \\ \sin(\theta_c) + \mu_{Tl}\cos(\theta_c) \end{bmatrix} \begin{bmatrix} \hat{i} & \hat{j} & \hat{k} \end{bmatrix} \right) d\theta_r \tag{3.15}$$

Given $\delta_n(\theta_r)$, the resultant force between the contactor and target can be calculated.

If the method used to acquire f_n vs. δ_n is based on the assumption of constant plane strain as an axisymmetric FEA typically is, then this assumption must be valid in our model. Ideal constant plane strain is a condition in an axisymmetic problem where the difference between the maximum and minimum strain in the angular direction does not vary significantly from the nominal strain in that direction. When a sphere is pressed straight down into a cone, the strain in the angular direction should be constant around the arc of contact. But, displacing the sphere from the center of the cone will result in varying amounts of angular strain around the cone. A derivation of the analysis used to determine a criteria and relate it to QKCs is provided in Appendix G. In general, the criteria is met for small ratios of δ_r / R_c, i.e. $\delta_r < 0.03\ R_c$.

3.3.2 Stiffness of QKCs

The actual load vs. displacement plot for the coupling may not be linear. Usually it follows a trend similar to the supplied f_n vs. δ_n curve. Calculating the instantaneous stiffness can be done, but is computationally intense, since the original equation is more than one page wide. Fortunately, it is not necessary, as a good estimate of the coupling stiffness can be obtained from linearizing the load vs. displacement plot locally. Given the resultant force, the stiffness of the coupling can then be estimated from the initial user supplied displacement, δ.

If the function is continuous and "well-behaved" around δ, then local linearization of the load vs. displacement plot provides a good approximation. The stiffness, i.e. slope, can be estimated through differential movements around the point of initial displacement using:

$$Stiffness = \frac{F(\delta + d\delta) - F(\delta - d\delta)}{d\delta} \tag{3.16}$$

3.3.3 Limits on the Estimation of QKC Stiffness

Constant Contact Assumption

The analysis assumes the contactors and targets remain in contact over the entire contact angle. This has already been address in section Section 3.2.3. The criteria for ensuring constant contact was given in equation 3.7, and is repeated here for convenience.

$$\frac{\delta_z(\theta_r)}{\delta_r(\theta_r)} \geq \tan(\theta_c) \quad \text{This must be satisfied for all } \theta_r! \tag{3.17}$$

Plane Strain Assumption

The substitution of a plane strain load vs. displacement function in 3.15 imposes a constant plane strain constraint on our model. How do we know when this is a good estimate? For small values of δ_r / R_c, i.e. $\delta_r < 0.03\ R_c$, the model is valid. A derivation of the analysis used to determine this value is provided in Appendix G.

Rigid Body Assumption

In our analysis, we have assumed that the relative movement of the kinematic elements is the same. This assumes no change in distance between the kinematic elements. For the rigid body assumption to be valid, the relative in-plane movement between coupling elements, i.e. axiphere centers, should be an order of magnitude less than the distance of approach between far field points in the kinematic elements (Slocum, 1992a).

Chapter 4

DESIGN AND MANUFACTURE OF QUASI-KINEMATIC COUPLINGS

4.1 Overview of the Quasi-Kinematic Coupling Design Process

The design process for QKCs consists of the four stages shown in Fig.4.1.

1. **Problem Definition** - Information gathering and detailed description of the problem. Description of design constraints, definition of what is required and how it will be done.
2. **Geometry Generation** - Given input from the first stage, the geometry of the coupling joint is generated using an algorithm which takes into account a multiplicity of variables and attempts to find the best solution. The placement and orientation of the joints is done manually.
3. **Design Check** - Checks to make sure all functional requirements are satisfied.
4. **Functional Design or Iteration Step** - If all design checks are satisfied, the process has found a solution or functional design. If not, the process starts over again with adjustments to the components of the Problem Definition Stage.

Sadly, there is not a closed-form solution for modeling the behavior of QKCs. The results is a an iterative design process (Culpepper et. al., 1999d). Though the process may be time consuming or possibly not converge to a solution, significant benefits may be realized if a functional solution is found. As will be shown in Chapter 5, coupling cost, the number of precision features, and the number of tools required to manufacture a coupling can be reduced up to 40 percent.

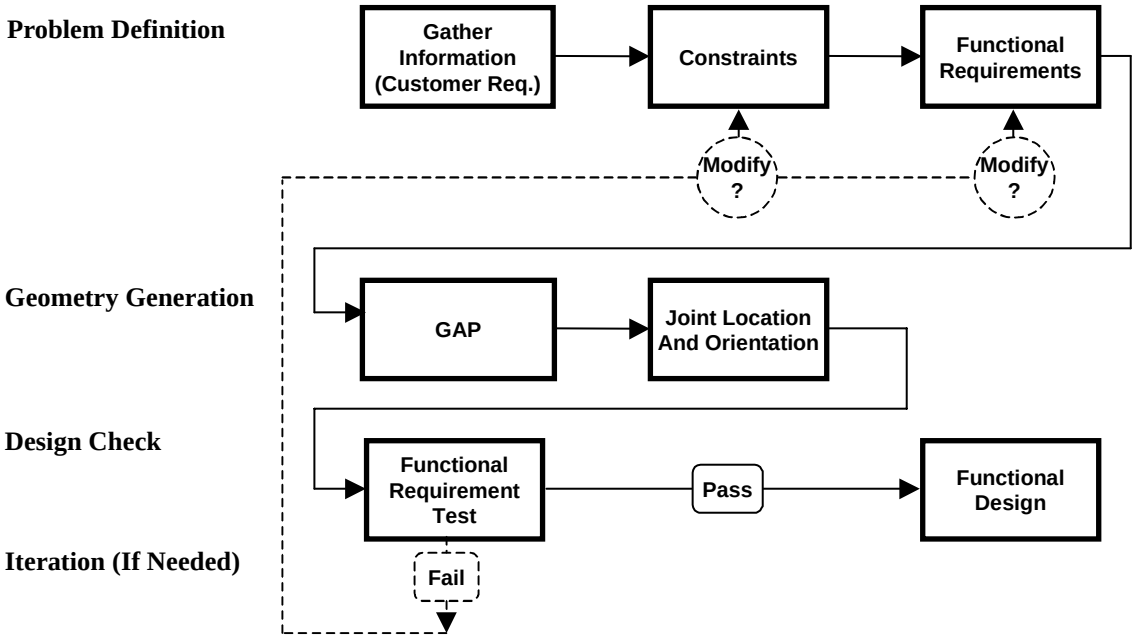


Figure 4.1 Design Procedure For Quasi-Kinematic Couplings

The remainder of this chapter follows the order of the design process. The goal of each section is to provide the reader with the general knowledge required to complete that design stage. Chapter 5 will demonstrate the use of these principles through a case study of an automotive assembly.

4.2 Problem Definition

The best way to begin is to gain a thorough understanding of the problem. This is best accomplished by gathering all pertinent information and defining the problem via sets of constraints and functional requirements. A set of design parameters, or those things which satisfy the design requirements can then be developed. These are often specific to the design/application, so the following will concentrate on making sure the designer can identify what is required of the design and how to best implement a solution. We begin by looking at constraints.

4.2.1 Constraints

Constraints put bounds on acceptable solutions (Suh, 1990); and these limits are lines which must not be crossed, i.e. there is no tolerance. The most common types of constraints are geometry, resources, manufacturing, or physical constraints. Geometry constraints, often called size constraints, place a limit on how large or small some aspect of the design should be. Resource constraints, place a limit on designs via the availability of material, monetary, or human resources. Manufacturing constraints limit the rate, precision, accuracy, and other factors which link a design to how it is/can made. Finally, physical constraints are limits which are placed by the laws of nature. For example, the second law of thermodynamics constrains the efficiency of machines/systems to be less than 100%.

Failing to understand the constraints imposed on a design can only lead to trouble. At best one may "get lucky" and the initial design will work. More often, the design must be "patched up" or redesigned, often after significant time, resources, and monetary investment. The sum total of these is often several times the investment which is required to determine the proper constraints.

4.2.2 Functional Requirements

Functional Requirements are required functions or outputs a design must deliver (Suh, 1990). A complete set of functional requirements consists of the least number of requirements needed to describe the desired functions of the design.

With respect to QKCs this can include:

- Stiffness
- Repeatability
- Sealing Contact
- Fool Proof Assembly - if the joints do not form an equilateral triangle, the coupling can only be assembled one way

4.2.3 Design Parameters

Design parameters are the means used to satisfy the functional requirements (Suh, 1990). Ideally, there is a unique relationship between the functional requirements and design parameters such that changing a design parameter does not affect, to within an acceptable level, the satisfaction of other functional requirements. For example, consider the following pairs of functional requirements (FRs) and design parameters (DPs).

TABLE 4.1 Example Quasi-Kinematic Coupling Functional Requirements and Design Parameters

Functional Requirement		Design Parameter
Repeatability	->	Stiffness of Coupling Elements
In Plane Stiffness	->	Friction Force Between Opposed Faces of Mated Components

Changing the coefficient of friction between the mated components will affect the in-plane stiffness of the coupling, but will not affect the coupling repeatability. This in essence decouples the stiffness requirements of the coupling from the repeatability requirements. A good designer will see this as a benefit, because the work needed to make changes or to redesign is reduced. When possible, one should strive to develop designs in this manner. For further discussion on functional requirements and design parameters, see Suh, 1990.

4.3 Geometry Generation

The performance of the coupling is very sensitive to the initial gap between the mated components, it often determines success or failure. Therefore we will use it as a starting point for the design. This reduces the amount of iteration which would result from starting with a different, less sensitive part of the design, say aesthetics.

4.3.1 Quasi-Kinematic Coupling Gap

Equation 4.1 through 4.4 provide the relations required to calculate the maximum and minimum gap of a coupling joint. Due to manufacturing errors, the gap will vary from the nominal value given in Equation 4.1. To ensure the existence of a gap, one sets the minimum gap, G_{MIN}, equal to the controllable gap variation, ΔG, plus a margin of safety, δG_{MS}.as seen in Equation 4.3.

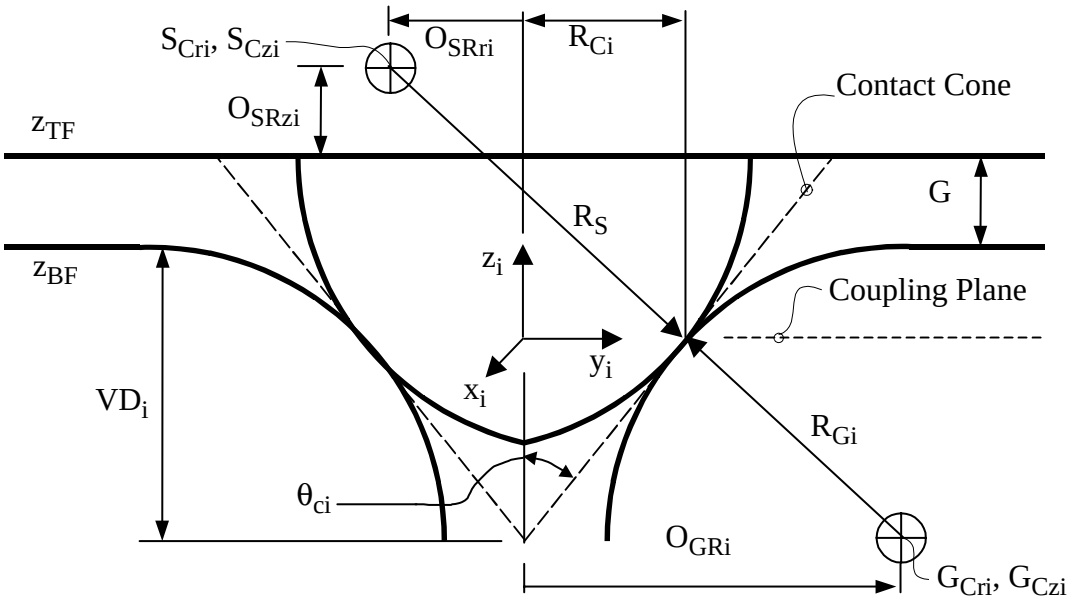


Figure 4.2 QKC Joint Showing Gap (G) and Related Variables

From equations 4.2 and 4.3, the maximum gap, G_{MAX} is found as a function of the variables seen in Fig.4.2. With so many variables, it becomes evident that some computational analysis will be needed to find the best, or a workable solution.

$$G = VD + \frac{R_S}{\sin(\theta_c)} + \frac{O_{SRr}}{\tan(\theta_c)} - O_{SR} - z_{BF} \tag{4.1}$$

$$\Delta G \sim \delta_{VD} + (\delta_{R_s})\frac{\partial G}{\partial Rs} + (\delta_{O_{SRr}})\frac{\partial G}{\partial O_{SRr}} + (\delta_{\theta_c})\frac{\partial G}{\partial \theta_c} + (\delta_{O_{SRz}})\frac{\partial G}{\partial O_{SRz}} + \delta_{zBF} \tag{4.2}$$

$$G_{MAX} = \Delta G + \delta G_{MS} \tag{4.3}$$

$$G_{MIN} = G + \Delta G = 2\Delta G + \delta G_{MS} \tag{4.4}$$

Gaps Resulting in Elastic Line Contact

When the deformation of the contacting elements is purely elastic, a Hertzian line contact solution can be used to estimate the stresses and displacements in arc contacts (Hale, 1999). However, with QKCs, the deformation is well into the full plastic region. This is due to the fact that most high volume manufacturing processes are incapable of holding the feature size and placement tolerances which are necessary to maintain a gap which will result in only elastic deformation upon closure. At best, one can expect +/- 25 microns (+/- 0.001 inches) reliable size and position control for dimensions such as VD (δ_{VD}) and z_{BF} (δ_{ZBF}). A quick look at the equations will show that the minimum gap will be at least 100 microns due to the effects of $\delta_{VD \text{ and }} \delta_{ZBF}$.

To verify whether plastic deformation has occurred, one solves for the force per unit length, f_{nYIELD}, required to induce plastic flow. A suitable relationship is given in equation 4.5 (Johnson, 1985).

$$f_{nYIELD} = \frac{2.8\pi R_e \sigma_Y}{E_e} \tag{4.5}$$

Here R_e is the equivalent radius of contact, σ_y is the yield stress of the materials, and E_e is the equivalent modulus of elasticity. The equivalent variables are common to hertzian analysis and calculated using equations 4.6 and 4.7. The radius of each i_{th} component at the point of contact is R_i. Poisons ratio and Young's Modulus for each component are denoted as ν_i and E_i. The subscripts 1 and 2 differentiate quantities for the two objects in contact.

$$R_e = \frac{1}{\left(\frac{1}{R_1} + \frac{1}{R_2}\right)} \tag{4.6}$$

$$E_e = \frac{1}{\left(\frac{1-\nu_1^2}{E_1} + \frac{1-\nu_2{}^2}{E_2}\right)} \tag{4.7}$$

With the value of f_{nYIELD}, one can use equation 4.8 modified from the analysis given in Johnson, 1985 to calculate the contact displacement which would induce plastic flow, thus providing the limit of elastic hertztian analysis.

$$\delta_n = \left(\frac{f_n}{\pi}\right)\left\{\frac{(1-\nu_1^2)}{E_1}\left(2\ln\left(2R_1\left(\frac{\pi E_e}{f_n R_e}\right)^{\frac{1}{2}}\right)-1\right)+\frac{(1-\nu_2^2)}{E_2}\left(2\ln\left(2R_2\left(\frac{\pi E_e}{f_n R_e}\right)^{\frac{1}{2}}\right)-1\right)\right\} \tag{4.8}$$

The associated displacement in the z direction or closure of the gap is:

$$\delta_z = G = \frac{\delta_n}{\sin(\theta_c)} \tag{4.9}$$

For most applications the allowable δ_n is on the order of 5-40 microns, well below the lowest possible gap of 50 microns.

Gaps Resulting in Plastic Line Contact

The solution to plastic herztian contact problems is not straight forward. There are limit analyses for plastic deformation of point contacts (Johnson, 1985) which can accurately predict the material state in the contacting elements. Due to the difference in conditions, these analyses are not applicable to line or arc contacts. An extensive literature review found no results to predict the behavior of plastic line contacts. This is curious given the fact that the backbone of the nation's industry was once the rail system which relies on line contact of rails and train wheels that must at sometimes be plastic. The author's attempts to find relationships via other means, i.e. dimensional analysis were not fruitful.

The necessary information, f_n vs. δ_n, can be found via a finite element analysis. Though we are able to obtain the information we desire, this is not the most desirable solution. Performing a non-linear FEA adds a step to the design which is temporally and computa-

tionally expensive, especially if the QKC design process is iterative. The author uses it here as it is the only means available to obtain the necessary data.

Iterative Modeling of Gap Using θ_c Minimization

As mentioned before, it is necessary to use a computational method to decide upon the best gap. Before discussing the details, an understanding of what must happen is needed. For now, it is enough to know that there are inputs which are incorporated into the analysis as functions or inequalities. For instance:

- **Constraints** - Absolute limits on the design. These would include the size of the QKC elements/joints. Figure 4.3 shows the variables which might be

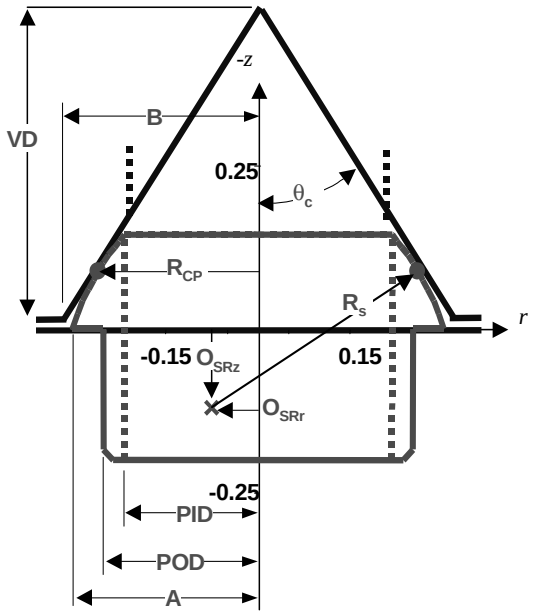


Figure 4.3 Model for Iterative Solution To Joint Geometry

used to describe the size of a QKC joint. Relations can be set between these quantities to constrain their values as is presented in Appendix A. Another example is cost. If the contactor is to be mass produced, the major contributor to its cost is material. A good cost estimate can be obtained from the mass required to make the peg. Equation 4.10 shows how the size/cost of the contactor could be estimated as a function of the geometry. The iteration

process would then use an inequality such as Equation 4.11 to enforce the cost constraint during the analysis.

$$Cost(Contactor) \propto \rho \times Volume \times \frac{Cost}{unitmass} \tag{4.10}$$

$$Cost(Contactor) \leq Constraint \tag{4.11}$$

- **Functional Requirements** - These are the desired functions of the design. Like constraints, these functions must be performed. However, they are assigned a tolerance within which a solution is acceptable. For instance the sealing pressure between opposed surfaces would be specified as some nominal value with a tolerance. Since we do not have a relationship between the variables which describe the geometry and the functional requirements, the design process is iterative. We can minimize the amount of iteration using rules of thumb.
- **Rules of Thumb** - We enter the iteration process without the information required to predict the contact stresses, radial stiffness (K_r), and stiffness of the coupling in the direction of mating (K_z). Therefore we must rely on rules of thumb to force the analysis to consider such quantities. A good rule of thumb is to minimize θ_c to the lowest limit allowed by manufacturing constraints. This is explained below.

It is fortuitous that minimizing θ_c has the desired affects on the following quantities:

TABLE 4.2 Affect of Minimizing θ_c on Important QKC Constraints/Functional Requirements

Contact Stress	**Kr** **Radial Stiffness**	**Kz** **Stiffness in z Direction**
Decreases	Increases	Decreases

Decreasing the contact stress is desirable to avoid material failure of the kinematic elements. Increasing the radial stiffness will make the coupling more resistant to error causing loads in the plane of mating. These loads are often proportional to the loads from the method used to clamp the joint. For instance, when using a bolt, the friction between the bolt head and the coupled component it slides against is proportional to the force in the bolt. This in turn is dependent upon the stiffness of the QKC joint in the z direction.

Therefore, lowering the stiffness in the z direction can help reduce error causing loads in the plane of mating.

Parenthetically, it should be noted that the ratio in Equation 4.12 can be used as a means to compare the performance of geometrically identical couplings with similar means of clamping, but different θ_c. This ratio increases as θ_c decreases.

$$\frac{K_z}{K_r} \tag{4.12}$$

There is a limit on how small θ_c, can become. As θ_c, decreases, the gap becomes increasingly more sensitive to variations in θ_c. This is illustrated in Fig.4.4 which shows the sensitivity of the nominal gap used in the case study. From a manufacturing perspective, the ideal θ_c would be 45 degrees or larger. From a material and/or stiffness perspective, we would like to decrease this value.

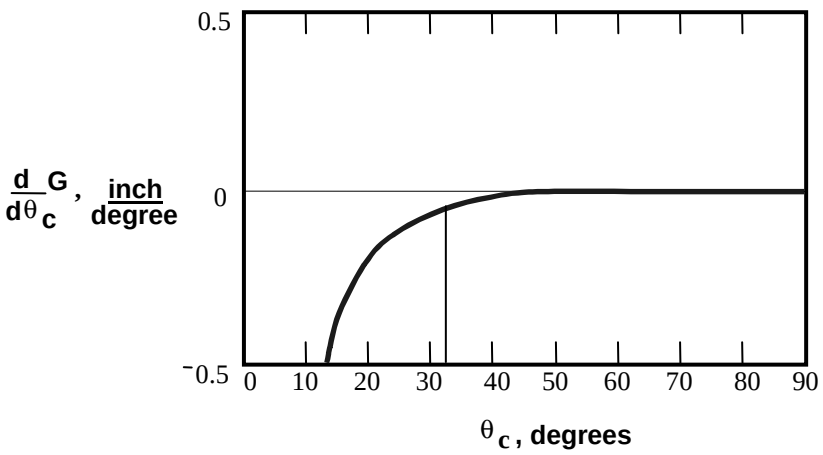


Figure 4.4 Sensitivity of Nominal Gap to θ_c For the QKC Described in the Case Study

A good approach to the problem is to set θ_c at 45 degrees, solve for the kinematic element dimensions, then perform the stress and stiffness design checks to determine if the design is feasible. If not, the iterative solver in Appendix A can be used to find a lower, feasible θ_c. The design checks can then be run again to determine feasibility. If a solution is still

not found, one should try to "loosen" the constraints of the design. The goal of the case study was to minimize the stress and maximize the radial stiffness, i.e. in plane stiffness, so the iterative solver was used to find a minimum acceptable solution of 32 degrees.

Joint Location and Orientation

The repeatability of a coupling under load is primarily dependent upon the applied error loads and the stiffness of the coupling. In a kinematic or quasi-kinematic coupling, the choice of joint location has a strong influence on the rotational stiffness of the coupling. This can be explained qualitatively by examining Fig.4.5. Two coupling triangles are pre-

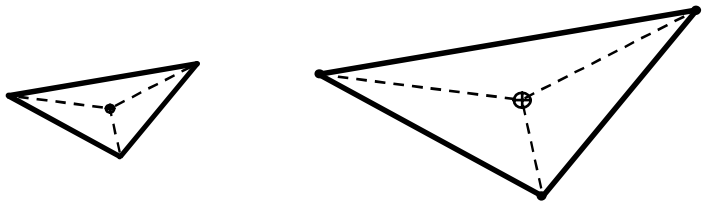


Figure 4.5 Comparison of Two Coupling Triangles

sented, the left is half the size of the right. The direction of coupling is parallel to the z axis, i.e. out of the page. If the joints of both couplings are similar, the coupling on the left will have a lower torsional stiffness about the z axis. Therefore, locating the coupling joints to define the widest possible triangle is desirable. This of course is subject to the geometry/size constraints of the design. The same line of thinking applies to rotation about the other axes. The exact affect on the stiffness of the coupling can be determined using the tool detailed in Appendix B. This tool is based on the models introduced in Chapter 3 for finding the stiffness of a QKC joint.

Joint orientation also affects the stiffness of the coupling. In traditional kinematic couplings, stability and good overall stiffness can be achieved if the grooves are oriented such that the normals to the planes containing the contact forces bisect the angles of the coupling triangle (Slocum, 1992b). This is illustrated in Fig.4.6. This orientation may be

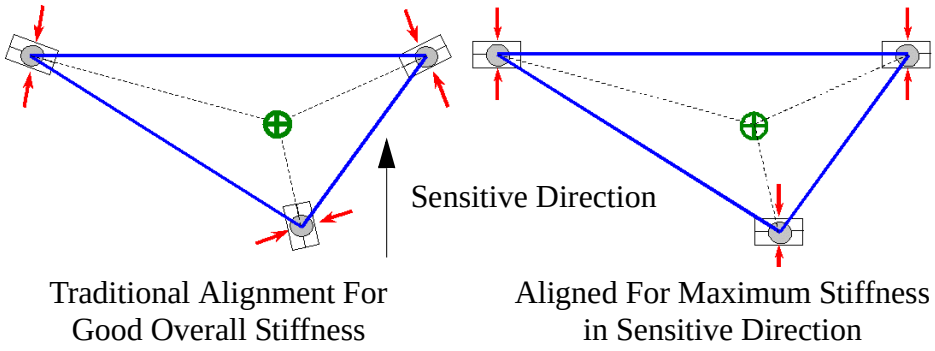


Figure 4.6 Comparison of Groove Orientations in Traditional and Aligned Kinematic Couplings

changed to allow for higher stiffness in a certain direction, but doing so adversely affects overall coupling stability. The right side of Fig.4.6 provides an example. Though able to provide maximum resistance to error causing loads in the direction in which we wish to prevent errors, this coupling provides no constraint in the perpendicular, i.e left-right direction as the balls can slide right and left in the grooves.

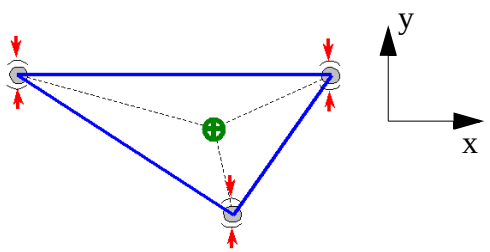


Figure 4.7 Aligned Grooves in Quasi-Kinematic Couplings

Quasi-Kinematic Couplings on the other hand, due to the curvature of their groove seats, can be aligned to provide maximum resistance to error causing loads in one direction, while still providing reasonable stiffness in the perpendicular direction. For example, the coupling in Fig.4.7 is positioned to provide maximum stiffens in the y direction.

Figure 4.8 is a typical polar plot of the in-plane stiffness (K_r) of a kinematic coupling which resembles the one shown in Fig.4.7. This particular plot is for an aligned coupling

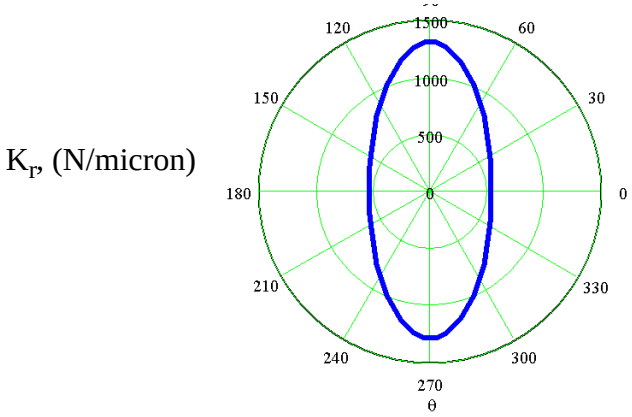


Figure 4.8 Stiffness Plot of Aligned Kinematic Coupling

with contact angles, θ_{CT}, equal to 120 degrees and θ_c equal to 32 degrees. The independent variable is θ_r, measured from the x axis. The maximum stiffness occurs at θ_r = 90 and 270 degrees, in line with the sensitive directions. The ratio of stiffness in the sensitive to non-sensitive direction is approximately 2.4 for this contact angle. Assuming similar error causing loads in both directions, the errors motions in the non-sensitive direction will be about a factor of 2.4 times the error in the sensitive direction. Close agreement with this relationship has been measured during testing of the coupling which was integrated into the automotive application discussed in Section 5.8.

4.4 Design Check

The next step is to verify that all functional requirements which were modeled as rules of thumb, not by inequalities in the iteration process, are met. The following should be checked:

- **Contact Stresses** - Given the joint geometry and gap, a finite element analysis can be preformed to determine the stresses in the contact region. Depending upon the application, these can then be compared to the stress needed to brinell out surface contacts and the yield or ultimate stress to determine if the coupling will fail.

- **Radial Stiffness (Kr)** - Using the tool detailed in Appendix B, the design is tested to determine if it meets the stiffness requirements in the sensitive and non-sensitive directions.
- **Axial Stiffness (Kz)** - The same tool is used to determine if the stiffness in the z direction is acceptable.

4.5 Iteration If Needed

If any of the design checks fail, an iteration is required. Either one or more of the constraints or functional requirements must be modified to make it possible for the solver to find a solution. Which constraint or functional requirement to change depends on the constraint or functional requirement which failed the design check. The designer must make an educated decision based on the sensitivity of the failed constraint to those variables which can be changed.

4.6 Design Specific Quasi-Kinematic Coupling Constraints

4.6.1 Enhancing QKC Performance Via Moderate Plastic Deformation

In this section we will explain the reason(s) why plastic deformation enhances the function of a Quasi-Kinematic Coupling. A means for estimating the required load to achieve this is provided.

It is common knowledge that the repeatability of couplings is dependent upon the surface finish of the mating components. The customary method for minimizing surface effects is to impart a very fine surface via expensive and time consuming processes, such as polishing. It is undesirable if not impossible to integrate these types of processes into the manufacture of high volume, low-cost goods, i.e. QKC elements. An ideal method for eliminating the effects of surface roughness would minimize the need for these processes. Fortunately, a mechanism for halving the number of finishing operations is built into the QKC. We will see that only one kinematic element requires a fine surface finish. How-

ever, before this is discussed, some background on the details of surface finish effects is necessary.

After a coupling has worn in, this affect has been found to be on the order of 1/3 μm Ra (Slocum, 1992a). However, during the first few mates of a coupling, the surfaces are not worn-in and one can expect, as a worst case scenario, that the repeatability of the coupling to be approximately equal to half the waviness spacing, λ, of the surface. This is explained with help from Fig.4.9 and some simplifying assumptions.

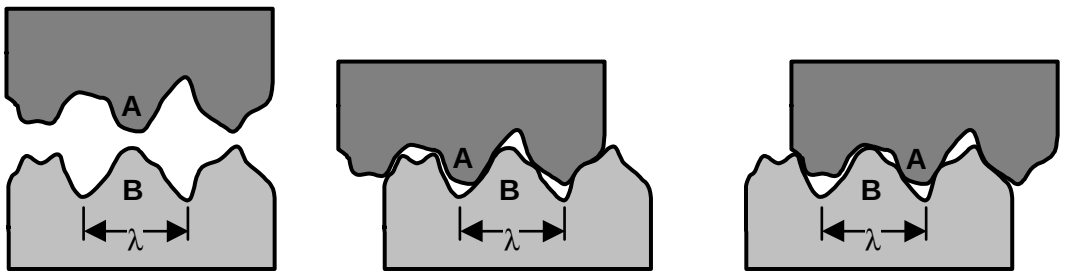


Figure 4.9 Rough Model Of Surface Finish Affects on Couplings

A general rule of thumb is that the roughness profile height, or peak-to-valley height, is about 4 times the measured average surface roughness (Oberg, et. al., 1992). This is a rough simplification, but we make it for convenience in illustrating the following point. If we assume the waviness spacing is approximately the same value, then the relative position of A and B in Fig.4.9 will vary between +/- $\lambda/_2$. We say that this is approximately the error in coupling repeatability due to surface finish affects. So the surface affects on the early cycle repeatability of a coupling can be estimated as:

$$\frac{\lambda}{2} \sim Repeatability \sim 2R_a \tag{4.13}$$

Therefore, if we are looking for sub-micron repeatability, the surface finish of the part should be less than 0.5 μmRa. This is the same as an average ground or roughly lapped

surface. The above is a rough estimate, but a designer can follow the same procedure given their specific surface topography.

Regardless, attaining fine surfaces with a machining process is very expensive. In the QKC, this is accomplished by another, less expensive means, a three step burnishing process of the contacting surfaces. Figure 4.10 shows an example trace of a QKC target surface as burnished after this process.

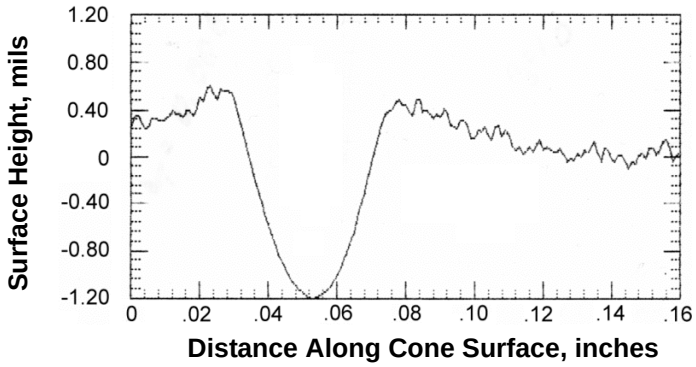


Figure 4.10 Profile Trace of Burnished Quasi-Kinematic Coupling Groove Surface

Stage 1: Elastic Deformation

In the first stages of burnishing, the contacting asperities deform elastically. Generally, these deflections are very small compared with the plastic deformation required to "smash" the asperities flat. In our analysis we will assume the deformations from this step are negligible. This assumption can be checked by modeling the asperity contacts as herztian contacts.

Stage 2: Plastic Flow Due to A Normal Force (From Johnson, 1985)

In stage two, significant plastic flow is seen as the result of a normal load. Through the use of plastic slip line theory with the models of Fig.4.11 and Fig.4.12, one can estimate the shape of the surfaces after the initial impression. This model assumes a flat, rigid

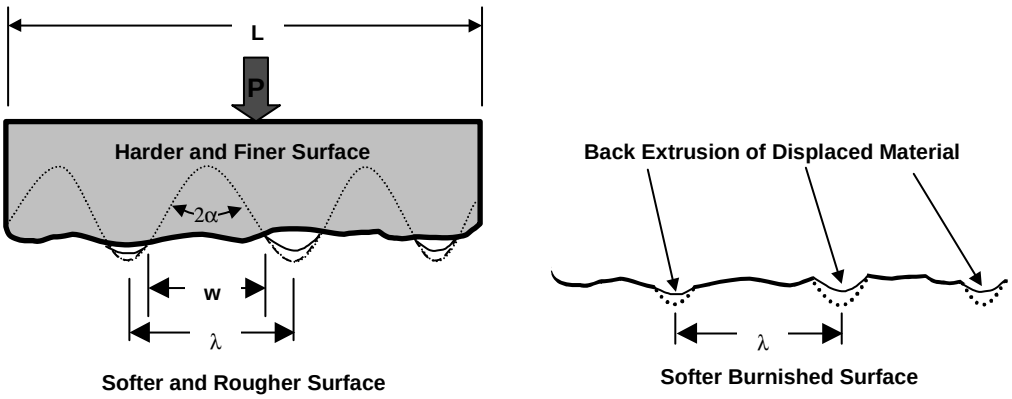


Figure 4.11 Model For Analyzing Surface Asperity Deformation Due To Normal Loads

indentor, plain strain conditions, perfectly plastic material, a periodic rough surface, and peak-to-valley height h_o. The asperities are modeled as two dimensional pyramids with a half included angle, α. For our purposes, we will estimate this angle as 65^o.

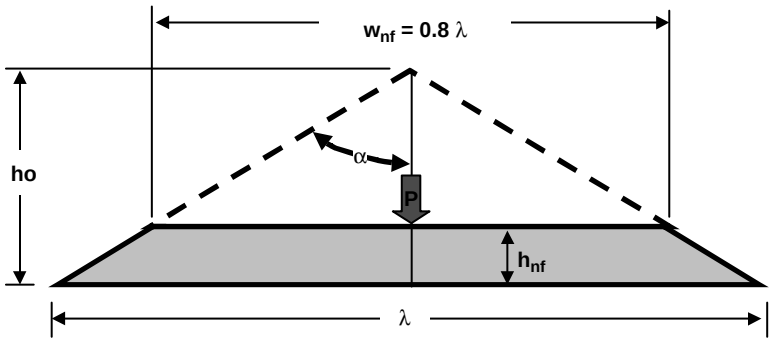


Figure 4.12 Simple Model of Asperity Before and After Deformation

Under load, the rigid indentor forces the asperities to comply. As a side note, the material will back extrude as shown, but exaggerated in Fig.4.11, effectively reducing the error causing surface features. Plastic deformation of the asperity will continue until the crushed width of the asperity, w_{nf}, reaches 0.8 λ. At this point, the normal pressure and interaction of the slip line fields from adjacent asperities are such that increased pressure will deform the sub-surface material, not the asperities. This is why asperities can not be

completely burnished by normal loads as was shown by Childs, 1973. At this point, the average pressure, $\bar{p}$, on the rigid indentor has been found to be 5 k where k is the yield stress in simple shear. This can be used to find the required burnishing load or average pressure, p, between an asperity and the indentor surface.

$$\bar{p} = \frac{P}{L} \approx \frac{p}{2k} \frac{w}{\lambda} \tag{4.14}$$

$$p \approx \frac{2k\lambda P}{Lw} = \frac{2k\lambda \bar{p}}{w} \tag{4.15}$$

Figure 4.11 illustrates the results of the surface before and after the second stage of burnishing. The author calculates the ratio of the final to initial asperity height, $^{hnf}/_{ho}$, to be approximately $^{1}/_{5}$. At this point, the usefulness of increasing the normal force to remove asperities has ended. Further deformation can only occur in the presence of a tangential traction or tangential displacement.

Stage 3: Plastic Flow Due To Normal & Tangential Traction (From Johnson , 1968)

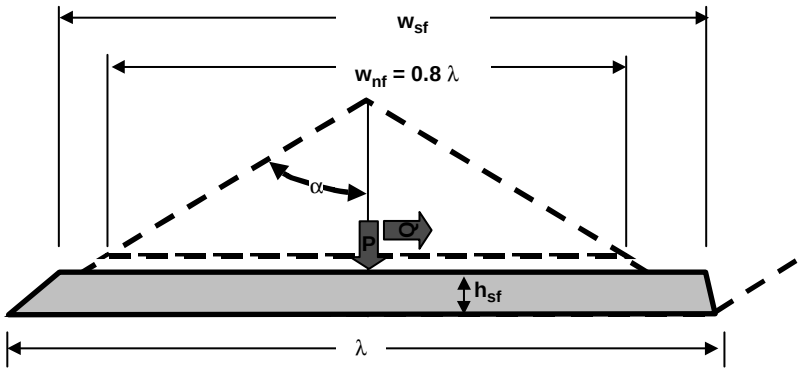


Figure 4.13 Plastic Deformation From Normal and Tangential Traction

In the third stage, we start from the final state of loading in stage 2. As stage three begins, a different slip line field emerges as a tangential traction begins to pull material from the asperity to the side, much like a knife smearing peanut butter. The "smearing" can be seen

on the right side of Fig.4.13. This model maintains the assumptions of a flat, rigid indentor, plain strain conditions, and a perfectly plastic rough surface, but two additions are made. First, it is assumed that there is no slip at the interface between the rigid member and the asperity. Second, the normal load, P, remains constant at the same value as in stage 2.

At this point, our analysis will break with Johnson's analysis and look at the remainder of the problem from a practical standpoint. Before we do so, the reader should realize that we have traveled this far to show that further deformation via tangential loading is possible. Johnson's method can be used to find a good approximation to continued asperity deformation, but this level of detail is not required.

We will assume that the tangential deformation required to entirely flatten the asperity is roughly 20% of the asperity spacing, λ, which is all that is left. Remember the top, w_{nf}, is already 80% as wide as the bottom, λ. If we maintain the no slip condition at the contact interface, the relative movement between the contacting elements need only be approximately 20% of the asperity spacing to work the asperity to a point where $w \sim \lambda$. In looking at QKCs, $0.2\ \lambda$ is about 0.5 - 5 microns, which is much less than KC preload displacements. This is several orders of magnitude larger the preload displacements which are often 100 - 300 microns. It is then quite reasonable to assume that the relative sliding between the kinematic elements provides the necessary means to finish the burnishing.

If the no slip condition is violated, i.e. due to unwanted lubrication, then the ability of the sliding contact to finish flattening the asperity will be diminished. This is a reason for avoiding lubrication of QKC elements during the first couple mates, i.e. the wear-in period. Regardless, even without sliding deformation, the increase of w to $0.8\ \lambda$ achieved by the normal indention, including the back extrusion, provides some filter for surface effects.

4.6.2 Affects of Localized Plastic Deformation on QKC Performance

The Consequence of Interrupted Contact

Depending upon the end conditions of a line contact, the local stress state can decrease, increase, or become theoretically infinite. Unfortunately, QKC joints exhibit the third behavior, which leads to gross local plastic deformation. This happens at the edge of a contactor flat where the contactor & target lose contact. At this location, one surface ends in a sharp corner, while the other has a continuous profile. If the constraints of the process/application allow, the sharp edge can be rounded by secondary processing. If not, then we must deal with the deformation.

Gross Plastic Deformation in QKCs

In the context of a quasi-kinematic coupling, this is undesirable. This is best explained with the help of Fig.4.14 which shows a cross section of a QKC joint through the arc of contact. To start, the contactor is seated in an unloaded state. When the contactor is

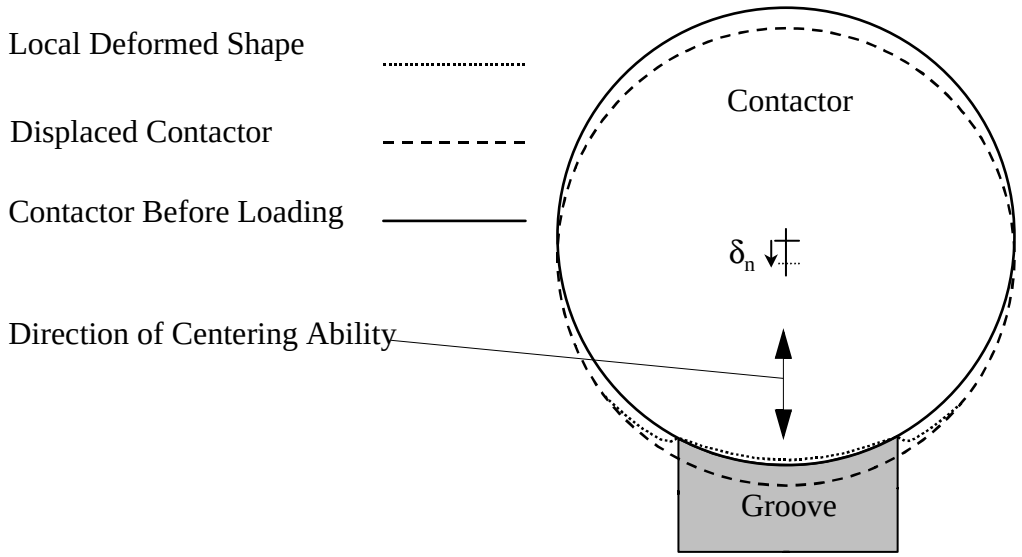


Figure 4.14 Simple Model of Edge Contact in Quasi-Kinematic Couplings

pressed or displaced into the groove, the edges of the groove flats will press into the surface of the contactor. As long as the contactor is made of roughly three to four times harder material than the target surfaces, the edges of the groove will be rounded off to some extent. When increasing load/displacement is applied, the contactor surface will begin to plastically deform as shown in Fig.4.15. This is undesirable as the high stress and sliding contact in these areas can make them prime sources for wear/particle generation.

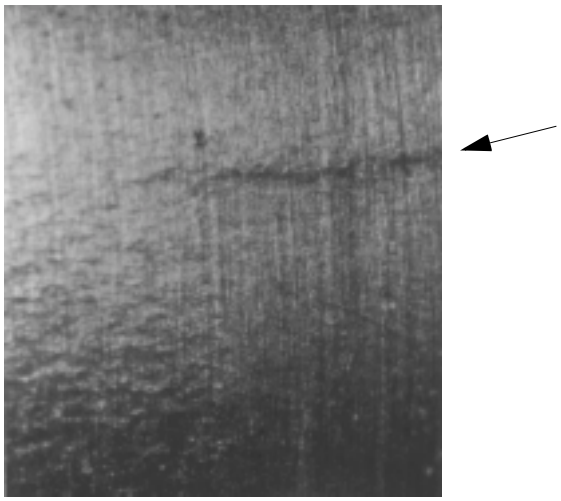


Figure 4.15 Deformed Contactor Surface, Cleaned For Viewing

This has been observed in the testing of QKCs. Silver bands were observed on the surface of the contactors which corresponded with the location of the edges of the target surfaces. This area is pointed out in Fig.4.16. These bands consisted of a fine aluminum powder which had worn away from the edges of the target surface. Once a coupling exhibited these symptoms, repeatability quickly degraded as additional wear particles were generated.

This has two negative effects. First, the introduction of wear particles between the contacting elements increases the friction between them. Accounting for the effects of friction in precision couplings is a notoriously difficult task, especially because friction is not

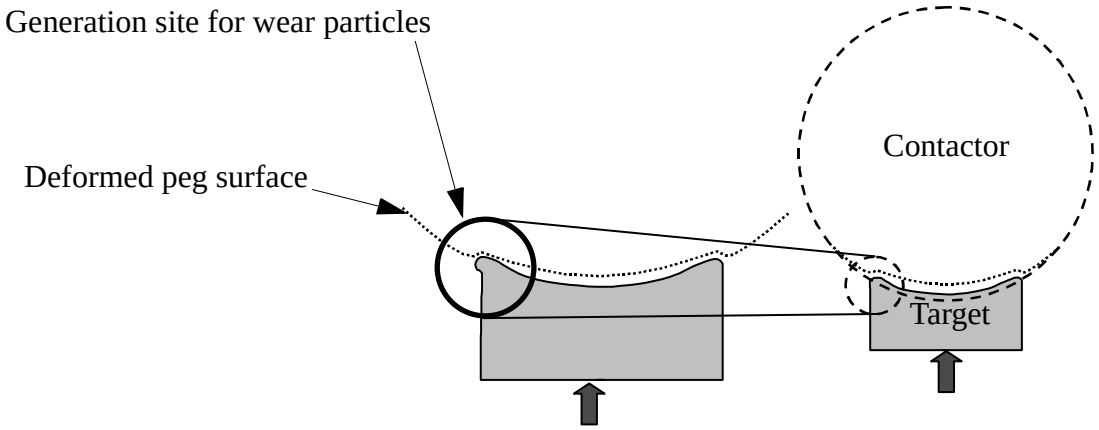


Figure 4.16 Location For Wear Particle Generation in QKCs

always constant. This situation introduces a variation in coupling performance which can only be determined by testing. As a designer, the author finds this most unpalatable!

The second effect is the error from the wear particles themselves. As with any coupling, contamination between mated surfaces ruins coupling performance. A reasonable estimate for the affects of wear particles on repeatability can be obtained by modeling the wear particles as asperities as discussed in Section 4.6.1. For instance, when a one micron particle comes between the contactor and target, a coupling error on the order of 1 micron can be expected. Regardless, this situation is to be avoided at all costs.

Quantifying the Limits of Plastic Deformation in QKCs

There are several problems in quantifying the limit for acceptable indentation. First, some means is needed to determine the shape of the kinematic elements as a function of load or displacement. Three dimensional FEA analysis of this problem is not a feasible solution as an incredibly fine local-mesh is needed to pick up the small deformations, approximately one to five microns, which we are looking for. This considered, the computational costs for a three dimensional model with the non-linear effects of friction, contact, and plasticity are extremely high.

In light of the above, three dimensional FEA analysis does not seem a practical solution. Despite this, a 3D FEA was attempted. Several unsuccessful attempts were made to obtain data from very coarsely meshed three dimensional FEA model. The model shown in Fig.4.17 shows three mesh densities which were tried, from fine to coarse, in attempting

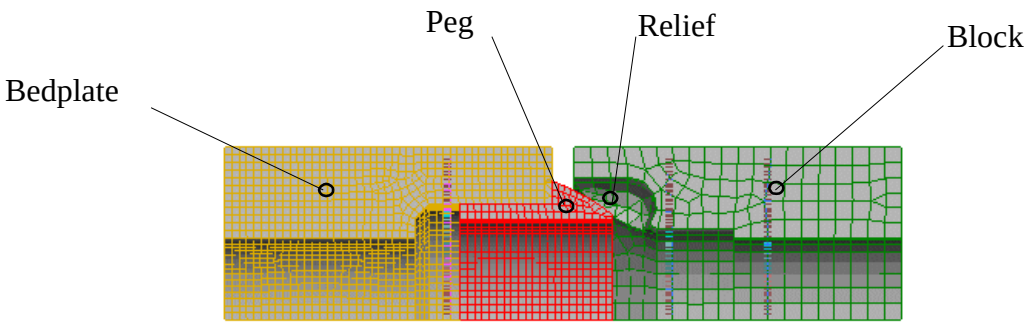


Figure 4.17 Side View of 3D FEA Mesh, Shows Examples of Mesh Densities Used in Finite Element Analysis, Symmetry of Model Allowed Use of 1/4 of Joint Geometry

to solve the problem. Note that all of these are far too coarse to capture the small features we are interested. On a high end computer, two FEA program failed to begin the analysis because sufficient memory was not available. Faced with these difficulties, the three dimensional FEA method was abandoned.

Instead, the small and inexpensive test fixture in Fig.4.18 was used to determine the limits

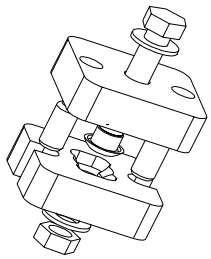


Figure 4.18 Quasi-Kinematic Coupling Plastic Deformation Test Fixture

on the QKC gaps. In one half, the fixture housed a QKC contactor, in the other, QKC target surfaces. These could be bolted together to simulate loading of a real QKC joint. Two dowel pins provide resistance to rotation between the components during testing. With this fixture, one can use shims to vary the distance between the mated halves, thereby obtaining a full range of test gaps.

Avoiding Local Plastic Deformation

If cost constraints permit, one should use a low modulus, high yield stress material, such as titanium for the contactors. The combination of these properties provides a wider range of strain before plastic deformation sets in.

With respect to geometry of the contactor in the case study, contact angles smaller than 120 degrees allow ovaling of hollow contactors, i.e. contactors with through holes for bolts. Figure 4.19 shows the arc of contact between the contactor and target surfaces as a

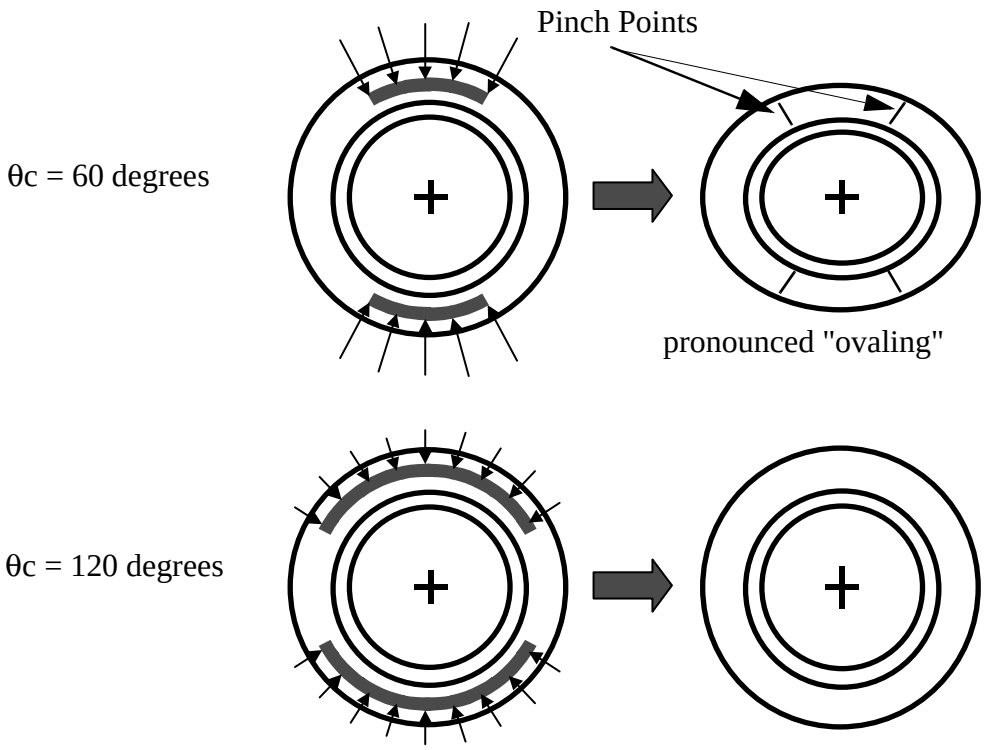


Figure 4.19 Axial View of Contactor, Effect of Contact Angle on Ovaling On Similarly Loaded Pegs

red line. The arrows signify the pressure loading on each arc. Unfortunately, when a con-

tactor "ovals," the target surface does not. This leads to pinching of the contactor at the edges of the target flats. The result is local plastic deformation on the contactor surface.

4.6.3 Load and Displacement Behavior of QKC Joints

Depending upon the gap between opposing faces of the mated components, the deformation in the kinematic elements can be elastic or elastic and plastic. This is important as the load-displacement behavior of the coupling is dependents upon the nature of the deformation. If the deformation is purely elastic, then the load-displacement plot will follow a curve with increasing slope. If the deformation is elastic and plastic, the slope of the curve will increase during the initial elastic deformation, then decrease as the material begins to flow plastically. This is due to the fact that the subsurface material can no longer provide as much resistance (per unit depth of penetration) as it could during the elastic deformation. In some cases, the plastic deformation extends beyond the contact interfaces, such that the bulk of the kinematic elements deforms plastically. Figure 4.20 shows the rela-

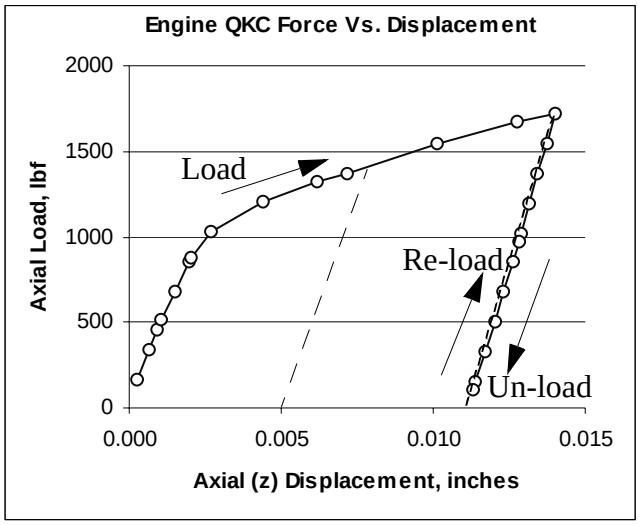


Figure 4.20 Axial Load-Displacement Plot for Engine QKC Joint

tionship between the displacement and axial force, i.e. along the cone axis of symmetry,

for the QKC joint used in the case study. The initial and final loading of the curve are not shown due to difficulties in obtaining the data.

What is important in designing QKCs is the "moment of mate" stiffness, or the stiffness at the instant the surfaces of the coupled components mate. This is the slope of the load-displacement curve at the instant the displacement equals the gap. Consider the following in the context of Fig.4.20. During the first mate, a joint being loaded will exhibit of the loading portion of the curve in Fig.4.20. When the coupling is "un-mated", the behavior will follow the "un-loading" portion of Fig.4.20. For subsequent assembly and disassembly of the coupling, the load-displacement behavior will follow the "un-loading" curve. This is illustrated by the "un-load" and "re-load" arrows in the figure.

4.6.4 Ratio of Contactor to Target Hardness

As discussed in Section 4.6.1, we wish to minimize the affects of surface geometry on coupling performance. When the contactor and target are pressed together, normally with no sliding, the surfaces of each material will deform and conform to each other. However, it has been shown (Suh, 1993) that if component *A* is approximately four times harder than component *B*, then the surface of A will not be affected by the geometry of surface B.

It is simpler and less expensive for manufacturers to obtain a better surface finish on the contactor. Section 4.7.2 discusses this in detail. Therefore, the ratio of contactor hardness to target hardness should be approximately four. Since the brinell hardness of metals is proportional to the tensile strength, this allows one to use the ratio of contactor to target tensile strength in place of the hardness ratio.

The ratio for the application in the case study is actually 2.5. Though lower than the ideal ratio of four, the affect of the target geometry, rougher and softer aluminum with $\sigma_y \sim 27$ ksi did not affect the surface of the contactor, with $\sigma_y \sim 72$ ksi. This may be due to the fact that the analysis upon which this ratio is based does not account for sliding contact. Sliding between the two components as discussed in Section 4.6.1 enhances the "flattening" of

surface asperities. Therefore, any deformation of the contactor surface may be hidden by this phenomena. It is fortuitous that sliding acts to help the cause.

This raises the question, "How low can the hardness ratio be?". To answer this, an analysis similar to that in Section 4.6.1 is needed which does not consider the harder element as infinitely rigid. The literature appears to be absent of such an analysis and it is beyond the scope of this thesis to provide one. Therefore, the designer should think of the hardness ratio as a guideline, or target to shoot for. If this is impractical, one can try a ratio of 2.5, or lower if the cost of prototyping and testing a test joint is allowable.

4.7 Manufacturing of Quasi-Kinematic Coupling Elements

The Quasi-Kinematic Coupling was developed for high volume manufacturing processes. Because each assembly needs 3 contactors and 3 sets of target surfaces, the means used to manufacture them must be able to make large quantities at low-costs. They must also be of sufficient quality to maintain a functional gap between the mated components. The following sections present an economical method for making the elements.

4.7.1 Manufacture of Target Surfaces

The "manufacturing equation" in Fig.4.21 shows a way to economically create target surfaces. The reliefs are manufactured first, preferably by casting/molding in their shape. It is possible to machine these features with an end mill or by spot drilling, but this adds more complex machining tasks and tooling to the manufacturing process. To make the groove seats, a form tool is used to machine a hole which is coaxial with the outer contours of the pre-cast reliefs.

There are several benefits to this method.

- **Clamping** - It provides a through hole for a bolt which can be used to apply the clamping load.
- **Retrofitting existing pinned joint processes** - Retrofitting an existing pinned joint is made easy as the reliefs can be placed coaxial with the loca-



Figure 4.21 Method For Inexpensive Manufacture of Target Surfaces

tion of the old dowel holes. A form tool similar to the one in Fig.4.21 is then used in place of the old tooling which formed the dowel hole. This type of form tool is compatible with most standard tooling holders, so tooling changes are minimal.

4.7.2 Manufacture of Contactors

An inexpensive way to manufacture small, axisymmetric parts is to use screw machines. It is not atypical for screw machines to produce millions of a particular part per year for pennies apiece. This is particularly impressive when considering the size tolerance on these parts can be +/- 10 microns.

Figure 4.22 shows an example of such a piece made for press fit into the components of a Quasi-Kinematic Coupling. Note the through hole which allows for placement of clamp-

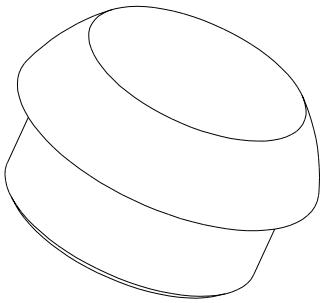


Figure 4.22 Spherical Peg For Press Fit in Quasi-Kinematic Couplings

ing bolts. ***This is important as clamping loads should be placed directly over the kinematic joints to avoid excessive rocking of the components before the mating.*** If this is not avoided and there is a large coefficient of friction, or if the edges contact via burrs between the mated surfaces, one could clamp in an error during mating. Typically, however, for clean surfaces with coefficients of friction less than 0.5, the stiffness of the quasi-kinematic coupling joints will resist these forces, and pull the coupling into its most stable equilibrium. Regardless, friction is an unreliable variable in design, so one should be safe and design the clamping loads coaxial or in the closest proximity to the QKC joints.

If the clamping means is not bolted joints, then another inexpensive way to produce contactors is to use ball bearings. These items are inexpensive and can be purchased in large quantities from bearing manufacturers.

4.7.3 Feature Size and Placement Tolerances

Within a pinned joint pattern, if the axes of a mating dowel and hole pair is off by more than the clearance, it is nearly impossible to assemble the coupling. Quasi-Kinematic Couplings do not have this problem as it is easy to fit a convex part into a conical groove with a little mismatch. After applying a certain load, the mating members are forced to conform during the initial deformation. Thus the Quasi-Kinematic Coupling is a form-in-place coupling. In comparison, pinned joints are incapable of eliminating initial misalignment. Depending upon the application, the tolerance range for QKC placement can be a factor of two to three times wider than pinned joints. The limit is set by the formation of indentions on the pegs surface as shown in Fig.4.15.

A clever designer will realize that it is possible to place a substantial portion of the joint's precision in the contactor. This is desirable as most high volume manufacturing lines can hope to hold at best +/- 25 to +/- 50 microns tolerances, while screw machines can easily hold +/- 10 microns. Manufacturers will generally find it beneficial to purchase these pegs from screw machining companies rather than run their own machines. As such, assigning tighter tolerances to the component made on the screw machine enables the designer to

specify wider tolerance ranges at the manufacturers factory where it is most needed. This is especially important in light of tool wear which will happen at the factory, and must be considered.

4.8 To QKC or Not To QKC?

In comparing the Quasi-Kinematic Coupling to a pinned coupling, one might say that the moderate complexity of the analysis needed to design the QKC does not justify the change from pinned joints because pinned joints are "so much easier" to design.

For some designs this may be true, for instance if only 250 microns (0.010 inches) repeatability is required, it is much easier to design, implement, and manufacture the pinned joint. On the other extreme, if 5 micron repeatability is required in a high volume application, the design, implementation, and manufacturing costs associated with the QKC will probably be much lower than the pinned joint. There would seem to be a fuzzy boundary on either side of which the use of one type of coupling is best. This is illustrated in Fig.4.23.

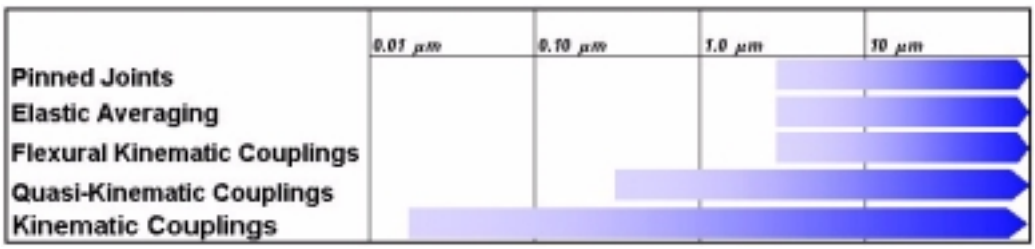


Figure 4.23 Practical Performance Ranges For Common Couplings

Drawing an absolute line in Fig.4.23 to mark the best range for each type of coupling. Common sense will tell us the choice will depend on many factors. For instance:

- Repeatability requirement
- Machine capability

- Materials
- Cost of the dowel pins vs. cost of contactors
- Cost of boring the dowel holes vs. cost of making the contactor surfaces
- Change in process
- Change in equipment
- Scrap/rework costs associate with poor alignment

All of these are highly dependent on application and machinery. It is up to the designer to set up the cost model to determine which joint will be less expensive to manufacture.

Chapter 5

CASE STUDY: ASSEMBLY OF A SIX CYLINDER AUTOMOTIVE ENGINE

This chapter demonstrates the analysis, design, and manufacturing of a Quasi-Kinematic Coupling via a case study of the precision alignment of automotive components. The chapter layout follows the design process presented in Chapter 4. We begin with problem definition.

5.1 Problem Definition

5.1.1 Application: The Six Cylinder Engine.

Figure 5.1 shows a fully assembled six cylinder automotive engine. This engine is manufactured in large volumes, typically in annual quantities of 300, 000 units, and is a fair rep-



Figure 5.1 2.5 Liter Six Cylinder Engine

resentative of the next generation of automotive engines. For example, to reduce the

weight of the engine, the block and most other large components of the engine are made from cast 319 aluminum. In addition, many of the parts and subassemblies in this engine are manufactured to race engine tolerances (Minch, 1999a). Of these, the most critical and difficult to machine is the crankshaft-journal bearing assembly.

5.1.2 Main Journal Bearing Assembly

A cross section of this assembly is shown in Fig.5.2. In virtually all automotive engines, the assembly is the same. The crankshaft resides between two main journal bearing halves

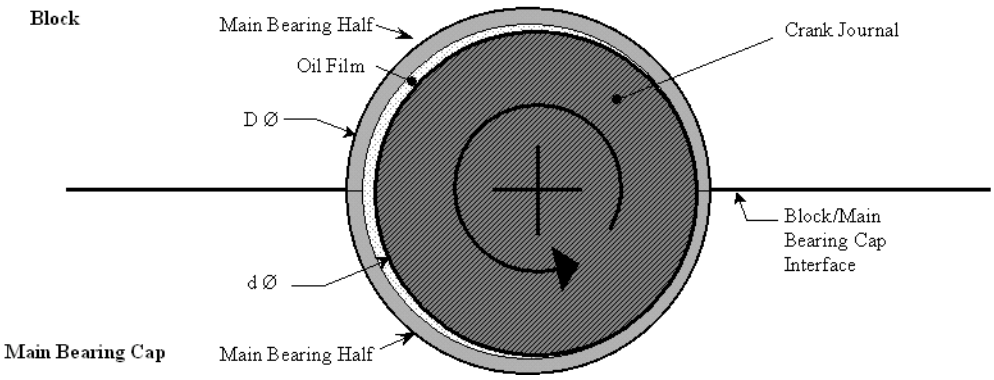


Figure 5.2 Cross Section of Typical Journal Bearing Assembly

with clearance on the order of 0.002". During operation, the rotation of the crankshaft induces a pressure profile in the bearing which acts to separate the crankshaft from the bearings. The crankshaft then rotates within the bearing halves on a film of oil. Misalignment between the main bearing halves has detrimental effects on the performance of the bearing. Some affected characteristics include:

- Decreased load capacity - The ability of the pressure film to maintain the gap between the bearings and the crank shaft can decrease with increasing mismatch.
- Increased coefficient of friction - If the mismatch is large enough, the gap between the bearings and the crankshaft could become very small or even close. This could lead to boundary lubrication for which the coefficient of friction can be an order of magnitude larger than hydrodynamic lubrication

(Heywood, 1988). Additional energy is required to overcome the increased friction, which in turn leads to lower gas mileage.

- Increased wear - If the mismatch is large enough to close the gap, direct metal to metal contact will lead to wear.
- Seizure or fatigue failure - An increased bearing coefficient of friction leads to overheating of journal bearings. This in turn can lead to thermal fatigue or in extreme cases, the bearing can seize (Shigley and Mischke, 1989).

In automotive engines, an analytic solution for the relationship between these quantities and the misalignment is not known. This is due to the complexity of the fluid dynamics which govern the pressure and velocity profiles in the bearing. In these bearings, the flow is typically turbulent, the bearing geometry is eccentric, and the bearing is dynamically loaded. Some software packages are available for dynamic journal bearing analysis, however results from the best of these packages compare poorly with experimental data (Brower, 1999). Sadly, experimental misalignment data for this engine is not available for publication. What can be said about the affects of misalignment on this engine's bearing performance is summarized in Table 5.1.

TABLE 5.1 Qualitative Effect of Bearing Centerline Misalignment

Misalignment	Affect on Bearing Performance
0 - 5 microns	Low
5 - 10 microns	Moderate
Over 10 microns	Severe

5.1.3 The Need For Repeatability

Main bearing halves are made from very soft materials, usually babbit, thus they conform to the shape of the elements into which they are pressed. In this engine, the block and bedplate house the halves of the main journal bearings, so misalignment of these components becomes the "precision problem". Ideally, no mismatch between the journal bearing center lines is desired, but practically some will exist due to manufacturing and assembly errors. Figure 5.3 shows the components disassembled, Fig.5.4 shows a partially assem-

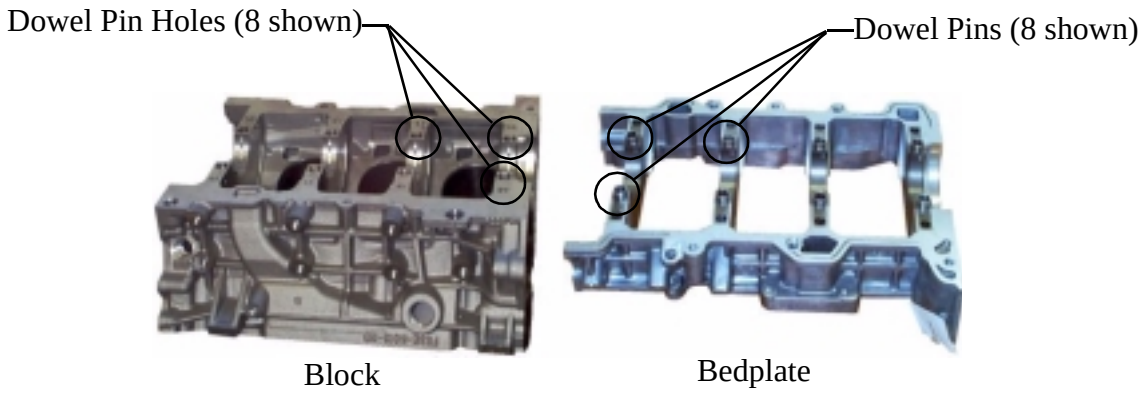


Figure 5.3 Block and Bedplate Components

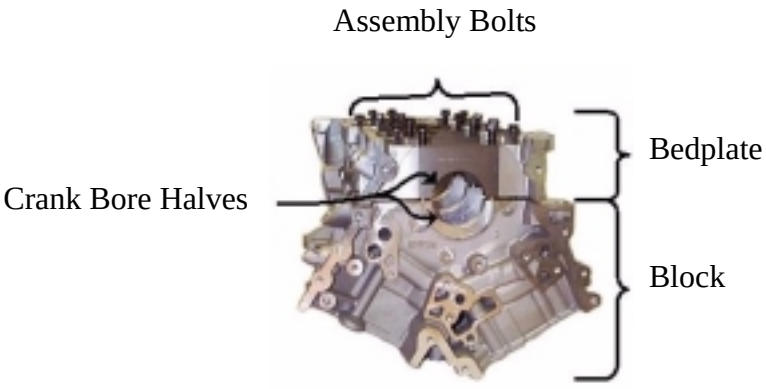


Figure 5.4 Six Cylinder Block - Bedplate Assembly

bled block-bedplate pair with the crankshaft and main bearings removed for clarity, and Fig.5.5 shows the full block-bedplate-crankshaft assembly.

Because the half bore sizes and alignment are critical, it is best to manufacture them simultaneously. Presently, the block and bedplate are aligned via the eight hollow dowel pin joints shown in Fig.5.3 and clamped together with eight bolts which are coaxial with the pinned joints. The crank bore is then simultaneously bored into each component. Afterwards, the block and bedplate are disassembled, the crankshaft and main bearings are put in place, then the two components are reassembled. Maintaining alignment of the half

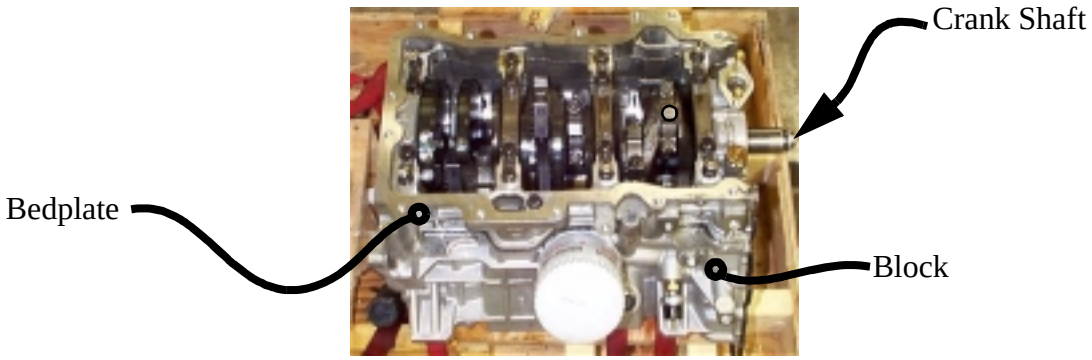


Figure 5.5 Block and Bedplate Assembled With Crankshaft and Main Bearings In Place

bore center lines with respect to their freshly machined position is the need. Due to relative rotation and translation, the maximum center line mismatch will occur at either of the outer journals. The error, δ_e, is illustrated in Figure 5.6.

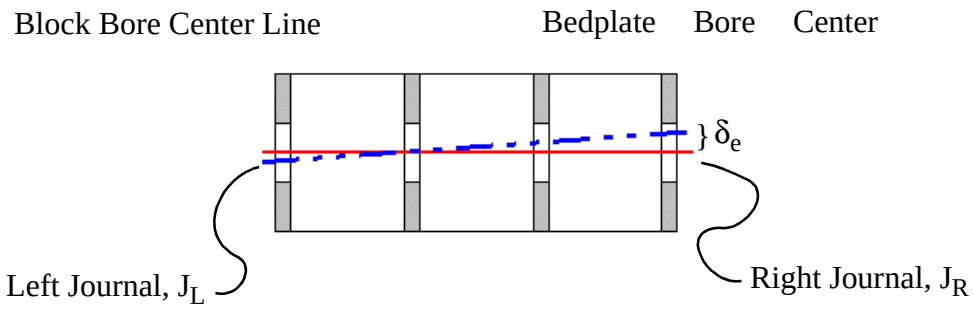


Figure 5.6 Center Line Error Between Block and Bedplate

5.1.4 Rough Repeatability Error Budget

There are several sources of error which contribute to the centerline mismatch.

- Relaxation of residual stresses during operation
- Geometry changes of the components due to thermal effects during machining
- Geometry changes of the components due to removal of residually stressed material
- Error loads between the block and bedplate

Relaxation of residual stresses during operation has recently been shown to be a problem. This is not a major concern for the bearing center lines unless the engine is disassembled after considerable running time. Before disassembly, friction between the block and bedplate surface prevent significant movement of material surrounding the crank bores. After disassembly, this constraint is removed and the components can change size. There is no database of such measurements in the vicinity of the crank bore, but limited measurement of other areas of the engine have shown up to 75 microns movement (Minch, 1999a). There is little a practical mechanical coupling can do to correct this. Determination of an exact value for errors due to relaxed stresses is beyond the scope of this thesis, but further research by the manufacturer is strongly recommended.

A limited database of in-factory measurements has shown the cumulative effect of geometry changes due to machining of residually stressed materials. This error seen in the location of the half bore center lines has been measured at approximately 5 microns (Minch, 1999a). Considering these facts and Table 5.1, this leaves little room for error from a mechanical coupling. Given that the present pinned joint coupling is at best capable of 4.9 micron repeatability, one can expect the effect of the total misalignment on bearing performance to be near the severe level shown in Table 5.1.

5.2 Constraints

As this was a retrofit application, there were many constraints imposed on the design.

Cost - An increase in coupling cost per engine was not allowed. The new coupling had to be less expensive than the pinned coupling.

Manufacturing - The new method had to be implemented with minimal change in the transfer line's core machinery. This included spindles, machine tools, fixtures, and anything else which would require a large capital investment to alter.

Joint location and size - The new coupling was constrained to fit within the footprint of the pinned joint pattern. The joints themselves were constrained to be located at positions previously occupied by the pinned joints. With respect to joint size, the new joints had to fit within the footprint of the old joint plus a small margin of safety, roughly 0.030" on the diameter. This was necessary as the transfer line was designed around "knowing" that pins of certain size would stick out of the bedplate surface at certain locations. Using joints of different size or at different locations from the dowel pins would result in interference problems.

Loose pieces - The engine components are flipped several times during the manufacturing process to bare different surfaces for machining. This eliminates the use of any loose pieces in the coupling. For instance one could not use ball bearings with through holes for the contactor in the coupling.

Material / Material Treatment - The material and heat treatment of the block and bedplate were not subject to change.

5.3 Functional Requirements

The functional requirements of the design were to:

Repeatability - Minimize the bearing centerline mismatch. A range of acceptable solutions exists from 0 to 5 microns.

Mating of Opposed Faces - The opposing faces of the block and bedplate needed to mate with a certain contact pressure. This actually translates into the percentage of bolt load which is dedicated to compressing the joint. The change in this percentage was not to exceed 25% from the initial loading of 11,000 lbf per bolt (Yerace, 1999). Strictly speaking, the functional requirement is: Maintain 8300 lbf in the bolt after mating of the coupling.

Fatigue - Prevent fatigue of the engine components before and up to the normal lifetime of an engine.

5.4 Gap

The iterative solver illustrated in Appendix A was used to find the minimum θ_c and corresponding coupling element dimensions. The goal of the iteration was to find the minimum θ_c, which could provide a plausible solution. This approach was taken to maximize the lateral stiffness, minimize the axial stiffness, and reduce the stress at the coupling interface. Several constraints, i.e. joint footprint, were placed on the size of the QKC elements which forced the solver to converge to the nominal values given in Table 5.2

TABLE 5.2 Nominal Dimension and Associated Tolerances for QKC Kinematic Elements

Dimension	**Nominal mm (inches)**	**+/- Tolerance mm (inches)**
VD	-12.59 (-0.4955)	+/- 0.08 (0.0030)
O_{SRz}	3.05 (0.1202)	+/- 0.01 (0.0005)
z_{BF}	0.00 (0.0000)	+/- 0.03 (0.0010)
O_{SRr}	-1.92 (-0.0757)	+/- 0.01 (0.0005)
θ_{cTool}	32 deg	+/- 0.01 deg
θ_{cWear}	N/A	+ 0, - 0.01 deg
R_s	10.04 (0.3951)	+/-

Using these values and Equation 4.4, the characteristics of the gaps were calculated and tabulated in Table 5.3.

TABLE 5.3 Quasi-Kinematic Coupling Gap

Minimum mm (inches)	**Nominal mm (inches)**	**Maximum mm (inches)**
0.03 mm (0.0013)	0.20 (0.0077)	0.36 (0.0143)

As an exercise in understanding, if we consider the sensitivity of the gap to the angle θ_c, it can be seen from Fig.5.7, that the solver sought a solution until the sensitivity of the gap

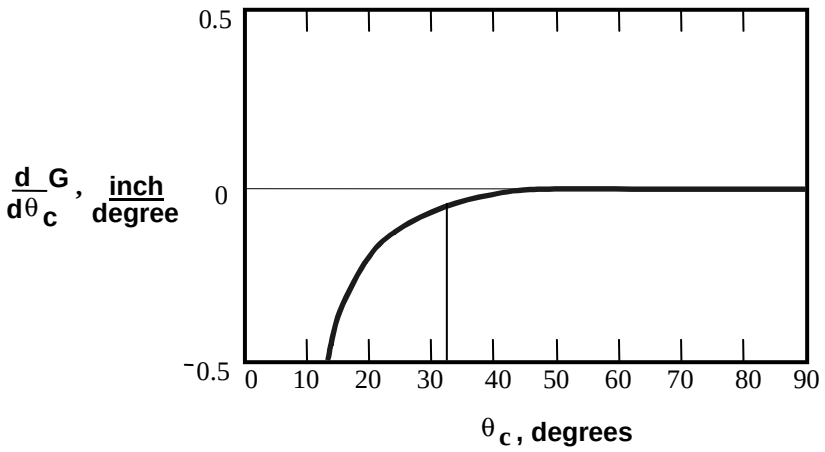


Figure 5.7 Sensitivity of Nominal Six Cylinder Engine QKC Gap to θ_c

began to increase, stopping before the magnitude of the sensitivity became too large.

5.5 Joint Location and Orientation

5.5.1 Review of Sensitive Directions

The sensitive directions are the rotation about the z axis and the direction perpendicular to the bore centerline and in the plane of mating. Both of these contribute to the error between the center lines of the bearing half bores.

5.5.2 Error Loads

When this Quasi-Kinematic Coupling is clamped down, friction between the bolt heads and the bedplate can cause errors in the alignment of the coupling. The coupling must be stiff enough in the sensitive directions to prevent error loads from resulting in displacement greater than the desired repeatability.

The loads acting to produce errors in the sensitive directions are:

- Friction torques between the bolt heads and the bedplate
- Forces parallel to the plane of mating, i.e. parallel to the x-y plane

These are estimated using a conventional bolt head friction model. The coefficient of friction used for steel on steel (Avallone et. al., 1996) was 0.8.

TABLE 5.4 Error Loads on Six Cylinder Assembly

Parameter	English	Metric
Maximum Bolt Load	2300 lbf	10 kN
Total Friction Torque	60 ft-lbf	80 N-m
Total Engine Side Load Varies direction as wrench rotates	60 lbf	260 N

5.5.3 Joint Location/Orientation

To provide maximum resistance to motion due to the friction induced torques between the bolts and bedplate, the joints are positioned such that they form the largest triangle possible. Note the ideal place to put the joints would be on the outer perimeter of the engine, as explained in Section 5.2, the location of the QKC joints was constrained to be coaxial with the pinned joint locations.

The coupling target surfaces were oriented as illustrated in Fig.5.8 and Fig.5.9 to maximize the centering ability and stiffness of the coupling in the sensitive direction.

5.5.4 Coupling Stiffness

The methods described in Chapter 3 were implemented via a finite element analysis, discussed in Appendix C, and a MathCad^{TM} worksheet discussed in Appendix B.

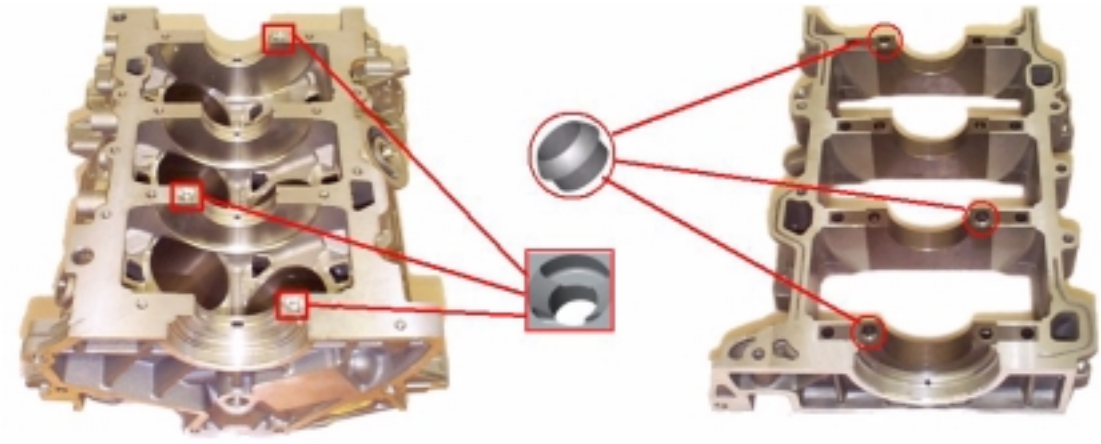


Figure 5.8 Position of QKC Joint in Six Cylinder Engine

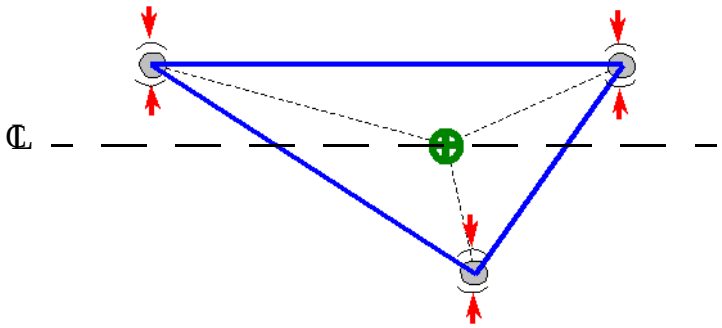


Figure 5.9 Orientation of QKC Coupling Joints To Maximize Repeatability In Sensitive Direction

5.6 Functional Requirement Tests

Repeatability - The average repeatability of the coupling was found to be 0.65 microns in the sensitive direction and 1.35 microns in the axial or non-sensitive direction. More detail is provided in Section 5.8.

Fatigue - Fatigue and durability testing is currently scheduled to be completed by the manufacturer's engineers, but sadly not before this thesis is finished. This is troublesome to the author, as the information from these tests was required do a proper analysis of the

fatigue characteristics of the joint. However, the designer takes some confidence in the following:

- Prototype Car - One prototype has been integrated into a functioning test car. The car has over 30, 000 miles of normal use and exhibits no problems.

The issues with respect to fatigue in this engine are not a trivial "plug and chug" problem. First there are the residual stresses in the castings which are of significant magnitude to affect any mean stress fatigue analysis, ie. Modified Goodman. The author has seen the effects of these stresses first hand while sectioning pieces of the engine. Several times, loud popping noises were heard as cracks propagated throughout the casting from the saw blade kerf. On several occasions, this was accompanied by relative movement, across the crack, of $^1/_8$ inch to $^1/_4$ inch. It is safe to assume that the stresses required to resist these displacements in a large casting, close to 24" x 20" x 20", are not small. Determining these stresses and using them in fatigue analysis of these engines via analytic means is currently a research topic for the manufacturer. Unfortunately, this subject is very complicated and the research is still in its infancy. The author has recently become aware of non-destructive means for measuring sub-surface residual stresses. Unfortunately, data will come too late for incorporation into this thesis, but will be the subject of future research.

Another issue complicating the fatigue analysis is the superposition of time varying thermal loading and mechanical loading. There is very little information on this subject in the literature. The author found only one publication which shows that traditional methods used to analyze the fatigue in common automotive cast aluminums compare poorly with experimental results, particularly with superimposed time varying thermal and alternating mechanical loading (Bressers et. al., 1995). The publications further describes complications from strain softening and creep which occur over time. Unfortunately, this data is not available for the engine under consideration. The author has determined that any meaningful fatigue analysis will have to be obtained through experiment, or several Ph.D. dissertations. Though the experimental means is undesirable because it adds time and cost

to the design process, it seems to be the only method until more fatigue knowledge/data is available for this engine and its materials.

Though this problem has not been solved in this thesis, the author wishes to emphasize the fact that a working prototype was been built and is functioning fine after 30 000 miles. For an average trip of 20 miles, this is roughly 1500 thermal cycles. Though not a complete fatigue test, it adds some comfort to the design. The reader should also not forget the comparison of stress states between the threads in the block just below the QKC joints and the QKC interface.

Sealing of Opposed Faces - The force required to close the maximum gap was determined for the FEA analysis at 2300 lbf. The remaining load in the bolt dedicated to closing the gap is 11, 000 - 2300 or 8700 lbf, which is greater than required by the QKC design.

5.7 Verification of Plastic Deformation Range

It is necessary to ensure that the given geometry and material properties of the kinematic elements do not result in plastic deformation of the peg surfaces. As has been explained, there is a maximum gap beyond which closure of the gap will result in gross plastic deformation of the peg surfaces. For the geometry generated in Section 5.4, experimental testing found this gap to be 0.015 inches. This is comfortably above the maximum gap of 0.012 inches.

Figure 5.10 shows a trace of the cone surface along the *l* direction after the initial mate with the peg. Because the steel peg was harder than the aluminum groove, the surface of the groove was burnished. As the discussion in Section 4.6.1, covered this in detail based on data from this case study, the author will refer the reader to the previous discussion. The plot of the burnished surface is provided for those who may have skipped the previous section.

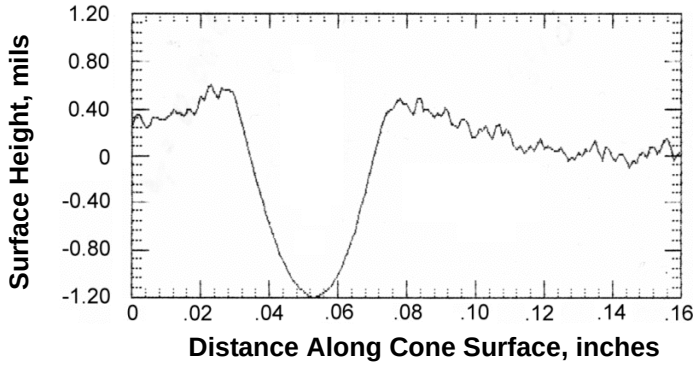


Figure 5.10 Profile Trace of Burnished Quasi-Kinematic Coupling Groove Surface

Ideally, following the reasoning of Section 4.6.4, one would like to have the ultimate strength ratio, or hardness ratio of the contactor/target materials to be about four. The ratio for this application is (72 ksi / 27 ksi) or about 2.5. Though lower than the ideal ratio of four, the affect of the target geometry (rougher and softer aluminum) did not affect the surface of the contactor. This may be due to the fact that the analysis upon which this ratio is based does not account for sliding contact. Sliding between the two components (as shown in Section 4.6.1 enhances the "flattening" of surface asperities. Therefore, any deformation of contactor surface may be hidden by this phenomena. It is fortuitous that sliding acts to help the cause. More expensive, hardened pegs could have been used, but the results of testing and the observation of the contactor surface show this was not necessary. The hardness ratio should then be thought of as a guideline, not a rigid requirement.

5.8 Testing and Performance Verification

5.8.1 Coupling Repeatability

The block and bedplate were assembled in a test stand as shown in Fig.5.11 and Fig.5.12. The bedplate and block fixtures were rigidly attached to their respective components. Relative movement between the block and bedplate was determined by measuring the movement of the bedplate fixture with three capacitance probes attached to the block fixtures. The entire assembly was mounted on a coordinate measuring machine which was used to

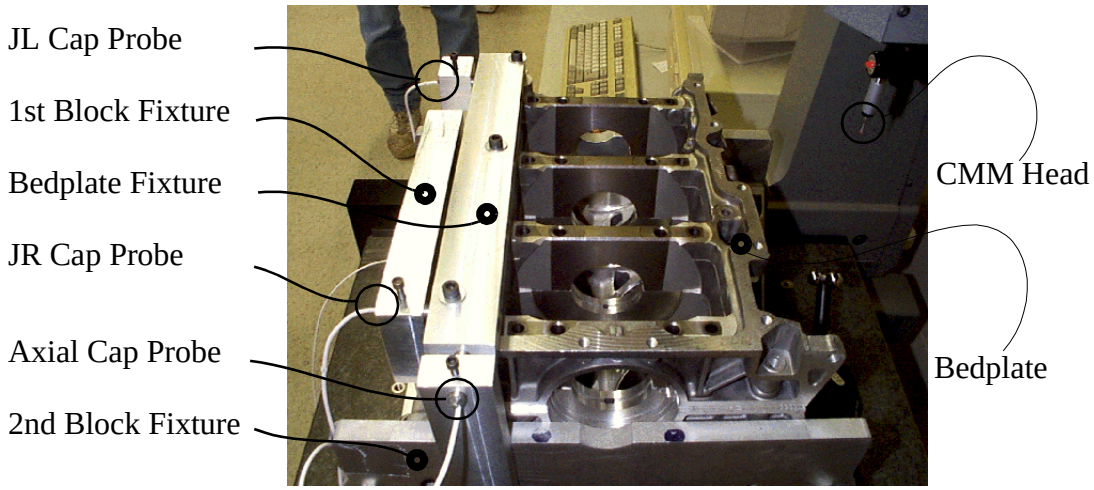


Figure 5.11 Top View of Test Setup For Six Cylinder Engine QKC

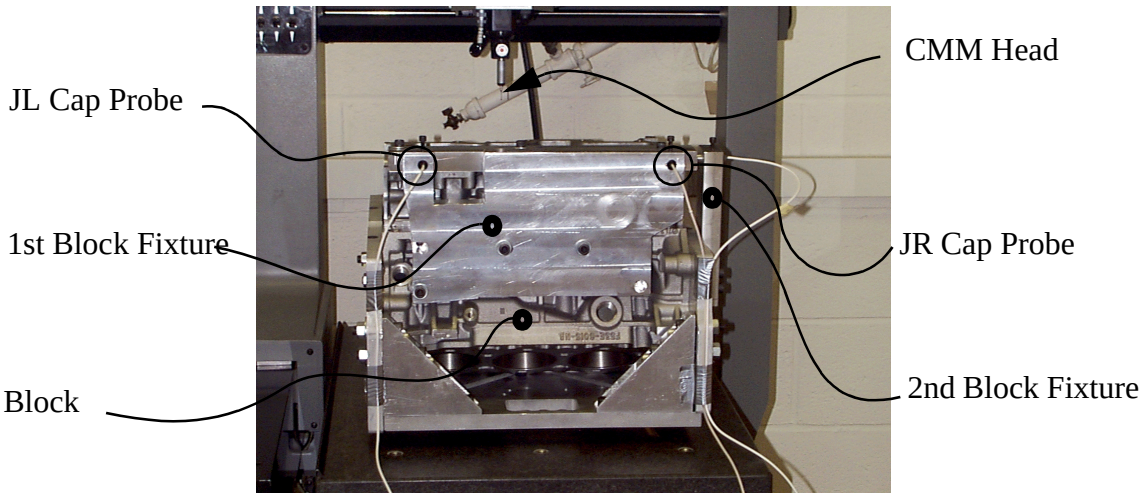


Figure 5.12 Front View For Six Cylinder Engine Quasi-Kinematic Coupling

measure the pre-mate and post-mate gap between the bedplate and block by measuring the height of the bedplate's top surface. Each mate, represented by a data point, involved bolting the components together, taking position readings, disassembling the components, reassembling them, then taking the final readings. Note that the resolution of the CMM and capacitance probes was five and 0.05 microns respectively.

Repeatability of the couplings is calculated by dropping the high and low readings, then dividing the maximum difference, or range, between the remaining data points by two. The repeatability in the sensitive direction at the JL and JR journals is 0.55 and 0.75 microns respectively, giving an average repeatability of 0.65 microns. The axial repeatability is found to be 1.35 microns. The difference in performance in the two directions is expected as the coupling uses a 120 degree groove seat which when orientated as shown in Fig.5.9 are 2.4 times more stiff in the sensitive direction than in the axial direction. Con-

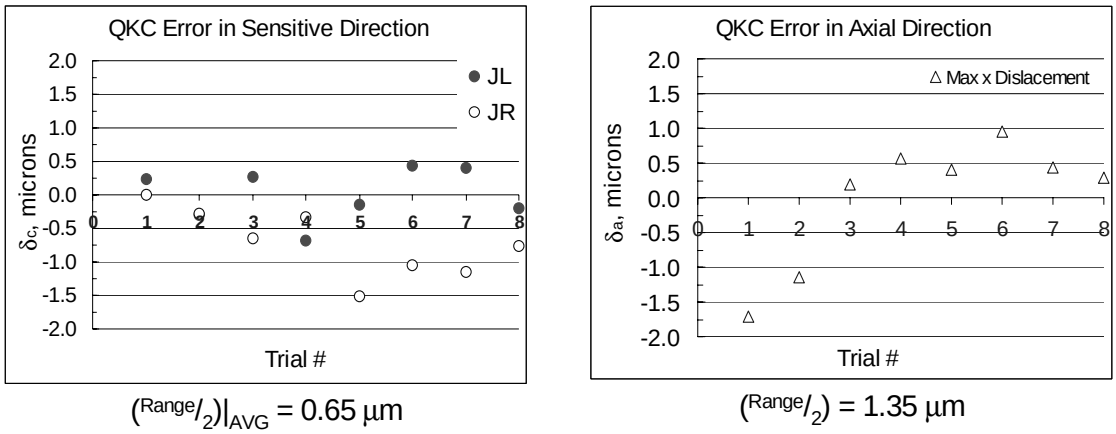


Figure 5.13 Repeatability Measurements For Six Engine QKC

sidering the application of error loads can take on random orientations, it is fair to compare the repeatability in the two directions by taking a ratio of the stiffness in the two directions.

$$\frac{Repeatability_{non-sensitive}}{Repeatability_{sensitive}} \sim \frac{K_r\big|_{sensitve}}{K_r\big|_{non-sensitive}} \tag{5.1}$$

The repeatability ratio is calculated as 2.1 which compares favorable with the in-plane stiffness ratio, 2.4. The difference can most likely be attributed to friction effects which can not easily be modeled.

5.8.2 The Affect of Contact Angle on Repeatability

As discussed in Section 4.6.2, small contact angles can lead to ovaling of the contactor, then plastic deformation at the pinch points. A test was run to determine the affect of contact angle on repeatability. Figure 5.14 shows the best angle for the QKC was 120

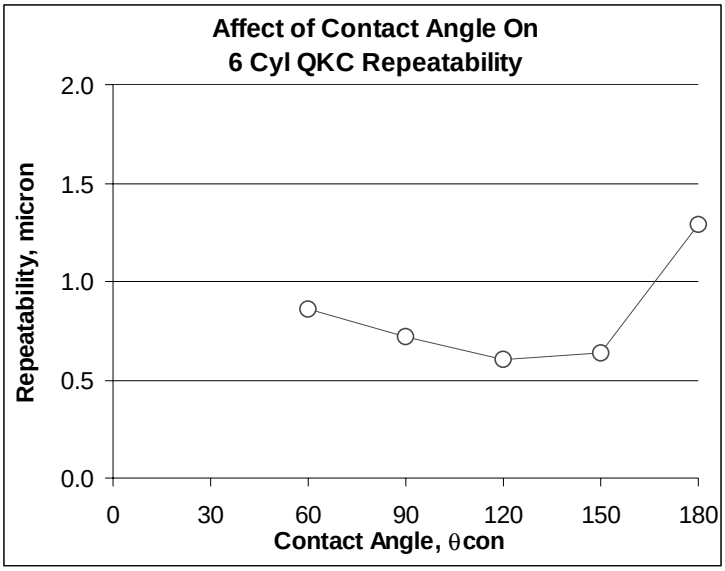


Figure 5.14 Effect of θc (shown as θcon) on Coupling Repeatability

degrees. It is fortuitous that at 120 degrees +/- 30, the repeatability does not vary significantly. This is important as the contact angle geometry will be dependent upon the ability of the casting process, which is not a precision process, to place the side reliefs. The loss of repeatability on the other end (150 - 180 degrees) is attributed to the inability of the coupling joints to adjust for misalignment between the three joints. The stiffer the joint, the more severe the effect on repeatability.

Clearly it is best to decouple the testing of joint misalignment and contact angle. This was done to the best of the author's ability. Precautions such as allowing the engine components to stabilize thermally over night and the use of a temperature controlled room were

taken. The patterns of the kinematic coupling joints in each component were measured with a CMM before mating. Those with close matching patterns were used in the contact angle study. This was a long and arduous process. Most of those which did not have close matching patters were used in the following study.

5.8.3 The Effect of Joint Misalignment on Repeatability

In this study, one of the coupling joints was moved a distance r, with equal components in the x and y directions illustrated in Fig.5.15. What is of interest here, is that one can mis-match a coupling joint by up to +/- 0.04 mm with little affect on coupling performance. This is nearly twice as wide as the tolerance allowed for misplacement of the pinned joint elements.

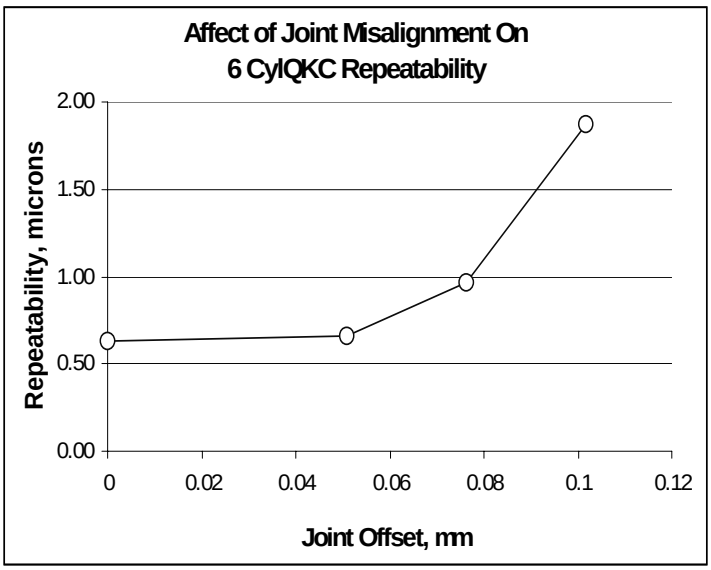


Figure 5.15 Affect of Joint Misalignment on Repeatability

5.9 Comparison of QKC and Pinned Joint Methods

5.9.1 Manufacturing Comparison

Figure 5.16 shows the basic operations of interest in the machining of the locating members in the pinned and QKC couplings. The only change needed to switch between the two designs is a tooling change from drill to the form tool, which fits in the same tool holder as the replaced drill, and the elimination of 13 of the 16 bored dowel pin holes. Note that three of the bored dowel holes were kept to accommodate the pegs.

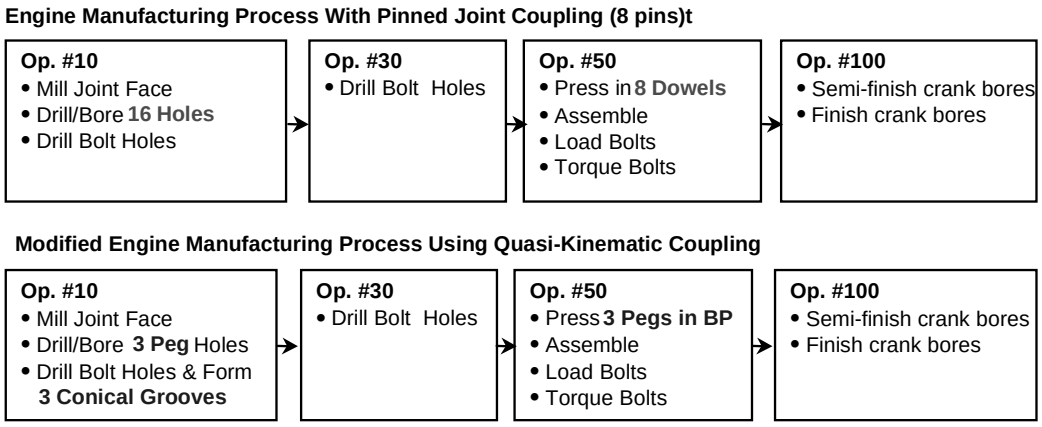


Figure 5.16 Comparison of Manufacturing Processes For Different Pinned and QKC Couplings

5.9.2 Design Comparison

A comparison of important characteristics and the performance of the pinned and QKC couplings is provided in Section 5.5. In all areas, the QKC out performs or has more desirable characteristics.

TABLE 5.5 Comparison of Six Cylinder Pinned and Quasi-Kinematic Coupling Designs

	QKC	**Pinned Joint**
Feature Placement Tolerance	+/- 0.08 mm	+/- 0.04 mm
Feature Size Tolerance	+/- 0.02 mm	+/- 0.02 mm
Precision Pieces	3	8
Boring Tools	3	16
Precision Features	3	16
Average Centerline Repeatability	0.65 microns	4.85 microns
Normalized Cost Per Engine	0.64	1.00

Chapter 6

SUMMARY AND FUTURE WORK

6.1 Implications of the QKC

6.1.1 Manufacturing

It is very satisfying to have developed a new technology which will change the way people think about precision high volume manufacturing. The two major implications of the Quasi-Kinematic Coupling are increased precision and wider manufacturing tolerances. To a designer or manufacturer, these are items for which a change for the better usually has a large influence on the bottom line. This was demonstrated for one application in the case study (Section 5.9) which has shown that the use of the QKC can provide near magnitude of order increased precision at substantially lower costs. In addition, the doubling of feature location tolerances in that application will enable the manufacturer to decrease scrap, rework, and the associated labor costs which plagued the use of the previous pinned joint.

6.1.2 Economic and Technological (Other Applications)

In a larger context, the quality of life and the economy in the Untied States are strongly dependent on the ability of manufacturers to produce quality goods at low cost. The author anticipates that there will be a large need for the QKC in areas which are highly dependent on precision, i.e. the automotive, aerospace, and machine tool industries. It is

difficult to estimate the affect on the economy, but the importance to the economy can be qualitatively understood by considering that these industries make up a substantial portion of the GNP.

The information storage industry may also benefit from QKCs. Portability of data, i.e. Zip Drives, DVDs, and CDs, has now passed from being a "nice feature of a product" to being a must. Would you buy a computer now without some form of portable media storage? Increasing storage needs will result in increase storage density and smaller feature sizes. The ability of the mechanisms to properly locate its internal components as well as the storage media to its receptor will become increasingly important. This opens the door for the Quasi-Kinematic Coupling.

6.2 Future Work

6.2.1 Plastic Line Contact

The ease of designing and analyzing a QKC would increase dramatically were there a general solution for plastic line contacts. The development of the plastic line contact theory is better suited for a thesis on mechanics of materials. As such, it fell outside the scope of this thesis, but the author believes it should be the first area of research in the extension of general QKC theory. The solution of such a process will reduce the time and effort spent on running finite element analysis. This can become quite costly given the iterative nature of the design process.

6.2.2 Displacement and Coupling Disturbances

This thesis has addressed the two major factors, shown in Fig.6.1 with check marks, influencing the performance of a precision coupling: momentum and geometric disturbances. Strictly speaking, though the analysis presented in Chapter 3, is displacement based, it is not meant to account for the motion of flexures and creep or thermal effects, therefore it

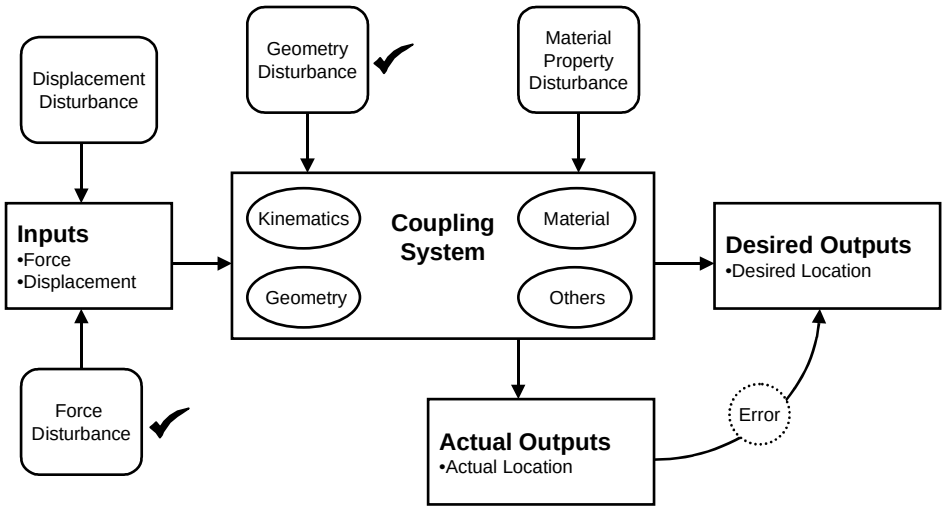


Figure 6.1 Model of a Mechanical Coupling System

does not address displacement disturbances. Material property disturbances also are not addressed as these tend to cover specific applications, and therefore fall outside the goals of this thesis. The determination of the affects of material property and displacement would be important to some applications where for instance the material properties of the coupling changed significantly with temperature. This might be the case in the alignment of journal bearings in jet engines, or the alignment of cryogenic components. As stated earlier, these would make interesting research topics, but the author does not anticipate the theory of these couplings to extend into these areas unless motivated by specific applications.

6.2.3 Metric For Degree of Over-Constraint

Quasi-Kinematic Couplings are not truly kinematic, but not grossly over-constrained either. A subject of future work would include a means to evaluate the degree of over-constraint. This is probably primarily dependent upon the contact arc length. Such a quantity would be useful as it could be used to quantify the limit to which a traditional kinematic coupling solution could be used. This would allow for a closed form solution to the analysis of some QKCs. For example, if the contact arc lengths were near zero, then

the direction of the contact force vectors could be approximated and a kinematic coupling solution could be performed.

REFERENCES

[Avallone et. al., 1996] Avallone, E. A., Baumeister, T., "Marks' Standard Handbook For Mechanical Engineers", McGraw-Hill, New York, NY, 1996, p. 3-23.

[Bressers et. al., 1995] Bressers, J., Remy, L., Steen, M., Valles, J. L., "Fatigue Under Thermal and Mechanical Loading: Mechanisms, Mechanics and Modeling", Proceedings of the Symposium Held At Petten, 1995, pp. 361 - 370.

[Brower, 1999] Brower, C., Conversation with Calvin Brower, Engineer, Ford Research Laboratory, Dearborn, MI, October, 13, 1999.

[Clark, 1996] Clark, T. R., Herman, W. A., Hertzberg, R. W., Jaccard, R., "A Technical Note. Influence of Mean Stress on Fatigue in Several Aluminum Alloys Utilizing $K_c$max Threshold Procedures", Fatigue and Fracture of Engineering Materials and Structures, Vol. 19, No. 7, 1996, pp. 949-954.

[Childs, 1973] Childs, T. H., "The Persistence of Asperities in Indentation Experiments", Wear, 1973, pp. 3 - 17.

*[*Couper, et. al., 1989*]* Couper, M. J., Neeson, A. E., and Griffiths, J. R., "Casting Defects and the Fatigue Behavior of An Aluminum Casting Alloy", Fatigue Fracture of Engineering Materials and Structures, Vol. 13, pp. 213 - 227.

[Culpepper et. al., 1998] Culpepper, M. L., Slocum, A. H., Shaikh, F. Z., 1998, "Compliant Kinematic Couplings For Use In Manufacturing And Assembly", Proceedings of the 1998 ASME International Mechanical Engineering Congress and Exposition, pp. 611 - 618.

[Culpepper et. al., 1999a] Culpepper, M. L, Slocum, A. H., Shaikh F. Z, 1999 "Quasi-Kinematic Couplings For Precision Automotive Assemblies," Proceedings of the 1999 ASME Fall ICE Technical Conference, Ann Arbor, MI, October, 1999, pp. 61-66.

[Culpepper et. al., 1999b] Culpepper, M. L., Slocum, A. H., Shaikh, F. H., "Quasi-Kinematic Coupling and Method For Use in Assembling and Locating Vehicle Components and the Like", U.S. Patent Application, Cambridge, MA, 1999.

[Culpepper and Slocum, 1999c] Culpepper, M. L. and Slocum, A. H., "Quasi-Kinematic Coupling and Method For Use in Assembling and Location of Mechanical Components and the Like", U.S. Patent Application, Cambridge, MA, 1999.

[Culpepper et. al., 1999d] Culpepper, M. L, Slocum, A. H., Shaikh F. Z, "Quasi-Kine-

matic Couplings: A Low-Cost Method For Precision Coupling of Product Components and the Like in Manufacturing Processes," Abstract for the Proceeding of the 1999 Annual Meeting of the American Society for Precision Engineering, Monterey, CA, 1999, pp. 571 - 574.

[Hale, 1999] Hale, L. C., "Principles and Techniques for Designing Precision Machines", Ph.D. Thesis, M.I.T., Cambridge, Massachusetts, 1999, p. 422.

[Heck, 1997] Heck, K., December 1997, Conversations with Kevin Heck, Manufacturing Engineer, Ford Engine Plant #2, Cleveland, OH.

[Heywood, 1988] Heywood, J. B., "Internal Combustion Engine Fundamentals", McGraw-Hill Inc., 1988, p. 717.

[Johnson, 1968] Johnson, K. L., "Deformation of a Plastic Wedge by a Rigid Flat Die Under the Action of a Tangential Force", Journal of Mechanics and Physics of Solids, pp. 395 - 402.

[Johnson, 1985] Johnson, K. L., "Contact Mechanics", Cambridge University Press, 1985, pp. 154 - 155, 170 - 179, 204-210, 233 - 237.

[Lasecki, 1999] Lasecki, J., Conversation with John Lasecki, Engineer, Ford Scientific Laboratory, Dearborn, MI, October, 22, 1999.

[Lubliner, 1990] Lubliner, J. "Plasticity Theory", Macmillan Publishing Co., New York, NY, 1990, pp 18 - 19.

[Minch, 1999a] Minch, G., Conversation with Greg Minch, Process Engineer, Ford Cleveland Engine Plant #1, Cleveland, OH, January 1999.

[Minch, 1999b] Minch, G., Conversation with Greg Minch, Process Engineer, Ford Cleveland Engine Plant #1, Cleveland, OH, December, 1999.

[Oberg, et. al., 1992] Oberg, E., Jones, F. D., Horton, H. L., and Ryffel, H. H., "Machinery's Handbook", Industrial Press Inc., New York, NY, 1992, p. 672.

[Schmiechen and Slocum, 1996] Schmiechen P. and Slocum, A., H. "Analysis of Kinematic Systems: a Generalized Approach", Precision Engineering, July 1996, Vol. 19, No. 1, pp. 11 - 18.

[Shigley and Mischke, 1989] Shigley, J. E., Mischke, C. R., 1989, "Mechanical Engineering Design," McGraw-Hill, Inc., New York, New York, pp. 508 - 509.

[Slocum, 1988a] Slocum, A. H., April 1988, "Kinematic Couplings for Precision Fixturing -Part I: Formulation of Design Parameters", Precision Engineering, Vol. 10, No. 2, pp. 85-91.

[Slocum and Donmez, 1988b] Slocum A. H. and Donmez A., "Kinematic Couplings For Precision Fixturing- Part 2: Experimental Determination of Repeatability and Stiffness", Precision Engineering, July 1988, Vol. 10, No. 3, pp. 115-122.

[Slocum, 1992a] Slocum, A. H., "Design of Three-Groove Kinematic Couplings", Precision Engineering, April 1992, Vol. 14, No. 2, pp. 67-73.

[Slocum, 1992b] Slocum, A. H., 1992, "Precision Machine Design", Prentice-Hall, Inc., Englewood Cliffs, New Jersey , pp. 401-412 and pp. 228-235.

[Slocum et. al., 1997] Slocum, A. H., Mueller, L., Braunstein, D., 1997, "Flexural Mount Kinematic Couplings and Method", United States Patent No. 5,678,944, pp. 1 - 10.

[Slocum, 1998a] Slocum, A. H., Conversations with Prof. A. H. Slocum of MIT, Cambridge, MA, May 1998.

[Slocum, 1998b] Slocum, A. H., "Kinematic Coupling Method and System For Aligning Sand Mold Cores and the Like and Other Soft Objects and Surfaces", United States Patent No. 5,769,554, pp. 1 - 6.

[Suh, 1990] Suh, N. P., 1990, "The Principles of Design", Oxford University Press, New York, pp. 1 - 40.

[Suh, 1993] Suh, N. P., "In Pursuit of the Lower Limit of Friction Coefficient in Dry Sliding", Proceedings of the 1993 ASME Winter Annual Meeting, New Orleans, LA, 1993, pp. 1-8.

[Swokowski, 1988] Swokowski, E. W., "Calculus With Analytic Geometry", PWS Kent Publishing Co., Boston, MA, p. 557.

[Ting and Lawrence, 1993] Ting, J. C., and Lawrence, F. V., "Modeling the Long-Life Fatigue Behavior of a Cast Aluminum Alloy", Fatigue Fracture of Engineering Materials and Structures, Vol. 16, 1993, p. 631 - 647.

[Vallance and Slocum, 1999] Vallance, R. R. and Slocum, A. H., "The Design of Split-Groove Kinematic Couplings", Draft Paper For ASPE Journal, Cambridge, MA, 1999, pp. 1-34.

[Vrsek, 1997] Vrsek, G., Conversations with Gary Vrsek, Powertrain Research Manager, Ford Scientific Laboratory, Dearborn, MI, December 1997.

[Yerace, 1999] Yerace, D., E-mail from Daniel Yerace, Engineer, Ford Scientific Research Laboratory, Dearborn, MI, November 1, 1999.

Appendix A

EXCEL SPREADSHEET USED TO ITERATE BEST SOLUTION

The iterative analysis used to minimize the contact angle and find dimensions of the joint elements was implemented in an Excel™ spreadsheet. There are three components to the spreadsheet.

- **User Input** - Section for user provided values which describe some parts of the coupling joint. The user can specify custom dimensions.
- **Graphical Representation of QKC Joint** - Using the data provided by the user, Excel™ plots a cross section of the joint so the user can visually verify a model. As an aside, the author has found this to be an invaluable tool for debugging spreadsheet calculations.
- **Constraint Matrix** - The constraint matrix contains the calculations and logic needed to determine if the constraints have been met. The equations contained within help drive the iteration.

To use the spreadsheet:

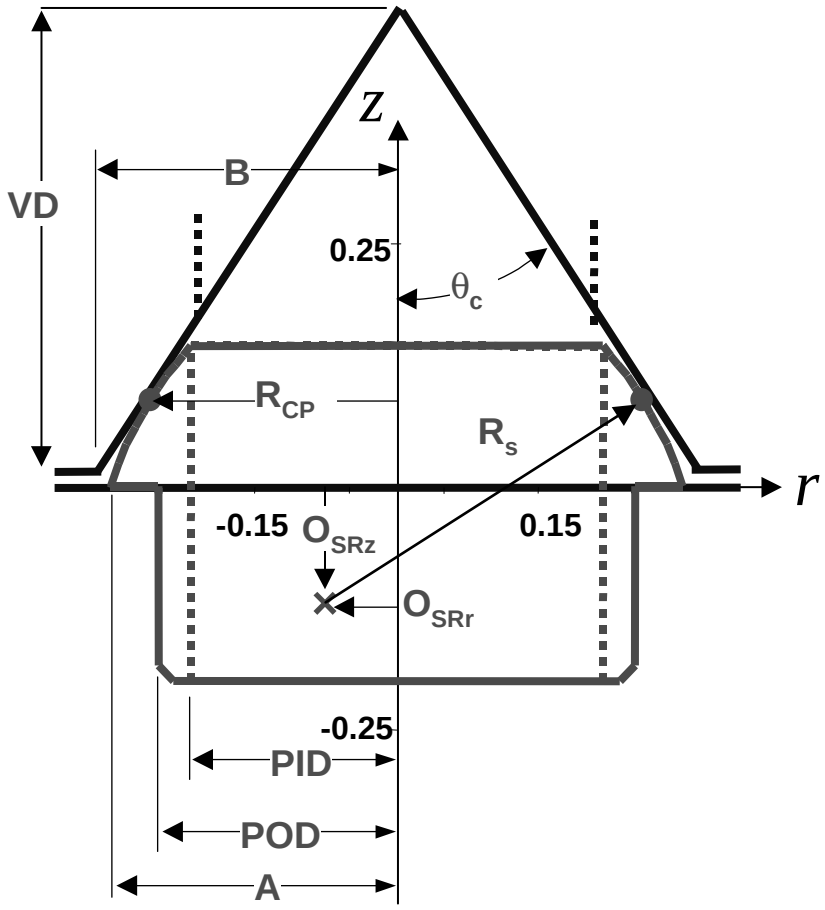
- 1. With the spreadsheet open, enter the nominal values the sheet requires
- 2. Choose: Tools > Solver
- 3. In the "Set Target:" cell, select the numerical value for θ_c (boxed value)
- 4. In the "Equal To:" cell, choose minimize (this tells Excel™ to minimize θ_c)
- 5. In the "By Changing Cells:" cell, select the values for R_s, θ_c, O_{SRr}, O_{SRz} (boxed values)
- 6. In the "Subject To Constraints:" area, input the solver constraint values for each constraint and set their values to be greater than or equal to 0
- 7. Click the solve button

If the solver does not find a solution, the solver constraints or margins of safety must be loosened to allow convergence to a workable design.

User Input

Units **in** (enter in or mm)

	Nominal Values		**Tolerance Inputs**		**Description of Variable**
General Variables					
θc	**32.0**	+/-	**0.0000**	deg	Half Cone Anggle
GAP	**0.007**	+/-	**0.0000**	*inches*	Nominal Pre-Mate Gap
Sphere Dimns-Coords					
Rs	**0.3946**	+/-	**0.0000**	*inches*	Sphere Radius
OSRr	**-0.0752**	+/-	**0.0000**	*inches*	r Coord. Of Sphere Center (Use Curve in 1st Quadrant)
OSRz	**-0.1207**	+/-	**0.0000**	*inches*	z Coord. Of Sphere Center (Use Curve in 1st Quadrant)
Peg-Hole Dimns					
DBH	**0.4331**	+/-	**0.0000**	*inches*	M10 Diameter of Bolt Hole
DH	**0.5000**			*inches*	Diameter of Peg Hole
INT	**0.0010**			*inches*	Peg-Hole Interference (DIAMETER)
LPEG	**0.2000**			*inches*	Length of Peg Shank
DR	**0.2756**			*inches*	Dowel Pin Radius (For Constraint)
COD	0.3004			*inches*	PEG Forced Crown OD @ y=0
t	0.0335			*inches*	Peg Wall Thickness
DP	0.5010			*inches*	Diameter of Peg Shank
Chamfers					
CHx-b	**0.0150**			*inches*	X Width of Bottom Peg Chamfer
γb	**45.0**			deg	Bottom Chamfer Angle
Contact Coordinates (r,z)					
Xcp	0.2594			*inches*	X Coord. Of Contact Point
Ycp	0.0884			*inches*	Y Coord. Of Contact Point



Excel Plot Of Peg Geometry For Visual Check

Geometry Constraint Checks					
#	Constraint	Check	MOS	Solver Constraint	Units
1	Contact Point-Bolt Hole Xcp-(DBH/2+N41)	OK	0.0400	0.0029	inches
2	V RAD @ y=0 < DR dr-(COD+MOS)	OK	-0.0300	0.0052	inches
3	Peg Indent Check	OK	0.0100	0.0057	inches
4	Reference Check COD>DP/2+MOS?	OK	0.0450	0.0049	inches

Description of Constraint

1 Constraint Which Keeps Contact Point Away From Bolt Hole

2 Enforces Largest Diameter on Peg Crown to be Less Than Diameter of Dowel Pin + MOS

3 Enforces Cone Diameter at Surface to be Less Than Peg Crown Diameter at Surface

4 Enforces Peg Reference Stop (A-POD in Fig.) to be Greater Than Margin of Safety

Note:

1 "MOS" = Margin of Safety

2 Solver Constraint must be greater than 0!

3 The "Check" States if Constraint is Met

Appendix B

MATHCAD WORKSHEET FOR FINDING COUPLING STIFFNESS

The analysis to determine the stiffness of Quasi-Kinematic Couplings was implemented in a MathCad^{TM} worksheet. A sample program is provided on the following pages and can be used with ease for those who understand the terminology presented in Chapter 2 and understand the analysis detailed in Chapter 3. The worksheet is broken into several steps to make it easier to follow the analysis. These steps are outlined below with the required inputs and calculated outputs.

TABLE 6.1 Steps in MathCad^{TM} Worksheet for QKC Stiffness Determination

#	Step Label	Inputs and Calculations
1	Define Joint Parameters	User Supplies Dimension of Coupling Elements
2	Define Coefficients of Friction	User supplies coefficients of friction for l and s directions (Conical coordinates)
3	Define Joint Positions	User provides location of coupling joints relative to arbitrary coordinate system
4	Define Target Surface Geometry	User defines angles over which contactors and targets make contact.
5	Joint Position Vectors	Program calculates coupling centroid and position of joint relative to coupling centroid.
6	Define Displacements	User specifies magnitude and direction of imposed displacement
7	Solve For ε_z Direction Angles	No input required, program calculates direction of maximum δ_n due to user imposed rotations of coupling about the z axis.
8	Calculate Normal Displacements	No input required, program calculates the normal displacements (of far field approach) between the contactor and target surfaces
9	Normal Force Per Unit Length	User inputs unit load vs. normal displacement curve obtained for FEA analysis
10	Integration of Contact Profiles	No input required, program integrates force per unit length profile over contact surfaces
11	Solution For Total Force/Torque	Program calculates total load on coupling due to resultant contact forces
12	Solution for Total Force Application Point	Program calculates the application point of total load from torque balance
13	Stiffness Calculation	Program calculates stiffness of coupling for given displacements and directions

SAMPLE PROGRAM FOR QKC, VALUES FOR CASE STUDY HELD FOR CONFIDENTIALITY

QUASI KINEMATIC COUPLING FORCE - DISPLACEMENT MODEL

BY: MARTIN L. CULPEPPER

STEP 1: USER INPUT

JOINT DIMENTIONS:

$\theta_c := 32 \cdot \frac{\pi}{180}$ $O_{SRr} := -0.0752 \cdot in$ $R_s := 0.3946 \cdot in$

FRICTION COEFFICIENTS:

$\mu_{Tl} := 0$ $\mu_{Ts} := 0$

IMPOSED DISPLACEMENTS:

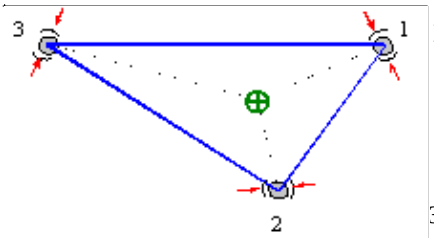
$\Delta r := \frac{1}{10^6} \cdot in$ $\phi := 45deg$ $\delta_{zcc} := -0.003 \cdot in$

$\varepsilon_x := 10^{-99} \frac{\pi}{180 \cdot 10^6} \cdot rad$ $\varepsilon_y := 10^{-99} \frac{\pi}{180 \cdot 10^6} \cdot rad$ $\varepsilon z := 10^{-99} \frac{\pi}{180 \cdot 10^6} \cdot rad$

JOINT POSITIONS RELATIVE TO ARBITRARY COORDINATE SYSTEM:

Joint 3 Must Be Leftmost In x-y Plane

$p_3 := \begin{pmatrix} -10.8366 \cdot in \\ 6.772 \cdot in \\ 1 \cdot in \end{pmatrix}$



$p_1 := \begin{pmatrix} 1.7618 \cdot in \\ 6.772 \cdot in \\ 1 \cdot in \end{pmatrix}$

$p_2 := \begin{pmatrix} 394 \cdot in \\ 3.2677 \cdot in \\ 1 \cdot in \end{pmatrix}$

CONTACT FLAT INTEGRATION ANGLES:

θ_{ri} is always less than θ_{rf}!!!

Joint 1, Flat 1:

$$\theta_{ri11} := 30 \cdot \frac{\pi}{180} \qquad \theta_{rf11} := 150 \cdot \frac{\pi}{180}$$

Joint 1, Flat 2:

$$\theta_{ri12} := 210 \cdot \frac{\pi}{180} \qquad \theta_{rf12} := 330 \cdot \frac{\pi}{180}$$

Joint 2, Flat 1:

$$\theta_{ri21} := 30 \cdot \frac{\pi}{180} \qquad \theta_{rf21} := 150 \cdot \frac{\pi}{180}$$

Joint 2, Flat 2:

$$\theta_{ri22} := 210 \cdot \frac{\pi}{180} \qquad \theta_{rf22} := 330 \cdot \frac{\pi}{180}$$

Joint 3, Flat 1:

$$\theta_{ri31} := 30 \cdot \frac{\pi}{180} \qquad \theta_{rf31} := 150 \cdot \frac{\pi}{180}$$

Joint 3, Flat 2:

$$\theta_{ri32} := 210 \cdot \frac{\pi}{180} \qquad \theta_{rf32} := 330 \cdot \frac{\pi}{180}$$

VARIABLES FOR FEA FORCE VS DISPLACEMENT CURVE FIT:

Joint 1

$$b_1 := 0.43$$

$$K_1 := 28456 \frac{\text{lbf}}{\text{in}^{1.43}}$$

Joint 2

$$b_2 := b_1$$

$$K_2 := 28456 \frac{\text{lbf}}{\text{in}^{1.43}}$$

Joint 3

$$b_3 := b_1$$

$$K_3 := 28456 \frac{\text{lbf}}{\text{in}^{1.43}}$$

STEP 2: SOLUTION FOR JOINT POSITION VECTORS RELATIVE TO COUPLING CENTER

$\theta_1 := \text{atan2}\left(p_{2_0} - p_{1_0}, p_{2_1} - p_{1_1}\right)$ $\theta_2 := \text{atan2}\left(p_{3_0} - p_{1_0}, p_{3_1} - p_{1_1}\right)$ $\theta_3 := \text{atan2}\left(p_{2_0} - p_{3_0}, p_{2_1} - p_{3_1}\right)$

$\theta_4 := \frac{1}{2} \cdot \left(\theta_3 + \theta_2 - \pi\right)$ $\theta_5 := \frac{1}{2} \cdot \left(\theta_1 + \theta_2\right)$ $\theta_6 := \frac{1}{2} \cdot \left(\theta_1 + \theta_3\right)$

$x_{cc} := \frac{\left(p_{3_1} - p_{1_1} + \tan\left(\theta_5\right) \cdot p_{1_0} - \tan\left(\theta_4\right) \cdot p_{3_0}\right)}{\tan\left(\theta_5\right) - \tan\left(\theta_4\right)}$ $y_{cc} := \tan\left(\theta_5\right) \cdot \left(x_{cc} - p_{1_0}\right) + p_{1_1}$ $z_{cc} := p_{3_2}$

Coupling Center Position Relative To Arbitrary Coordinate System:

$p_{cc} := \begin{pmatrix} x_{cc} \\ y_{cc} \\ z_{cc} \end{pmatrix}$ $p_{cc} = \begin{pmatrix} -3 \times 10^0 \\ 5 \times 10^0 \\ 1 \times 10^0 \end{pmatrix}$ in

Joint Coordinate System Positions Vectors Relative To Coupling Center

$r_{cs1} := p_1 - p_{cc}$ $r_{cs2} := p_2 - p_{cc}$ $r_{cs3} := p_3 - p_{cc}$

$\left|r_{cs1}\right| = 4.85041$ in $\left|r_{cs2}\right| = 1.89755$ in $\left|r_{cs3}\right| = 8.19166$ in

STEP 3: CALCULATION OF IMPOSED DISPLACEMENT VARIABLES AND DIRECTIONS

$$\delta_{xcc} := \Delta r \cdot \cos\left(\phi \cdot \frac{\pi}{180}\right) \qquad \delta_{ycc} := \Delta r \cdot \sin\left(\phi \cdot \frac{\pi}{180}\right) \qquad \delta_{rcc} := \left(\delta_{xcc}^{\ 2} + \delta_{ycc}^{\ 2}\right)^{\frac{1}{2}}$$

$$\theta_{\delta rmax} := \operatorname{atan2}\left(\delta_{xcc}, \delta_{ycc}\right) \qquad \gamma := \operatorname{atan2}\left(\varepsilon_x, \varepsilon_y\right) \qquad k := \begin{pmatrix} 0 \\ 0 \\ 1 \end{pmatrix}$$

$$\varepsilon z = 0 \times 10^{0}\ \text{deg} \qquad \varepsilon_z := \begin{pmatrix} 0 \\ 0 \\ \varepsilon z \end{pmatrix} \qquad r_{\varepsilon z} := \begin{pmatrix} 0 \\ 0 \\ 0 \end{pmatrix} \cdot \text{in}$$

$$\varepsilon xy := \left(\varepsilon_x^{\ 2} + \varepsilon_y^{\ 2}\right)^{\frac{1}{2}} \cdot \text{rad} \qquad \varepsilon_{xy} := \begin{pmatrix} \varepsilon xy \cdot \cos(\gamma) \\ \varepsilon xy \cdot \sin(\gamma) \\ 0 \end{pmatrix} \qquad r_{\varepsilon xy} := \begin{pmatrix} 0 \\ 0 \\ 0 \end{pmatrix} \cdot \text{in}$$

STEP 4: DIRECTION ANGLES FOR ε_z DISPLACEMENTS

$$\delta_{rmax1\varepsilon z} := \varepsilon_z \times \left(r_{cs1} - r_{\varepsilon z}\right) \qquad \delta_{rmax2\varepsilon z} := \varepsilon_z \times \left(r_{cs2} - r_{\varepsilon z}\right) \qquad \delta_{rmax3\varepsilon z} := \varepsilon_z \times \left(r_{cs3} - r_{\varepsilon z}\right)$$

$$\theta_{\delta rmax1\varepsilon z} := \operatorname{atan2}\left(\delta_{rmax1\varepsilon z_0}, \delta_{rmax1\varepsilon z_1}\right) \qquad \theta_{\delta rmax2\varepsilon z} := \operatorname{atan2}\left(\delta_{rmax2\varepsilon z_0}, \delta_{rmax2\varepsilon z_1}\right) \qquad \theta_{\delta rmax3\varepsilon z} := \operatorname{atan2}\left(\delta_{rmax3\varepsilon z_0}, \delta_{rmax3\varepsilon z_1}\right)$$

TS

$$\left|\varepsilon_z \times \left(r_{cs1} - r_{\varepsilon z}\right)\right| \cdot \cos\left(\theta_r - \theta_{\delta rmax1\ \varepsilon z}\right)\Big] \cdot \cos\left(\theta_c\right) + \Big[\delta_{zcc} - \varepsilon xy \cdot \left(R_s \cdot \cos\left(\theta_c\right) + O_{SRr}\right) \cdot \sin\left(\theta_r - \gamma\right) + k \cdot \left[\varepsilon_{xy} \times \left(r_{cs1} - r_{\varepsilon xy}\right)\right]\Big] \cdot \sin\left(\theta_c\right)\Big]$$

$$\left|\varepsilon_z \times \left(r_{cs2} - r_{\varepsilon z}\right)\right| \cdot \cos\left(\theta_r - \theta_{\delta rmax2\ \varepsilon z}\right)\Big] \cdot \cos\left(\theta_c\right) + \Big[\delta_{zcc} - \varepsilon xy \cdot \left(R_s \cdot \cos\left(\theta_c\right) + O_{SRr}\right) \cdot \sin\left(\theta_r - \gamma\right) + k \cdot \left[\varepsilon_{xy} \times \left(r_{cs2} - r_{\varepsilon xy}\right)\right]\Big] \cdot \sin\left(\theta_c\right)\Big]$$

$$\left|\varepsilon_z \times \left(r_{cs3} - r_{\varepsilon z}\right)\right| \cdot \cos\left(\theta_r - \theta_{\delta rmax3\ \varepsilon z}\right)\Big] \cdot \cos\left(\theta_c\right) + \Big[\delta_{zcc} - \varepsilon xy \cdot \left(R_s \cdot \cos\left(\theta_c\right) + O_{SRr}\right) \cdot \sin\left(\theta_r - \gamma\right) + k \cdot \left[\varepsilon_{xy} \times \left(r_{cs3} - r_{\varepsilon xy}\right)\right]\Big] \cdot \sin\left(\theta_c\right)\Big]$$

STEP 6: UNIT FORCE VS DISPLACEMENT LINE FIT EQUATIONS

$$f_{n1}(\theta_r) := K_1 \cdot \left(\left|\delta_{n1}(\theta_r)\right|\right)^{b_1} \qquad f_{n2}(\theta_r) := K_2 \cdot \left(\left|\delta_{n2}(\theta_r)\right|\right)^{b_2} \qquad f_{n3}(\theta_r) := K_3 \cdot \left(\left|\delta_{n3}(\theta_r)\right|\right)^{b_3}$$

STEP 7: CONTACT FORCES

Flat 11:

$$F_{ARC11} := \left(R_s \cdot \cos(\theta_c) + O_{SRr}\right) \cdot \begin{bmatrix} \int_{\theta_{ri11}}^{\theta_{rf11}} -f_{n1}(\theta_r) \cdot \left(-\cos(\theta_r) \cdot \cos(\theta_c) - \mu_{Ts} \cdot \sin(\theta_r) + \mu_{Tl} \cdot \cos(\theta_r) \cdot \sin(\theta_c)\right) d\theta_r \\ \int_{\theta_{ri11}}^{\theta_{rf11}} -f_{n1}(\theta_r) \cdot \left(-\sin(\theta_r) \cdot \cos(\theta_c) + \mu_{Ts} \cdot \cos(\theta_r) + \mu_{Tl} \cdot \sin(\theta_r) \cdot \sin(\theta_c)\right) d\theta_r \\ \int_{\theta_{ri11}}^{\theta_{rf11}} -f_{n1}(\theta_r) \cdot \left(\sin(\theta_c) + \mu_{Tl} \cdot \cos(\theta_c)\right) d\theta_r \end{bmatrix}$$

Flat 12:

$$F_{ARC12} := \left(R_s \cdot \cos(\theta_c) + O_{SRr}\right) \cdot \begin{bmatrix} \int_{\theta_{ri12}}^{\theta_{rf12}} -f_{n1}(\theta_r) \cdot \left(-\cos(\theta_r) \cdot \cos(\theta_c) - \mu_{Ts} \cdot \sin(\theta_r) + \mu_{Tl} \cdot \cos(\theta_r) \cdot \sin(\theta_c)\right) d\theta_r \\ \int_{\theta_{ri12}}^{\theta_{rf12}} -f_{n1}(\theta_r) \cdot \left(-\sin(\theta_r) \cdot \cos(\theta_c) + \mu_{Ts} \cdot \cos(\theta_r) + \mu_{Tl} \cdot \sin(\theta_r) \cdot \sin(\theta_c)\right) d\theta_r \\ \int_{\theta_{ri12}}^{\theta_{rf12}} -f_{n1}(\theta_r) \cdot \left(\sin(\theta_c) + \mu_{Tl} \cdot \cos(\theta_c)\right) d\theta_r \end{bmatrix}$$

$$F_{PEG1} := F_{ARC11} + F_{ARC12}$$

Flat 21:

$$F_{ARC21} := \left(R_s \cdot \cos\left(\theta_c\right) + O_{SRr}\right) \cdot \begin{bmatrix} \int_{\theta_{ri21}}^{\theta_{rf21}} -f_{n2}\left(\theta_r\right) \cdot \left(-\cos\left(\theta_r\right) \cdot \cos\left(\theta_c\right) - \mu_{Ts} \cdot \sin\left(\theta_r\right) + \mu_{Tl} \cdot \cos\left(\theta_r\right) \cdot \sin\left(\theta_c\right)\right) d\theta_r \\ \int_{\theta_{ri21}}^{\theta_{rf21}} -f_{n2}\left(\theta_r\right) \cdot \left(-\sin\left(\theta_r\right) \cdot \cos\left(\theta_c\right) + \mu_{Ts} \cdot \cos\left(\theta_r\right) + \mu_{Tl} \cdot \sin\left(\theta_r\right) \cdot \sin\left(\theta_c\right)\right) d\theta_r \\ \int_{\theta_{ri21}}^{\theta_{rf21}} -f_{n2}\left(\theta_r\right) \cdot \left(\sin\left(\theta_c\right) + \mu_{Tl} \cdot \cos\left(\theta_c\right)\right) d\theta_r \end{bmatrix}$$

Flat 22:

$$F_{ARC22} := \left(R_s \cdot \cos\left(\theta_c\right) + O_{SRr}\right) \cdot \begin{bmatrix} \int_{\theta_{ri22}}^{\theta_{rf22}} -f_{n2}\left(\theta_r\right) \cdot \left(-\cos\left(\theta_r\right) \cdot \cos\left(\theta_c\right) - \mu_{Ts} \cdot \sin\left(\theta_r\right) + \mu_{Tl} \cdot \cos\left(\theta_r\right) \cdot \sin\left(\theta_c\right)\right) d\theta_r \\ \int_{\theta_{ri22}}^{\theta_{rf22}} -f_{n2}\left(\theta_r\right) \cdot \left(-\sin\left(\theta_r\right) \cdot \cos\left(\theta_c\right) + \mu_{Ts} \cdot \cos\left(\theta_r\right) + \mu_{Tl} \cdot \sin\left(\theta_r\right) \cdot \sin\left(\theta_c\right)\right) d\theta_r \\ \int_{\theta_{ri22}}^{\theta_{rf22}} -f_{n2}\left(\theta_r\right) \cdot \left(\sin\left(\theta_c\right) + \mu_{Tl} \cdot \cos\left(\theta_c\right)\right) d\theta_r \end{bmatrix}$$

$$F_{PEG2} := F_{ARC21} + F_{ARC22}$$

Flat 31:

$$F_{ARC31} := \left(R_s \cdot \cos\left(\theta_c\right) + O_{SRr}\right) \cdot \begin{bmatrix} \int_{\theta_{ri31}}^{\theta_{rf31}} -f_{n3}\left(\theta_r\right) \cdot \left(-\cos\left(\theta_r\right) \cdot \cos\left(\theta_c\right) - \mu_{Ts} \cdot \sin\left(\theta_r\right) + \mu_{Tl} \cdot \cos\left(\theta_r\right) \cdot \sin\left(\theta_c\right)\right) d\theta_r \\ \int_{\theta_{ri31}}^{\theta_{rf31}} -f_{n3}\left(\theta_r\right) \cdot \left(-\sin\left(\theta_r\right) \cdot \cos\left(\theta_c\right) + \mu_{Ts} \cdot \cos\left(\theta_r\right) + \mu_{Tl} \cdot \sin\left(\theta_r\right) \cdot \sin\left(\theta_c\right)\right) d\theta_r \\ \int_{\theta_{ri31}}^{\theta_{rf31}} -f_{n3}\left(\theta_r\right) \cdot \left(\sin\left(\theta_c\right) + \mu_{Tl} \cdot \cos\left(\theta_c\right)\right) d\theta_r \end{bmatrix}$$

Flat 32:

$$F_{ARC32} := \left(R_s \cdot \cos(\theta_c) + O_{SRr}\right) \cdot \begin{bmatrix} \int_{\theta_{ri32}}^{\theta_{rf32}} -f_{n3}(\theta_r) \cdot \left(-\cos(\theta_r) \cdot \cos(\theta_c) - \mu_{Ts} \cdot \sin(\theta_r) + \mu_{Tl} \cdot \cos(\theta_r) \cdot \sin(\theta_c)\right) d\theta_r \\ \int_{\theta_{ri32}}^{\theta_{rf32}} -f_{n3}(\theta_r) \cdot \left(-\sin(\theta_r) \cdot \cos(\theta_c) + \mu_{Ts} \cdot \cos(\theta_r) + \mu_{Tl} \cdot \sin(\theta_r) \cdot \sin(\theta_c)\right) d\theta_r \\ \int_{\theta_{ri32}}^{\theta_{rf32}} -f_{n3}(\theta_r) \cdot \left(\sin(\theta_c) + \mu_{Tl} \cdot \cos(\theta_c)\right) d\theta_r \end{bmatrix}$$

$F_{PEG3} := F_{ARC31} + F_{ARC32}$

$$F_{ARC11} = \begin{pmatrix} 0 \\ 679 \\ -513 \end{pmatrix} \text{lbf} \qquad F_{ARC12} = \begin{pmatrix} 0 \\ -679 \\ -513 \end{pmatrix} \text{lbf} \qquad F_{PEG1} = \begin{pmatrix} 0 \\ 0 \\ -1026 \end{pmatrix} \text{lbf}$$

$$F_{ARC21} = \begin{pmatrix} 0 \\ 679 \\ -513 \end{pmatrix} \text{lbf} \qquad F_{ARC22} = \begin{pmatrix} 0 \\ -679 \\ -513 \end{pmatrix} \text{lbf} \qquad F_{PEG2} = \begin{pmatrix} 0 \\ 0 \\ -1026 \end{pmatrix} \text{lbf}$$

$$F_{ARC31} = \begin{pmatrix} 0 \\ 679 \\ -513 \end{pmatrix} \text{lbf} \qquad F_{ARC32} = \begin{pmatrix} 0 \\ -679 \\ -513 \end{pmatrix} \text{lbf} \qquad F_{PEG3} = \begin{pmatrix} 0 \\ 0 \\ -1026 \end{pmatrix} \text{lbf}$$

STEP 8: TOTAL FORCE AND TORQUE

$$F_{TOT} := F_{PEG1} + F_{PEG2} + F_{PEG3} \qquad F_{TOT} = \begin{pmatrix} 0.33 \\ 0.01 \\ -3077.53 \end{pmatrix} \text{lbf}$$

$$F_r := \left[\left(F_{TOT_0} \right)^2 + \left(F_{TOT_1} \right)^2 \right]^{\frac{1}{2}} \qquad F_r = 0.33\text{lbf}$$

$$T_{TOT} := r_{cs1} \times F_{PEG1} + r_{cs2} \times F_{PEG2} + r_{cs3} \times F_{PEG3} \qquad T_{TOT} = \begin{pmatrix} -1409 \\ -3273 \\ -0 \end{pmatrix} \text{lbf} \cdot \text{in}$$

STEP 9: STIFFNESS CALCULATION

THIS IS BEST DONE BY HAND. TO FIND STIFFNESS,
IMPOSE DEFLECTIONS (+/-ε) and follow procedure in Chapter 3

Appendix C

NON-LINEAR FINITE ELEMENT ANALYSIS

C.1 About the FEA Code

Following is the complete code for a Cosmos/M 2.5 two dimensional analysis of the Quasi-Kinematic Coupling joint used in the case study. This code can be typed into a text file and saved as: *problem_name.ses*. When this file, the session file, is loaded into Cosmos/M, the program will automatically create the geometry, mesh, boundary conditions, gap elements, and assign material properties. To change any values for the analysis, modify the session file accordingly, start a new problem, reload the new session file, and run the analysis.

C.2 What the Code Does

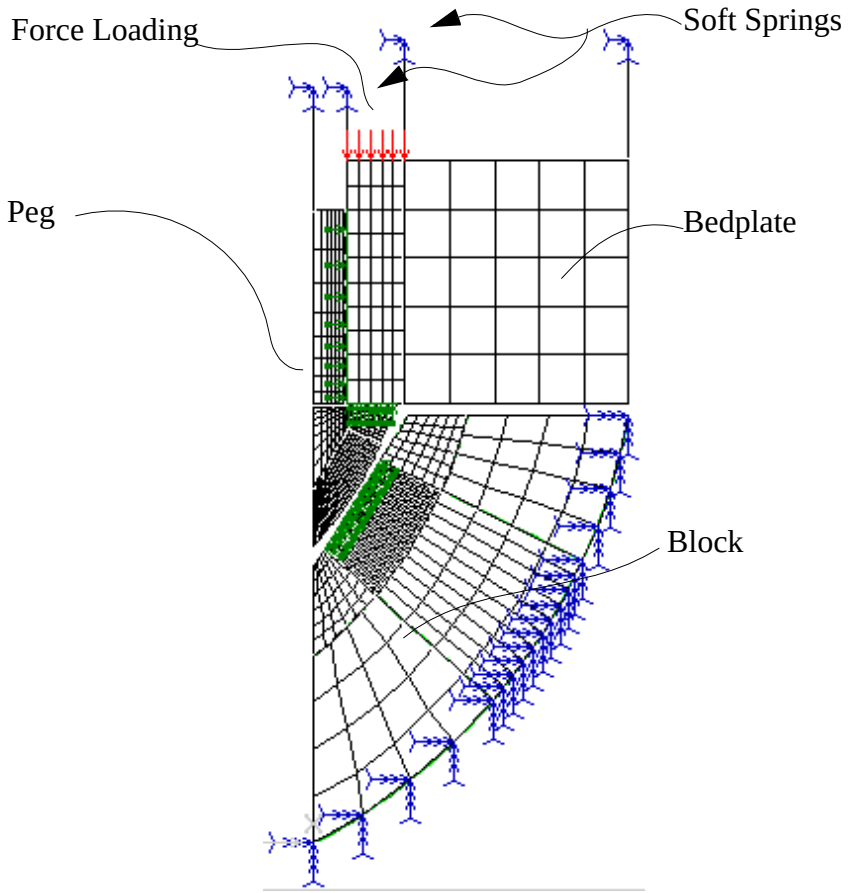


Figure C.1 Axisymmetric Mesh For FEA Model of QKC Joint, Note: Mesh Shown to Illustrate FEA Geometry, Actual Mesh Was Much Finer (Considerably More Cluttered)

The code generates the peg-groove geometry as a combination of points and curves, then defines surfaces using the curves of the geometry. Next, a series of soft springs are attached to the top surfaces/components. This is necessary to ensure stability of the model as the top component requires some constraint (soft springs) in the y direction for the analysis to run. Without the springs, the model is under defined.

Next the element types are defined followed by the material properties. As plastic flow is involved in this analysis, a representation of the stress-strain curve is input during this

stage. The curve is approximated by two straight lines, the first represents the elastic region and the second representing the plastic region starts at the end of the elastic curve and continues with a different (lower) slope. Figure C.2 shows the curve fit for the steel used for the contactors in the case study (12L14 steel). The behavior of the material is modeled as Von Mises Isotropic Hardening and as strain rate insensitive. A series of constants, i.e. gap friction, etc..., are then defined as real constants.

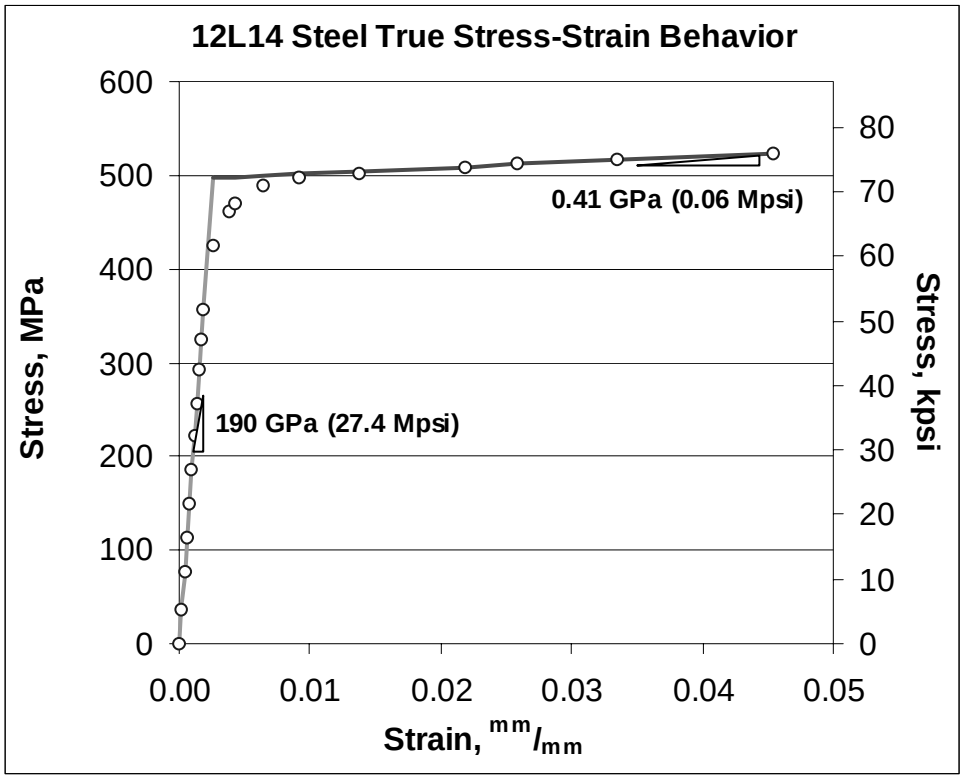


Figure C.2 Elastoplastic Model For Material Properties of 12L14 Steel

The surfaces are then meshed with the appropriate material and element properties. Then boundary conditions and gap elements between contacting components are defined. Next the type of solution control, force or displacement, and associated variables are input. This is followed by the temperature change the joint experiences during operation which can be used to determine the stress amplitude due to temperature change.

Various non-linear analysis options are then set. Next an alternate coordinate system which matches the *n* - *l* coordinate system introduced in Section 3.2.1 is defined to simplify calculation of displacements and stresses normal to and perpendicular to the groove surface (*n* direction). The final commands runs the non-linear analysis.

C.3 Complete Cosmos/M 2.5 Non-linear FEA Code

```
C*********************************************************
C* CONE-GROOVE CONTACT SIMULATION
C* THETAc = 32
C* MU = 0
C* MARTIN L. CULPEPPER
C* MIT DEPARTMENT OF MECHANICAL ENGINEERING
C* ROOM 3-449G
C* WORK: 617 - 452 - 2395
C* mculpepp@mit.edu
C*********************************************************

C*************************************************************
C********************  GEOMETRY  **********************
C*************************************************************

CRLCORD,1,0,0.25046143803,0.650391004320539,0.0,0.216502098435614,0.650391004320539,0.0
CRLCORD,2,0,0.25046143803,0.650391004320539, 0.0, 0.25046143803,0.450421791070732, 0.0
CRLCORD,3,0,0.284844051714361,0.392740759514652,0.0,0.313902435159875,0.439243893900624,0.0
CRLCORD,4,0,0.374454281581981,0.439243893900624,0.0,0.313902435159875,0.439243893900624,0.0
CRLCORD,5,0,0.216502098435613,0.192229845762822,0.0,0.216502098435613,0.283370771900562,0.0
CRACSE,6,0,0.0,-0.0751884237119689,0.552758210512732,0.216502,0.000000,0.400445,0.147298
CRACSE,7,0,0.0,-0.0751884237119835,0.571103210512729,0.216502,0.305438,0.285844,0.411991
CRLCORD,8,0,0.25046143803,0.450421791070732,0.0,0.300440673876797,0.450421791071432,0.0
CRLCORD,9,0,0.216502098435613,0.366579244869357,0.0,0.216502098435613,0.305438265058888,0.0
CRACSE,10,0,0.0,-0.0751884237119621,0.55275821051274,0.216502,0.192230,0.280014,0.254605
CRLCORD,11,0,0.216502098435613,0,0.0,0.216502098435613,0.192229845762822,0.0
CRLCORD,12,0,0.539416734030825,0.439243893900624,0.0,0.374454281581981,0.439243893900624,0.0
CRLCORD,13,0,0.216502098435613,0.283370771900562,0.0,0.227671035675278,0.30124480781789,0.0
CRLCORD,14,0,0.227671035675278,0.30124480781789,0.0,0.284844051714361,0.392740759514652,0.0
CRACSE,15,0,0.0,-0.0751884237119992,0.552758210512754,0.491957,0.290136,0.539417,0.439244
CRLCORD,16,0,0.34739903393138,0.361750610814435,0.0,0.491957327611912,0.290135483477866,0.0
CRACSE,17,0,0.0,-0.0751884237119906,0.552758210512752,0.400445,0.147298,0.491957,0.290136
CRLCORD,18,0,0.280014158285545,0.254605249363136,0.0,0.400444504321378,0.147297586320461,0.0
CRACSE,19,0,0.0,-0.075188423711971,0.552758210512748,0.280014,0.254605,0.347399,0.361751
CRLCORD,20,0,0.227671035675278,0.30124480781789,0.0,0.280014158285545,0.254605249363136,0.0
CRACSE,21,0,0.0,-0.0751884237119988,0.552758210512762,0.347399,0.361751,0.374454,0.439244
CRLCORD,22,0,0.284844051714361,0.392740759514652,0.0,0.34739903393138,0.361750610814435,0.0
CRACSE,23,0,0.0,-0.0751884237120159,0.571103210512743,0.285844,0.411991,0.300441,0.450422
CRLCORD,24,0,0.25046143803,0.417584400273011,0.0,0.25046143803,0.450421791070732,0.0
CRLCORD,25,0,0.25046143803,0.417584400273011,0.0,0.285844051714361,0.411990748269025,0.0
CRLCORD,26,0,0.216502098435613,0.366579244869357,0.0,0.25046143803,0.417584400273011,0.0
CRLCORD,27,0,0.216502098435613,0.450421791070731,0.0,0.216502098435613,0.366579244869357,0.0
CRLCORD,29,0,0.216502098435613,0.450421791070731,0.0,0.25046143803,0.450421791070732,0.0
CRLCORD,28,0,0.216502098435613,0.650391004320539,0.0,0.216502098435613,0.450421791070731,0.0
ACTSET,CS,0
VIEW,0,0,1,0
```

```
C***************************************************************
C*****************  SURFACES & SPRINGS  ******************
C***************************************************************

SF4CR,1,7,25,26,9,0
SF4CR,2,23,25,24,8,0
SF4CR,3,26,24,29,27,0
SF4CR,4,29,2,1,28,0
SF4CR,6,14,20,19,22,0
SF4CR,7,13,20,10,5,0
SF4CR,8,3,22,21,4,0
SF4CR,9,19,18,17,16,0
SF4CR,10,10,18,6,11,0
SF4CR,11,21,16,15,12,0
SF4CORD,12,0.25,0.451421791070731,0,0.310,0.451421791070731,0,0.31,0.7,0,0.25,0.7,0
SF4CORD,13,0.31,0.451421791070731,0,0.539416734030825,0.451421791070731,0,0.539416734030825
,0.7,0,0.31,0.7,0
CREXTR,1,2,1,Y,0.125
CREXTR,26,29,3,Y,0.125
SCALE,0

C***************************************************************
C******************  ELEMENT GROUPS  *******************
C***************************************************************

EGROUP,1,PLANE2D,0,2,1,0,1,2,0,1
EGROUP,2,PLANE2D,0,2,1,0,1,2,0,1
EGROUP,3,TRUSS2D,0,0,0,0,0,1,0,0;
EGROUP,4,GAP,1,2,0,1,3,0,0,0;
EGROUP,5,PLANE2D,0,2,1,0,1,2,0,1
EGROUP,6,GAP,1,2,0,1,3,0,0,0;
EGROUP,7,GAP,1,2,0,1,3,0,0,0;
EGROUP,8,GAP,1,2,0,1,3,0,0,0;


C***************************************************************
C******************  MAT'L PROPERTIES  ******************
C***************************************************************

MPROP,1,EX,27448448,NUXY,0.29,ALPX,06E-6,ALPY,06E-6,SIGYLD,72011,ETAN,059847;
MPROP,2,EX,09890683,NUXY,0.33,ALPX,15E-6,ALPY,15E-6,SIGYLD,27391,ETAN,524736;
MPROP,3,EX,20,NUXY,0.3;
MPROP,5,EX,27448448,NUXY,0.29,ALPX,06E-6,ALPY,06E-6,SIGYLD,72011,ETAN,59847;


C***************************************************************
C*******************  REAL CONSTANTS  *******************
C***************************************************************

RCONST,3,1,1,4,1,0,0,0
RCONST,4,2,1,2,0,1e-8,
RCONST,6,6,1,2,0,1e-8,
RCONST,7,7,1,2,0,1e-8,
```

```
RCONST,8,8,1,2,0,1e-8,

C*************************************************************
C***********************  MESH  ***********************
C*************************************************************

C*-----------------------------------------------------------
C* PEG MESH
C*-----------------------------------------------------------

ACTSET,EG,1,
ACTSET,MP,1,
M_SF,1,1,1,4,20,10,1,.5
M_SF,2,2,1,4,10,10,1,0.5
M_SF,3,3,1,4,10,12,1,1
M_SF,4,4,1,4,5,15,1,1
BONDDEF,1,1,1,1,3,2,1,1
BONDDEF,2,1,4,1,3,3,1,1

C*-----------------------------------------------------------
C* CONE MESH
C*-----------------------------------------------------------
ACTSET,EG,2,
ACTSET,MP,2,
M_SF,6,6,1,4,20,10,1,1
M_SF,7,7,1,4,8,10,1,1
M_SF,8,8,1,4,10,10,1,1
M_SF,9,9,1,4,10,10,1,1
M_SF,10,10,1,4,8,10,1,1
M_SF,11,11,1,4,10,10,1,1
BONDDEF,2,1,6,1,7,11,1,1

C*-----------------------------------------------------------
C* TRUSS MESH
C*-----------------------------------------------------------
ACTSET,EG,3,
ACTSET,MP,3,
ACTSET,RC,1,
M_CR,37,40,1,2,1,1
NMERGE;

C*-----------------------------------------------------------
C* HOLE MESH
C*-----------------------------------------------------------

ACTSET,EG,5,
C*ACTSET,MPC,5,
ACTSET,MP,5,
M_SF,12,12,1,4,5,10,1,1
M_SF,13,13,1,4,5,10,1,1
BONDDEF,3,1,12,1,13,13,1,1


C*************************************************************************
C*****************  BOUNDRY CONDITIONS  ******************
```

```
C*********************************************************************
DPT,30,AU,0,33,1,
DCR,6,UY,0,6,1,
DCR,17,UY,0,17,1,
DCR,15,UY,0,15,1,
NMERGE;
EMERGE;


C*****************************************************************
C*********************  GAP ELEMENTS  *********************
C*****************************************************************

C*---------------------------------------------------------
C* DEFINE BALL-GROOVE GAP ELEMENTS
C*---------------------------------------------------------
ACTSET,EG,4
ACTSET,RC,2
NL_GSAUTO,0,7,0,14,14,1,1

C*---------------------------------------------------------
C* DEFINE PEG-HOLE INTERFERENCE GAP ELEMENTS
C*---------------------------------------------------------
ACTSET,EG,6
ACTSET,RC,6
NL_GSAUTO,0,32,0,2,2,1,1
CURDEF,TIME,2,1,0,0,1,1;

C*---------------------------------------------------------
C* DEFINE PEG STOP - BEDPLATE SURFACE GAP ELEMENTS
C*---------------------------------------------------------
ACTSET,EG,7
ACTSET,RC,7
NL_GSAUTO,0,30,0,8,8,1,1

C*---------------------------------------------------------
C* DEFINE BEDPLATE-BLOCK SURFACE GAP ELEMENTS
C*---------------------------------------------------------
ACTSET,EG,8
ACTSET,RC,8
NL_GSAUTO,0,34,0,4,12,8,1

C*****************************************************************
C*******************  SOLUTION CONTROL  *******************
C*****************************************************************

C*---------------------------------------------------------
C*DEFINE SOLUTION CONTROL-FORCE
C*---------------------------------------------------------
CURDEF,TIME,1,1,0,0,2,0.01,100,1,110,1
FCR,31,FY,-80,31,1;
NL_CONTROL,0,1,

C*---------------------------------------------------------
```

```
C*DEFINE SOLUTION CONTROL-DISPLACEMENT (use either force or displacement, not both, comented
out)
C*-------------------------------------------------------
C*CURDEF,TIME,1,1,0,0,1,-.010,100,-0.017, 110,-0.017,
C*PCR,31,1,31,1,1,4
C*TIMES,0,110,1,
C*NL_CONTROL,1,1,431,UY,


C*****************************************************************
C******************  THERMAL CHANGE  *******************
C*****************************************************************
CURDEF,TIME,3,1,0,70,100,70,110,302
NTSF,1,1,13,1;
TREF,70;

C*-------------------------------------------------------
C* SET UP NONLINEAR ANALYSIS
C*-------------------------------------------------------

TIMES,0,100,1,
A_NON,S,1,1,100,0.0001,0,T,0,0,1E+010,0.0001,0.01,0,0.0,0,
NL_AUTO,1,1E-008,5,100,
STRAIN_OUT,1,1,1,1,1,1

C*************************************************************************
C***************  CONE COORDINATE SYSTEM  ****************
C*************************************************************************

CSANGL,3,0,0,0,0,0,0,58,0
ACTSET,CS,3
CSPLOT,3,3,1
ACTSET,CS,1


C*************************************************************
C*******************  RUN ANALYSIS  *********************
C*************************************************************
R_NON
```

Appendix D

GENERAL QUASI-KINEMATIC COUPLING PATENT

One of the most important steps in product development is the procurement of a patent to protect one's intellectual property. Therefore, the patent for the generic Quasi-Kinematic Coupling has been included. This patent is still pending, hence the claims have been omitted. The patent should issue by January, 2001 at which time the claims will be public knowledge, available at the library in each state capital or via the web.

Note that Appendix E contains a similar patent. The two are separate as they describe two distinct inventions. The patent in this Appendix covers the QKC in general, for all applications. The patent in the following Appendix is more specific, in that it covers an application to automotive assemblies.

On a side note, writing a patent is a very valuable experience for an engineer. It forces one to think about the economic and business side of design. This also saves money as the engineer (who is more familiar with the invention) can write a patent in a short amount of time (this patent took 10 days) compared to a patent attorney who might take several weeks at several hundred dollars per hour. This is the third patent the author has written.

QUASI-KINEMATIC COUPLING AND METHOD FOR USE IN ASSEMBLING AND LOCATING MECHANICAL COMPONENTS AND THE LIKE

TECHNICAL FIELD

The present invention relates to the coupling of mechanical component parts, surfaces or assemblies and the like (hereinafter sometimes generically termed "components"), where low cost and repeatable coupling are desired, as, for example, in applications and processes involving machine tool fixtures and other general assembly applications.

BACKGROUND

Better precision at lower cost is a major driving force in design and manufacturing. Traditionally, precision assemblies have used precision pins and holes for part alignments; but the demands of manufacturing processes have now pushed performance requirements beyond the approximately ten micron repeatability limits of such techniques. Next generation assemblies, such as, for example, machining fixtures, require low cost methods of assembly with consistently better than ten microns repeatability. The present invention is accordingly directed to a fundamentally new kinematic coupling, termed here a "quasi-kinematic" coupling, which meets the more stringent demands of these processes.

While certain types of prior kinematic couplings have been used to provide affordable sub-micron repeatability, their operation generally leaves gaps between the mated components, and they are therefore not well-suited for those types of precision assembly applications that require contact or sealing, such as in casting. This problem has been addressed in part by compliant kinematic couplings as described in US Patent No. 5,678,944, Flexural Mount Kinematic Coupling and Method, of common assignee Advanced Engineering Systems Operation and Products (AESOP) Inc. herewith. These types of couplings kine-

matically locate components and then allow translation parallel to the mating direction until contact is made between the desired surfaces. Though constituting a significant improvement, such couplings are not ideally suited for use in high volume manufacturing and assembly processes, due to the cost of manufacturing and assembling the flexural and kinematic components. Another limitation of these couplings resides in their inability to be arranged so that most of the resistance to error-causing loads is aligned in a common direction, while maintaining high stiffness in an orthogonal direction.

The present invention, on the other hand, as later more fully explained, overcomes such limitations by using conical shaped grooves with relieved sides which can direct a desired portion of their error resistance along a direction without seriously compromising the resistance to error in an orthogonal direction. Accomplishing this function in prior classical or flexural kinematic couplings is not achievable since their use of conventional straight V grooves leaves one degree of freedom and with very low stiffness.

In further US Patent No. 5,769,554, also of common assignee, an invention is described for use in sand casting and similar applications which incorporates kinematic elements into parts of the mold in a manner that admirably solves this problem, though only for low precision or sand mold assemblies and the like. The use of this coupling in large scale assembly and locating applications is, however, somewhat limited due to the fact that the kinematic elements must be pre-formed into the components. This technique, therefore, is not well suited for coupling situations requiring precision assemblies where machining of the mating surfaces is required, more specifically, in high precision assembly activities where the mating of the components is dependent upon the depth and size of the kinematic elements (i.e. grooves.) For such higher precision assemblies, this geometric relationship is sensitive enough that the capability of net shape manufacturing processes is insufficient to hold the relation between the kinematic features and the mating surface. While this problem may be addressed by machining the contact surfaces of the mated components, this would destroy the geometric relationship initially imparted to the components by the net shape process, nullifying the advantage of pre-formed elements.

In the absence of the ability to form, as, for example, by casting these kinematic features, they must be machined. Machining straight grooves into components requires translation motion in a minimum of two directions; depth perpendicular to the mating surface and translation in a direction contained in the plane defined by the contact surface. In comparison, the present invention, through using the principle of said patents, also introduces a novel way to form quasi-kinematic elements during a simple plunge operation using a rotating form tool, further providing a low cost method to manufacture these elements while simultaneously machining other features into the mated components.

OBJECTS OF THE INVENTION

An object of the present invention, accordingly, is to provide a new and improved low cost quasi-kinematic coupling and method which enable repeatably locating two or more components, surfaces, or assemblies or the like without any of the above-described or other limitations of prior couplings.

A further object is to provide such a novel coupling in which opposing surfaces of the components are allowed to come into intimate contact and form a sealable joint, and wherein repeatability is less sensitive to errors in the relative placement of the kinematic elements, and with the transverse stiffness of the coupling decoupled from the transverse quasi-kinematic coupling stiffness by relying on the resistance to motion due to friction between the surfaces of the mated components, and the stiffness of the coupling in the mated direction is decoupled from the quasi-kinematic coupling stiffness by relying on the resistance to motion due to a clamping force and the contact of the mated surfaces.

Another object of the invention is to provide a quasi-kinematic coupling in which the orientation of its kinematic elements can be set to provide maximum resistance to error-causing loads in a plane perpendicular to the mating direction, while maintaining resistance to motion in the same plane, but perpendicular (orthogonal) to the sensitive direction.

Other and further objects will be explained hereinafter and are more fully delineated in the appended claims.

SUMMARY

In summary, from one of its important aspects, the invention embraces a method of quasi-kinematic coupling of two matable components with repeatable location alignment of their mating surfaces, that comprises, providing the mating surfaces with correspondingly disposed respective sets of three grooves and corresponding mating protrusions, each of the grooves and protrusions being formed as surfaces of revolution, bringing the mating surfaces together to establish six lines of groove-protrusion contact, two lines at each mating groove and protrusion, and with a small gap maintained between the two components mating surfaces; and clamping by forcing the components together to seat the protrusions in the grooves and seal the gap to effect the coupling with the two component mating surfaces in contact.

This invention is a fundamentally new kinematic coupling for use in precision alignment of product components, tooling, and fixtures and the like which require a repeatable, low cost manufacturing and assembly process, and it incorporates conical grooves, sometimes with accompanying side reliefs, into one mated component and spherical members into the other component. These elements can either be machined directly into the mating components or attached to them. This is herein described as "quasi-kinematic" because the relative position of the mated components is defined by six lines of contact at the kinematic interfaces, as distinguished from six points of contact used in a true kinematic coupling. The line contact results from mating two surfaces of revolution, the conical groove and the spherical peg.

The six lines of contact (two at each sphere-groove interface) act to define the six relative degrees of freedom between the mated components. This is a weakly over-constrained

system that still effectively acts like a kinematic coupling. The interface is designed such that a small gap is left between the contacting surfaces in order to ensure the kinematic nature of the joint. A force is then applied to properly seat the spherical members in the grooves. Specific compliance characteristics can be designed into the kinematic elements, making it possible for them to deform under additional preload, even to the point where the opposed surrounding planar surfaces touch. When the clamping force is released, all or a fraction of the gap is restored through elastic or resilient recovery of the kinematic element material, thus ensuring that the next mate will still be quasi-kinematic.

The coupling is readily designed or incorporated into existing parts since the kinematic elements can be made by simple, low cost manufacturing processes. Its application is especially suited to applications which have traditionally heretofore used pinned joints, including many medium and large scale manufacturing processes such as casting, assembly, and fixturing.

Preferred and best mode design and operation methods are hereinafter detailed.

DRAWINGS

The aforementioned invention will now be described with reference to the accompanying drawing in which:

FIG. 1 is an illustration of a generic quasi-kinematic coupling constructed in accordance with a preferred embodiment of the invention;

FIG. 2 is a detail of a generic quasi-kinematic spherical element;

FIG. 3 is a detail of a hollow center crowned peg that allows a preload bolt to pass through it center;

FIG. 4 is a detail of a generic quasi-kinematic conical groove;

FIG. 5 is a two-dimensional view of several quasi-kinematic grooves with different contact angles;

FIG. 6 is a cross section of a generic quasi-kinematic joint clamped together by a bolt;

FIG. 7 details the contact lines in a quasi-kinematic coupling's conical groove;

FIG. 8 shows a tool which can simultaneously machine a conical groove and drill a hole;

FIG. 9 shows side reliefs of a conical groove cast in prior to the machining of the seats;

FIG. 10 shows a conical groove with cast in side reliefs after machining with a form tool;

PREFERRED EMBODIMENT(S) OF THE INVENTION

FIG. 1 shows the open coupling 2-4 of the invention in its generic form. The coupling consists of three spaced conical grooves 3a, 3b, and 3c attached to or machined into the inner surface 25 of the first (lower) component 4, and three corresponding spherical peg or protruding elements 1a, 1b, and 1c attached or machined into the opposing or inner surface 26 of the second (upper) component 2, FIGs. 1 and 2. When such a coupling is initially mated, each spherical protrusion element 1a, 1b, and 1c contacts its corresponding conical groove 3a, 3b, and 3c, and surfaces 25 and 26 will be parallel and separated by a small gap.

This contact takes place on seats of the conical grooves, as shown at 7a and 7b for the illustrative groove 3a, in FIG. 4 and FIG. 7. The contact can be modeled as along lines 17a and 17b, FIG. 7, since the surfaces of the spherical elements 1a, 1b, and 1c and the surfaces of the conical grooves 3a, 3b, and 3c are surfaces of revolution. With each conical groove 3a, 3b, and 3c having reliefs 8a and 8b at the appropriate location, the contact areas can be made to resemble those of a kinematic coupling.

FIG. 5 shows four views of conical grooves with varying contact angles (θ_0, θ_1, θ_2, θ_3) at 59a, 59b, 59c, and 59d, respectively. As the contact angle of the seats 10a, 10b, 10c, and 10d increases, as by decreasing relief zones 11a, 11b, 11c, and 11d, respectively, the coupling becomes more like a deterministic kinematic coupling. The benefit of reducing the contact angle 59 is limited by the contact stress, which increases with decreasing contact angle Q.

The resulting contact defines a near kinematic or "quasi-kinematic" definition of six degrees of freedom between the first component 2 and second component 4, as before described. Practically, due to manufacturing errors, only a portion of the seats 7a and 7b in a joint will contact the surface of the spherical member, such as the member 1a shown in FIG. 3. This situation, in addition to friction forces at the sphere-groove contact interface, can prevent the first component 2 from settling into its most stable equilibrium. This can further be prevented with a preload force (schematically shown as F in FIG. 1) that is ideally parallel to the mating direction and large enough to overcome the contact friction and properly seat the spherical member 1a in its groove 3a. Once the preload is applied, the coupling defines a repeatable mate. In addition, if the mating of the opposed faces 25 and 26 of components 4 and 2 respectively, is desired, compliance characteristics (elastic and plastic) can be designed into the kinematic elements 1a, 1b, 1c, 3a, 3b, and 3c so that additional preload force causes them resiliently to deform and allow the opposing surfaces 25 and 26 to contact, thereby forming a sealable joint.

Depending upon several factors, including the manufacturing capability of the machines used to make and locate the kinematic elements 1a, 1b, 1c, 3a, 3b, and 3c, shown generically in FIG. 1, the size of the mated gap 60 seen in the cross section in FIG. 6, will vary. Ideally, the gap variation will be such that mating of the opposed surfaces 25 and 26 will require only elastic deformation of the kinematic elements 1a, 1b, 1c, 3a, 3b, and 3c. However, when the manufacturing process is not capable of holding the required tolerances, plastic deformation of the kinematic elements 1a, 1b, 1c, 3a, 3b, and 3c may occur. In either case, after the initial mate, the material in the kinematic elements 1a, 1b, 1c, 3a,

3b, and 3c will recover elastically, restoring a portion of the initial gap 60. This is necessary to maintain the quasi-kinematic nature of the joint for future mating sequences.

The present invention provides a low cost alternative to prior methods. A quasi-kinematic coupling of the invention can readily use for example three conical grooves 35a, 35b, and 35c machined into a block and three crowned pegs pressed into a mating component. A crowned peg 1a, as shown in FIG. 3, can be inexpensively made as a semi-precision piece in a turning operation. Since conical grooves and press fit holes can be created by revolving tools, their placement is well suited, but not limited, to be aligned with features which are manufactured by revolving tools (i.e. drilled holes.) This allows the simultaneous machining of the conical grooves and additional features with a form tool 31 shown in FIG. 8. The form tool 31 can also be used in conjunction with pre-cast reliefs 22a and 22b, shown in FIG. 9, to form the joint seen in FIG. 10.

FIG. 3 and FIG. 4 show holes 50a and 49a in the kinematic elements through which bolts can pass. In addition, the joints should be located over features which form the largest triangle that will fit within the perimeter of the components. This is desired to provide maximum resistance to the torsion loads induced by the friction between the head(s) of the bolt(s) 12 and the surface of the component 2 which is bolted on.

As shown in FIG. 9, the pre-machined reliefs 22a and 22b can be economically manufactured by casting. This is permissible as the depth of the reliefs 22a and 22b need not be precisely located with respect to the mated surface 25. In addition, if the position of reliefs 22a, and 22b in the plane of the mated surface 25 is on the order of the capabilities of most the casting processes, it will not have a significant effect on the repeatability of the coupling.

Important design parameters of the quasi-kinematic joint of the invention will now be examined with reference to FIGS. 3, 4, 5, and 6. The two radii of the spherical member 1a, for example, the two radii of the corresponding conical groove 3a, the seat contact angle 59 (Q), the depth of the conical groove 3a, the depth of the side reliefs 8a and 8b,

and the materials used for the peg 1a and conical groove 3a are the most important parameters. With reference to FIG. 6, it has earlier been stated that quasi-kinematic couplings of the invention initially have a small gap 60 between the mating surfaces 25 and 26. This might, for example, be on the order of 0.10 mm, more or less. It is desired to choose the design parameters such that the gap 60 is not so large as to cause the surface of the spherical element such as 1a, to undergo plastic deformation during mating. If this is not avoided, the edges of the groove seats 62a, 62b, 62c, and 62d will leave indentations in the surface of the spherical element 1a, etc. This will adversely affect the repeatability of the coupling as during re-mating, the indentations will catch at random locations on the edges of the conical grooves 62a, 62b, 62c, and 62d. The result is an additional error in the location of the kinematic coupling which may not be correctable by additional preload. Choosing materials such that the spherical member 1a is harder than the conical groove 3a and optimizing the dimensions of the kinematic elements via finite element analysis are thus recommended.

Another important design consideration is the clamping force F. The clamping load and coefficient of friction should be chosen to provide an adequate friction force to resist all applied loads, even if the kinematic components were absent. In certain applications, a glue or sealing agent can be introduced between the mated components which will act to seal the interface or maintain joint position.

Transverse stiffness of the coupling is decoupled through the resistance to motion due to friction between the mating surfaces and the stiffness in the direction of mating is decoupled through the resistance to motion due to the clamping force and the contact of the mated surface.

In some applications where a kinematic joint is used coaxial with a tapped hole, an additional relief 45 may be required, as illustrated in FIG. 6. The deformation in the first threads 53 of the taped hole can cause deformation in the groove seats 63a and 63b. To avoid this, the threads 53 should start far enough from the seats 63a and 63b so that the

deformation in the threads 53 does not affect the geometry of the seats 63a and 63b. If space is limited, finite element analysis is well suited to determine the minimum size of the relief needed to accomplish this.

Quasi kinematic couplings of the invention have many benefits over traditional kinematic couplings and other alignment methods, such as pinned joints, as earlier pointed out. They are less expensive to manufacture than many pinned joints since the kinematic elements require little precision machining and can be made with standard manufacturing processes. This, in conjunction with fewer components, make their use more economical and less complex than pinned joints. When comparing repeatability, a quasi-kinematic coupling constructed in accordance with the present invention, such as shown in FIG. 1, can attain 1 micron repeatability at a fraction of the cost of a pinned joint, which is typically only capable of five - ten micron repeatability. In addition, quasi-kinematic coupling joint placements are less sensitive to misalignment, since a spherical element, such as 1a, can easily fit into a conical hole 3a which is somewhat misaligned; then, through elastic/plastic deformation, make it conform during the initial mate. Increased clamping force F causes the surfaces 25 and 26 to touch without a loss of relative repeatability, thereby allowing the joint to be sealed. In comparison, the pinned joint method is intolerant and incapable of eliminating initial misalignment. Another benefit is that clamping the components together in a quasi-kinematic coupling, forces each spherical element into a conical groove, thereby inducing a centering effect which forces the mated components 2 and 4 into a best overall position. When using the pinned joint method, on the other hand, a centering effect does not occur.

In alternative embodiments, this coupling may also be used, as before stated, in the precision alignment of product components, parts to machine tool fixtures, machine tool fixtures to machines, casting molds and the like. In some applications, the three sets of mating conical grooves and spherical plugs are spaced to form a symmetrical equilateral or substantially equilateral triangle as in FIG. 1, for example; whereas in other applications, particularly where the structure of the mating components does not permit such

symmetrical spacing, other and non-symmetrical spacing geometries may also be used. Other variations, modifications, and other implementations of what is described herein will also occur to those of ordinary skill in the art without departing from the spirit and the scope of the invention as claimed. Accordingly, the invention is to be defined not just by the preceding illustrative description, but instead by the spirit and scope of the following claims.

What is claimed is:

CLAIMS

This patent is still pending, therefore the claims must be omitted for confidentiality.

ABSTRACT

A quasi-kinematic coupling for mating components (mechanical parts, surfaces, assemblies and the like) employing mating sets of surface of revolution, (conical) grooves and cooperative surface of revolution (spherical/conical) protrusions for establishing six lines (not just prior points) of contact at the kinematic interfaces, and with elastic compliance therebetween and preferably with relief features to define the effective orientation as a clamping force seats the protrusions in the grooves and seals the component mating surfaces into contact.

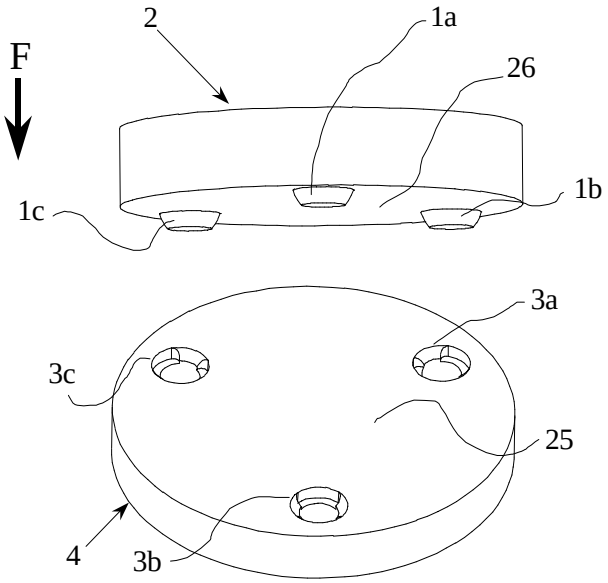


FIG. 1

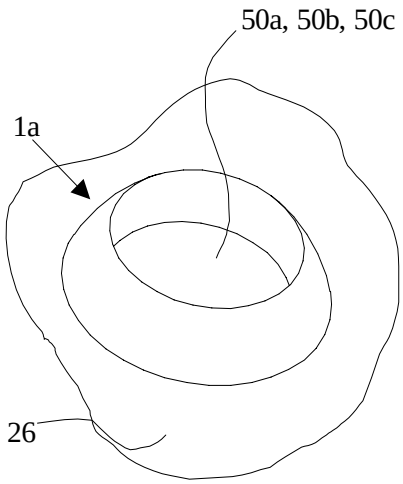


FIG. 2

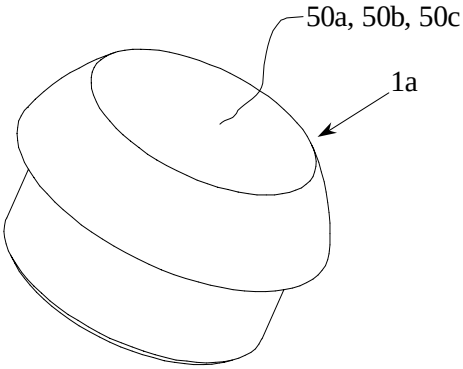


FIG. 3

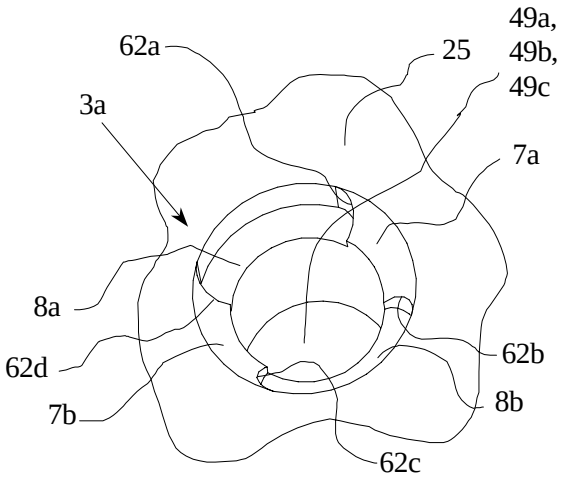


FIG. 4

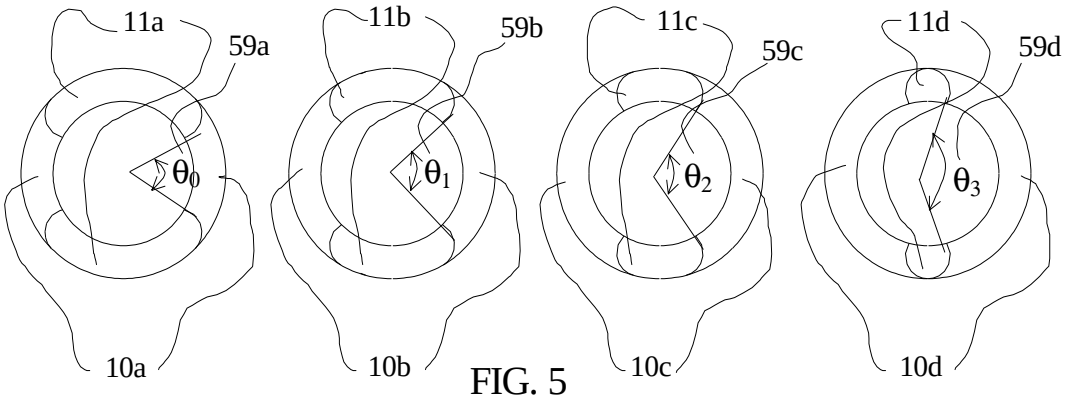


FIG. 5

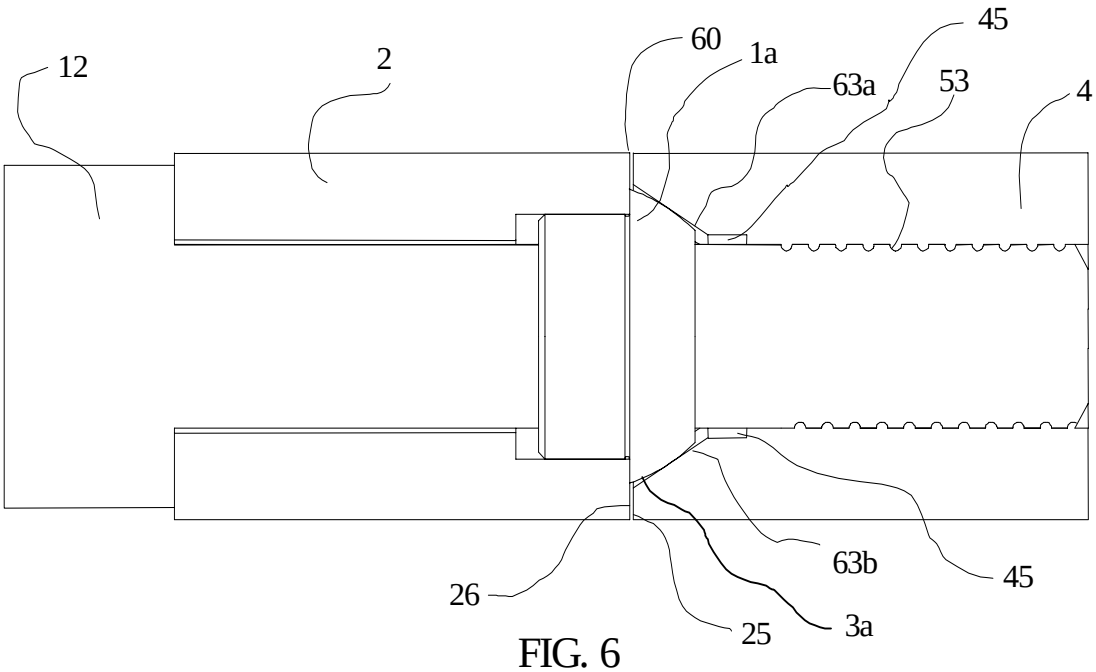


FIG. 6

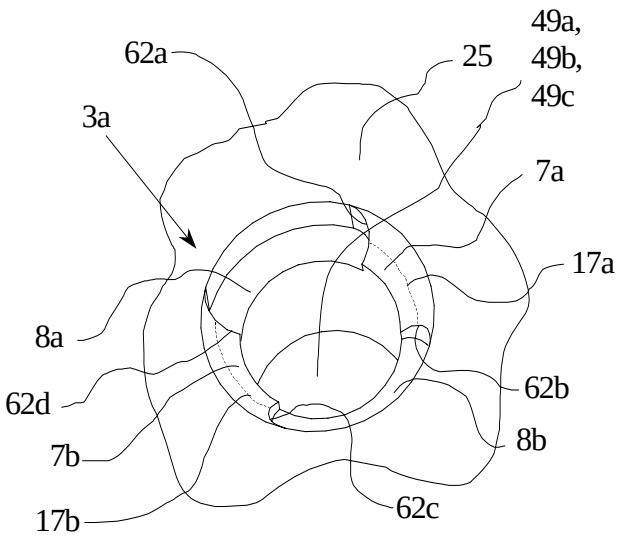


FIG. 7

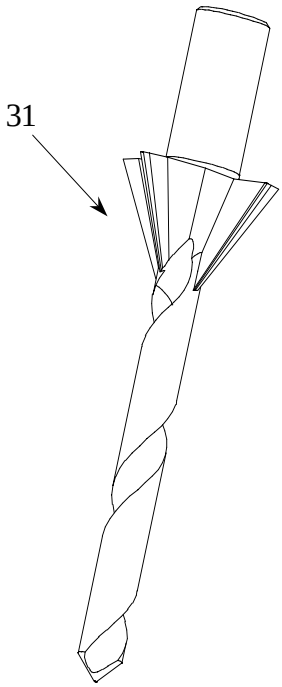


FIG. 8

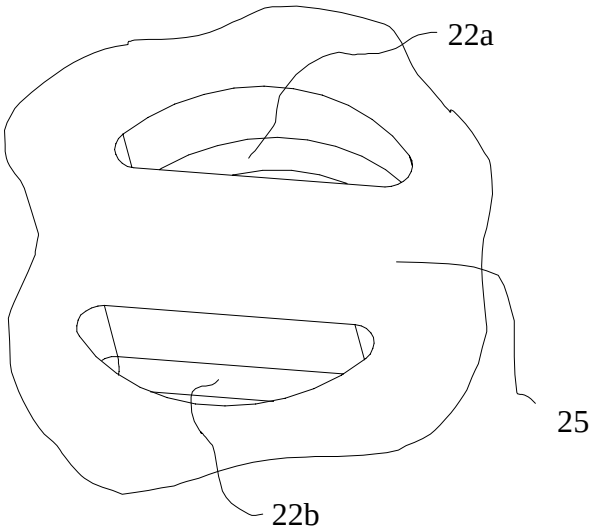


FIG. 9

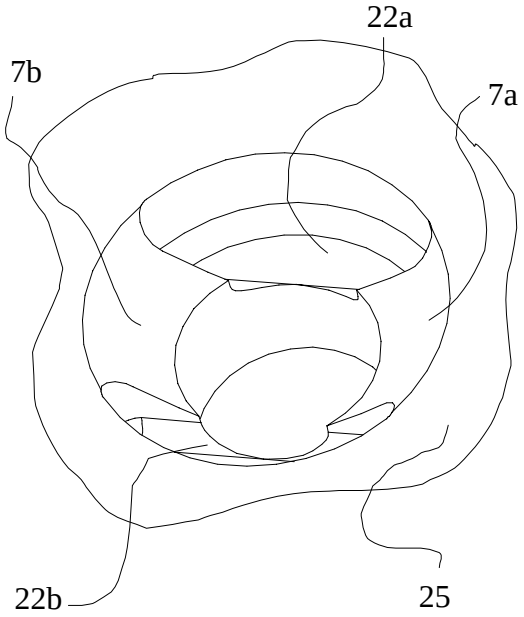


FIG. 10

Appendix E

AUTOMOTIVE QUASI-KINEMATIC COUPLING PATENT

This patent is still pending, hence the claims have been omitted. The patent should issue by January, 2001 at which time the claims will be public knowledge, available at the library in each state capital or via the web.

Note that Appendix D contains a similar patent. The two are separate as they describe two distinct inventions. The patent in Appendix D covers the QKC in general, for all applications. The patent in this Appendix is more specific, in that it covers an application, use in automotive assemblies.

QUASI-KINEMATIC COUPLING AND METHOD FOR USE IN ASSEMBLING AND LOCATING ENGINE VEHICLE COMPONENTS AND THE LIKE

TECHNICAL FIELD

The present invention relates to the coupling of mechanical component parts, surfaces or assemblies and the like (hereinafter sometimes generally termed “components”), where low cost and repeatable coupling are desired, particularly, in applications and processes involving the manufacture and assembly of automobile or similar engines, and the like.

BACKGROUND

Better precision at lower cost is a major driving force in design and manufacturing. Traditionally, precision assemblies have used precision pins and holes for part alignments; but the demands of manufacturing processes have now pushed performance requirements beyond the approximately ten micron repeatability limits of such techniques. Next generation assemblies, such as, for example, automotive assemblies and machining fixtures, require low cost methods of assembly with consistently better than ten microns repeatability. The present invention is accordingly directed to a fundamentally new kinematic coupling, termed here a “quasi-kinematic” coupling, which meets the more stringent demands of these processes.

While certain types of prior kinematic couplings have been used to provide affordable sub-micron repeatability, their operation generally leaves gaps between the mated components, and they are therefore not well-suited for those types of precision assembly applications that require contact or sealing, such as in casting. This problem has been addressed in part by compliant kinematic couplings as described in US Patent 5,678,944, Flexural

Mount Kinematic Coupling Method, of co-assignee Advanced Engineering Systems Operation and Products (AESOP) Inc. These types of couplings kinematically locate components and then allow translation parallel to the mating direction until contact is made between the desired surfaces. Though constituting a significant improvement, such couplings are not ideally suited for use in high volume manufacturing and assembly processes, due to the cost of manufacturing and assembling the flexural and kinematic components. Another limitation of these couplings resides in their inability to be arranged so that most of the resistance to error-causing loads is aligned in a common direction, while maintaining high stiffness in an orthogonal direction.

The present invention, on the other hand, as later more fully explained, and as a specific application to vehicular engine assembly of the invention of U.S. Patent application Serial No. _____ , filed _____, entitled Quasi-Kinematic Coupling and Method For Use in Assembling and Locating Mechanical Components and the Like and also assigned to said AESOP, overcomes such limitations by using conical shaped grooves with relieved sides which can direct a desired portion of their error resistance along a direction without seriously compromising the resistance to error in an orthogonal direction. Accomplishing this function in prior classical or flexural kinematic couplings is not achievable since their use of conventional straight V grooves leaves one degree of freedom and with very low stiffness.

In further, US Patent No. 5,769,554, also of common assignee, an invention is described for use in sand casting and similar applications which incorporates kinematic elements into parts of the mold in a manner that admirably solves this problem, though only for low precision or sand mold assemblies and the like. The use of this coupling in large scale assembly and locating applications is, however, somewhat limited due to the fact that the kinematic elements must be pre-formed into the components. This technique, therefore, is not well suited for coupling situations requiring precision assemblies where machining of the mating surfaces is required as with automobile engine components; more specifically, in high precision assembly activities where the mating of the components is dependent

upon the depth and size of the kinematic elements (i.e. grooves.) For such higher precision assemblies, this geometric relationship is sensitive enough that the capability of net shape manufacturing processes is insufficient to hold the relation between the kinematic features and the mating surface. While this problem may be addressed by machining the contact surfaces of the mated components, this would destroy the geometric relationship initially imparted to the components by the net shape process, nullifying the advantage of pre-formed elements.

In the absence of the ability to form, as, for example, by casting these kinematic features, they must be machined. Machining straight grooves into components requires translation motion in a minimum of two directions; depth perpendicular to the mating surface and translation in a direction contained in the plane defined by the contact surface. In comparison, though the present invention is based upon, uses, and embraces the principles of said patents and of said co-pending application, it introduces a novel design which orients the kinematic elements in a way which enhances the stiffness in a desired sensitive direction without substantially degrading the repeatability in the non-sensitive orthogonal direction.

OBJECTS OF THE INVENTION

An object of the present invention, accordingly, is to provide a new and improved low cost quasi-kinematic coupling and method which enable repeatably locating two or more vehicle components, surfaces, or assemblies or the like without any of the above-described or other limitations of prior couplings.

A further object is to provide such a novel coupling in which opposing surfaces of the engine components or the like are allowed to come into intimate contact and form a sealable joint, and wherein repeatability is less sensitive to errors in the relative placement of the kinematic elements, and with the transverse stiffness of the coupling decoupled from the transverse quasi-kinematic coupling stiffness by relying on the resistance to motion due to friction between the surfaces of the mated components, and the stiffness of the coupling in the mated direction is decoupled from the quasi-kinematic coupling stiffness by

relying on the resistance to motion due to a clamping force and the contact of the mated surfaces.

Another object of the invention is to provide a quasi-kinematic coupling of engine components and the like in which the orientation of its kinematic elements can be set to provide maximum resistance to error-causing loads in a plane perpendicular to the mating direction, while maintaining resistance to motion in the same plane, but perpendicular (orthogonal) to the sensitive direction.

Other and further objects will be explained hereinafter and are more fully delineated in the appended claims.

SUMMARY

In summary, from one of its important aspects, the invention embraces a method of quasi-kinematic coupling of two matable vehicle engine components with repeatable location alignment of their mating surfaces, that comprises, providing the mating surfaces with correspondingly disposed respective sets of three non-symmetrically space grooves and corresponding mating protrusions, each of the grooves and protrusions being formed as surfaces of revolution, bringing the mating surfaces together to establish six lines of groove-protrusion contact, two lines at each mating groove and protrusion, and with a small gap maintained between the two components mating surfaces; and clamping by forcing the components together to seat the protrusions in the grooves and seal the gap to effect the coupling with the two component mating surfaces in contact.

This invention is a fundamentally new kinematic coupling for use in precision alignment of product components, tooling, and fixtures and the like which require a repeatable, low cost manufacturing and assembly process, and it incorporates conical grooves, sometimes with accompanying side reliefs, into one mated component and spherical members into the other component. These elements can either be machined directly into the mating

components or attached to them. This is herein described as “quasi-kinematic” because the relative position of the mated components is defined by six lines of contact at the kinematic interfaces, as distinguished from six points of contact used in a true kinematic coupling. The line contact results from mating two surfaces of revolution, the conical groove and the spherical peg.

The six lines of contact (two at each sphere-groove interface) act to define the six relative degrees of freedom between the mated components. This is a weakly over-constrained system that still effectively acts like a kinematic coupling. The interface is designed such that a small gap is left between contacting surfaces in order to ensure the kinematic nature of the joint. A force is then applied to properly seat the spherical members in the grooves. Specific compliance characteristics can be designed into the kinematic elements, making it possible for them to deform under additional preload, even to the point where the opposed surrounding planar surfaces touch. When the clamping force is released, all or a fraction of the gap is restored through elastic or resilient recovery of the kinematic element material, thus ensuring that the next mate will still be quasi-kinematic.

The coupling is readily designed or incorporated into existing parts since the kinematic elements can be made by simple, low cost manufacturing processes. Its application is especially suited to applications which have traditionally heretofore used pinned joints, including many medium and large scale manufacturing processes such as casting, assembly, and fixturing.

Preferred and best mode design and operation methods are hereinafter detailed.

DRAWINGS

The aforementioned invention will now be described with reference to the accompanying drawing in which:

FIG. 1 is an illustration of a generic quasi-kinematic coupling constructed in accordance with the invention of said co-pending application and the principles of which are used in the vehicle engine application of the present invention;

FIG. 2 is a detail of a generic quasi-kinematic spherical element;

FIG. 3 is a detail of a crowned peg used in the assembly of an internal combustion engine;

FIG. 4 is a detail of a generic quasi-kinematic conical groove;

FIG. 5 is a two-dimensional view of several quasi-kinematic grooves with different contact angles;

FIG. 6 is a cross section of a generic quasi-kinematic joint clamped together by a bolt;

FIG. 7 details the contact lines in a quasi-kinematic coupling's conical groove;

FIG. 8 shows a tool which can simultaneously machine a conical groove and drill a hole;

FIG. 9 shows side reliefs of a conical groove cast in prior to the machining of the seats;

FIG. 10 shows a conical groove with cast in side reliefs after machining with a form tool;

FIG. 11 shows the error caused by misalignment of the bore and bedplate center lines;

FIG. 12 shows an engine block equipped for use with a quasi-kinematic coupling in accordance with the present invention;

FIG. 13 shows an engine bedplate equipped for use with a quasi-kinematic coupling;

FIG. 14 is an exploded view of a generic reciprocating internal combustion engine;

FIG. 15 shows the elements of a typical pinned joint incorporated into an engine bedplate;

FIG. 16 is a three-dimensional view of half of an aligned quasi-kinematic coupling;

FIG. 17 is a two-dimensional view of half of an aligned quasi-kinematic coupling;

FIG. 18 is a three-dimensional view of the half of an aligned kinematic coupling;

FIG. 19 is a two-dimensional view of the half of an aligned kinematic coupling;

FIG. 20 is a schematic illustrating the most stable orientation of a kinematic coupling;

FIG. 21 is a schematic illustrating an unstable orientation of a kinematic coupling;

FIG. 22 is a view further clarifying the orientation of the kinematic components in FIG. 20; and

FIG. 23 is a similar view further clarifying the orientation of the kinematic components in FIG. 21.

FIG. 24 is a view which illustrates how a quasi-kinematic coupling can be used to define a repeatable mate between engine heads and blocks for the purposes of the present invention.

PREFERRED EMBODIMENT(S) OF THE INVENTION

FIG. 1 shows the open coupling 2-4 of the invention of said co-pending application in its generic form. The coupling consists of three spaced conical grooves 3a, 3b, and 3c attached to or machined into the inner surface 25 of the first (lower) component 4, and three corresponding spherical peg or protruding elements 1a, 1b, and 1c attached or machined into the opposing or inner surface 26 of the second (upper) component 2 , FIGS. 1 and 2. When such a coupling is initially mated, each spherical protrusion element 1a, 1b, and 1c contacts its corresponding conical groove 3a, 3b, and 3c, and surfaces 25 and 26 will be parallel and separated by a small gap.

This contact takes place on seats of the conical grooves, as shown at 7a and 7b for the illustrative groove 3a, in FIG. 4 and FIG. 7. The contact can be modeled as along lines 17a and 17b, FIG. 7, since the surfaces of the spherical elements 1a, 1b, and 1c and the surfaces of the conical grooves 3a, 3b, and 3c are surfaces of revolution. With each conical groove 3a, 3b, and 3c having reliefs 8a and 8b at the appropriate location, the contact areas can be made to resemble those of a kinematic coupling.

FIG. 5 shows four views of conical grooves with varying contact angles (θ_0, θ_1, θ_2, θ_3) at 59a, 59b, 59c, and 59d, respectively. As the contact angle of the seats 10a, 10b, 10c, and 10d increases, as by decreasing relief zones 11a, 11b, 11c, and 11d, respectively, the coupling becomes more like a deterministic kinematic coupling. The benefit of reducing the contact angle 59 is limited by the contact stress, which increases with decreasing contact angle Θ.

The resulting contact defines a near kinematic or "quasi-kinematic" definition of six degrees of freedom between the first component 2 and second component 4, as before described. Practically, due to manufacturing errors, only a portion of the seats 7a and 7b in a joint will contact the surface of the spherical member, such as the member 1a shown in FIG. 3. This situation, in addition to friction forces at the sphere-groove contact interface, can prevent the first component 2 from settling into its most stable equilibrium. This can further be prevented with a preload force (schematically shown as F in FIG. 1) that is ideally parallel to the mating direction and large enough to overcome the contact friction and properly seat the spherical member 1a in its groove 3a. Once the preload is applied, the coupling defines a repeatable mate. In addition, if the mating of the opposed faces 25 and 26 of components 4 and 2 respectively, is desired, compliance characteristics (elastic and plastic) can be designed into the kinematic elements 1a, 1b, 1c, 3a, 3b, and 3c so that additional preload force causes them resiliently to deform and allow the opposing surfaces 25 and 26 to contact, thereby forming a sealable joint.

Depending upon several factors, including the manufacturing capability of the machines used to make and locate the kinematic elements 1a, 1b, 1c, 3a, 3b, and 3c, shown generically in FIG. 1, the size of the mated gap 60 seen in the cross section in FIG. 6, will vary. Ideally, the gap variation will be such that mating of the opposed surfaces 25 and 26 will require only elastic deformation of the kinematic elements 1a, 1b, 1c, 3a, 3b, and 3c. However, when the manufacturing process is not capable of holding the required tolerances, plastic deformation of the kinematic elements 1a, 1b, 1c, 3a, 3b, and 3c may occur. In either case, after the initial mate, the material in the kinematic elements 1a, 1b, 1c, 3a, 3b, and 3c will recover elastically, restoring a portion of the initial gap 60. This is necessary to maintain the quasi-kinematic nature of the joint for future mating sequences.

The use of this device is more clearly illustrated in the context of applications underlying the present invention such as the manufacture and assembly of reciprocating internal combustion engines, hereinafter referred to as RIC engines. FIG. 14 and FIG. 15 show the crankshaft 61, journal bearings 38a - 38j, alignment pins 32a - 32j, and fastening bolts 39a - 39t common to these types of engines. The crankshaft 61 is held between the journal bearings 38a - 38j which reside in the block 34 and the bedplate 30. In either case, during operation, the rotation of the crank 61 induces a pressurized oil film in the gap between the crank shaft 61 and main bearings 38a - 38j. There is an optimal gap (on the order of 0.01 to 0.10 mm) between the bearings 38a - 38j and the crank shaft 61 which results in a minimum coefficient of friction for a particular design. Deviation from the optimal gap results in an increased coefficient of friction and increased power loss.

As the relative location and size of the half bores 29a - 29e and 37a - 37e seen in FIG. 12 and 13 are critical, many RIC engines are manufactured by clamping the block 34 and bedplate 30 together, then simultaneously machining the bearing bore halves 29a - 29e and 37a - 37e. Later, the block 34 and bedplate 30 must be disassembled for crank shaft 61 and main bearing 38a - 38j installation, then reassembled. Error in relocating the bedplate 30 and block 34 results in a departure from the nominal gap between the journal bearings 38a - 38j and crank shaft 61. The allowable misalignment 64 seen in FIG. 11 between the

block bore center line 27 and bedplate bore center line 28 is quantified by specifications on the order of five microns.

FIGS. 14 and 15 show a traditional pinned joint often used to locate the block 34 and bedplate 30. The pins 32a - 32j are fitted into corresponding holes in the block 34. Often, good repeatability can only be achieved with the elastic averaging effect achieved with a multiplicity of pinned joints (8 or more.) This makes manufacture of the joints difficult as the location of the hole patterns in each component as well as the relative location of the individual holes must be held to tight tolerances (on the order of 0.02 mm). Many manufacturing operations which machine these features have high scrap or re-work rates due to the difficulty of holding these tolerances. Other methods for defining position such as slotted joints and V in flats can be used; such, however are grossly over-constrained and their performance is susceptible to contaminants.

The present invention provides a low cost alternative to these prior methods. A quasi-kinematic coupling of the invention can readily be incorporated into RIC engines in many ways, one of which is shown in FIG. 12 and FIG. 13. Three conical grooves 35a, 35b, and 35c are thereshown be machined into the block 34 and three crowned pegs 33a, 33b, 33c are pressed into corresponding holes in the bedplate 30. A crowned peg 1a, as shown in FIG. 3, can be inexpensively made as a semi-precision piece in a turning operation. Since the conical grooves 35a, 35b, and 35c and press fit holes can be created by revolving tools, their placement is well suited, but not limited, to be aligned with features which are manufactured by revolving tools (i.e. drilled holes.) This allows the simultaneous machining of the conical grooves 35a, 35b, and 35c and additional features with a form tool 31 shown in FIG. 8. In the case of an RIC engine, the placement of the joints is best suited to be coaxial with the bolt holes used to hold the components together. The form tool 31 can also be used in conjunction with pre-cast reliefs 22a and 22b, shown in FIG. 9, to form the joint seen in FIG. 10. The structures of the engine components-to-be-mated invariably provide non-symmetrical spacings amongst the three grooves and the corresponding three pegs or

protrusions, and do not lend themselves to symmetrical equilateral spacings as, for example, in the illustration of FIG. 1.

FIG. 3 and FIG. 4 show holes 50a and 49a in the kinematic elements through which bolts such as 39a (FIG. 14) can pass. In addition, the joints should be located over features which form the largest triangle that will fit within the perimeter of the components. This is desired to provide maximum resistance to the torsion loads induced by the friction between the heads of the bolts 39a, etc. and the lower surface 71 of the bedplate 30. The areas for this interface can most clearly seen in FIG. 14.

As shown in FIG. 9, the pre-machined reliefs 22a and 22b can be economically manufactured by casting. This is permissible as the depth of the reliefs 22a and 22b need not be precisely located with respect to the mated surface 25. In addition, if the position of reliefs 22a, and 22b in the plane of the mated surface 25 is on the order of the capabilities of most the casting processes, it will not have a significant effect on the repeatability of the coupling. In FIGS. 12 and 13, for example, plastic deformation of the kinematic elements 33a, 33b, 33c, 35a, 35b, and 35c during the initial mating, forces alignment of the elements 33a, 33b, 33c, 35a, 35b, and 35c. Alternatively, one could machine in these features, but in most cases at substantial added cost.

With reference to FIG. 6, it has earlier been stated that quasi-kinematic couplings of the invention initially have a small gap 60 between the mating surfaces 25 and 26. In an RIC engine, this gap is on the order of 0.10 mm. FIGS. 12 and 13 show the spherical members 33a, 33b, and 33c which are seated in the grooves 35a, 35b, and 35c. After seating, a series of bolts 39a - 39t are tightened, forcing the mating faces 40a, 40b and 41a, 41b of the block 34 and bedplate 30 respectively together. As this happens, the pegs 33a, 33b, and 33c mate with the conical grooves 35a, 35b, and 35c. Depending on system dimensions and bolt forces applied, some plastic yielding may occur. The machining of the engine then proceeds as normal. When the components are disassembled for crank shaft 61 and main bearing 38a - 38j installation, part or all of the initial gap 60 is restored

through elastic recovery. Whether the whole or a fraction of the gap 60 is restored depends on the nature of the initial deformation. If the deformation was purely elastic, all of the initial gap 60 will be recovered. If the initial deformation was elastic and plastic, only a fraction of the gap 60 will be recovered. Restoration of gap 60 is, however, necessary to maintain the quasi-kinematic nature of the coupling by insuring that the mating surfaces 40a, 40b, 41a, and 41b do not contact before the pegs 33a, 33b, 33c and conical grooves 35a, 35b, 35c. After the bearings 38a - 38j are installed in the engine, the block 34 and bedplate 30 are mated again and fastened together.

Important design parameters of the quasi-kinematic joint of the invention will now be examined with reference to FIGS. 3, 4, and 5. The two radii of the spherical member 1a, for example, the two radii of the corresponding conical groove 3a, the seat contact angle 59 (Θ), the depth of the conical groove 3a, the depth of the side reliefs 8a and 8b, and the materials used for the peg 1a and conical groove 3a are the most important parameters. It is desired to choose the design parameters such that the surface of the spherical element such as 1a, does not undergo plastic deformation. If this is not avoided, the edges of the groove seats 62a, 62b, 62c, and 62d will leave indentations in the surface of the spherical element 1a, etc. This will adversely affect the repeatability of the coupling as during re-mating, the indentations will catch at random locations on the edges of the conical grooves 62a, 62b, 62c, and 62d. The result is an additional error in the location of the kinematic coupling which may not be correctable by additional preload. Choosing materials such that the spherical member 1a is harder than the conical groove 3a and optimizing the dimensions of the kinematic elements via finite element analysis are thus recommended.

Another important design consideration is the clamping force F. For instance, consider again the RIC engine shown in FIG. 14. During operation, there are loads induced by the normal operation of the engine which could cause relative movement between the block 34 and bedplate 30 if the joint between them was not suitably rigid. The components normal to the mated surfaces 40a, 40b, 41a, and 41b are counteracted by the force supplied by the bolts 39a - 39t and the force supplied by the contact between the surfaces 40a, 40b,

41a, and 41b. The loads which act to shear the two apart are counteracted by friction resistance between mated faces 40a, 40b, 41a, and 41b. The clamping load and coefficient of friction should be chosen to provide an adequate friction force to resist all applied loads, even if the kinematic components were absent. In certain applications, a glue or sealing agent can be introduced between the mated components which will act to seal the interface or maintain joint position.

Transverse stiffness of the coupling is decoupled through the resistance to motion due to friction between the mating surfaces, and the stiffness in the direction of mating is decoupled through the resistance to motion due to the clamping force and the contact of the mated surfaces.

In some applications where a kinematic joint is used coaxial with a tapped hole, an additional relief 45 may be required, as illustrated in FIG. 6. The deformation in the first threads 53 of the taped hole can cause deformation in the groove seats 63a and 63b. To avoid this, the threads 53 should start far enough from the seats 63a and 63b so that the deformation in the threads 53 does not affect the geometry of the seats 63a and 63b. If space is limited, finite element analysis is well suited to determine the minimum size of the relief needed to accomplish this.

Quasi kinematic couplings of the invention have many benefits over traditional kinematic couplings and other alignment methods, as earlier pointed out. For instance, as shown in FIG. 11, repeatability (minimizing the error 64) is only important in one direction perpendicular to the bore center lines 27 and 28 and contained in the plane of the mated surfaces 40a, 40b, 41a, and 41b . In a traditional kinematic coupling, the grooves are orientated as shown in FIGS. 20 and FIG. 22. Ideally, the tangents 54a, 54b, and 54c to the planes containing the normal force vectors 51a, 51b, 52a, 52b, 53a, and 53b bisect the angles of the coupling triangle (sides 67a, 67b, and 67c.) Were one to align the grooves as shown in FIGS. 18, 19, 21, and 23, the tangents 57a, 57b, and 57c to the planes containing the normal force vectors 55a, 55b, 56a, 56b, 57a, and 57b would be parallel, as shown in FIG. 21.

This would result in a coupling which is better able to resist error-causing loads in the y (sensitive) direction. This coupling, however, would not constrain motion in the orthogonal x direction. FIG. 16 and FIG. 17 representing three and two-dimensional views of half an aligned quasi-kinematic coupling, show the curved seats 65a, 65b, 65c, 65d, 65e, and 65f of a quasi-kinematic couplings wherein this curvature allows nominal orientation of the conical grooves 42a, 42b, and 42c, thus maximizing resistance to errors in the y (sensitive) direction without greatly compromising the resistance to motion in the x direction. This is compared with the designs of kinematic couplings shown in the corresponding three and two-dimensional views of FIG. 18 and 19.

Quasi-kinematic couplings also have other benefits over pinned joints. They are less expensive to manufacture since the kinematic elements require little precision machining and can be made with standard manufacturing processes. This, in conjunction with fewer components, make their use more economical and less complex than pinned joints. When comparing repeatability, a quasi-kinematic coupling constructed in accordance with the present invention, such as shown in FIG. 1, can attain 1 micron repeatability at a fraction of the cost of a pinned joint, which is typically only capable of five - ten micron repeatability. In addition, quasi-kinematic coupling joint placements are less sensitive to misalignment, since a spherical element, such as 1a, can easily fit into a conical hole 3a which is somewhat misaligned; then, through elastic/plastic deformation, make it conform during the initial mate. Increased clamping force F causes the surfaces 25 and 26 to touch without a loss of relative repeatability, thereby allowing the joint to be sealed. In comparison, the pinned joint method is intolerant and incapable of eliminating initial misalignment. Another benefit is that clamping the components together in a quasi-kinematic coupling, forces each spherical element into a conical groove, thereby inducing a centering effect which forces the mated components 2 and 4 into a best overall position. When using the pinned joint method, on the other hand, a centering effect does not occur.

In alternative embodiments, this coupling may also be used, as before stated, in the precision alignment of product components, parts to machine tool fixtures, machine tool fix-

tures to machines, casting molds, RIC engine blocks and heads and the like. Fig. 24 shows an example of an engine head 72 equipped with quasi-kinematic elements 71a, 71b, 71c that mate with corresponding quasi-kinematic grooves in the block 34. In this application, repeatable coupling is desired to minimize misalignment between the combustion chambers 73a, 73b, 73c, 73d and the cylinders in the block. Other applications in RIC engines include fuel injector components, manifold to block mates, and other areas where close fit tolerances or bearing clusters are required. Variations, modifications, and other implementations of what is described herein will also occur to those of ordinary skill in the art without departing from the spirit and the scope of the invention as claimed. Accordingly, the invention is to be defined not just by the preceding illustrative description, but instead by the spirit and scope of the following claims.

What is claimed is:

CLAIMS

This patent is still pending, therefore the claims must be omitted for confidentiality.

ABSTRACT

A quasi-kinematic coupling for mating vehicle engine components and the like employing mating sets of surface of revolution, (conical) unsymmetrically spaced grooves and cooperative surface of revolution (spherical/conical) protrusions for establishing six lines (not just prior points) of contact at the kinematic interfaces, and with elastic compliance therebetween and preferably with relief features to define the effective orientation as a clamping force seats the protrusions in the grooves and seals the component mating surfaces into contact.

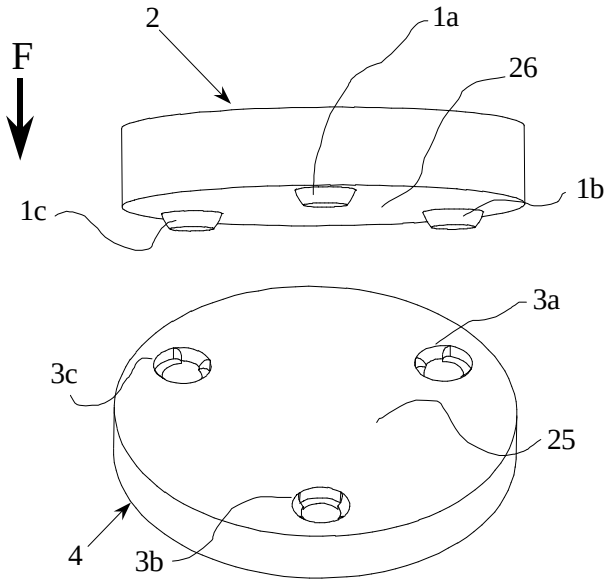


FIG. 1

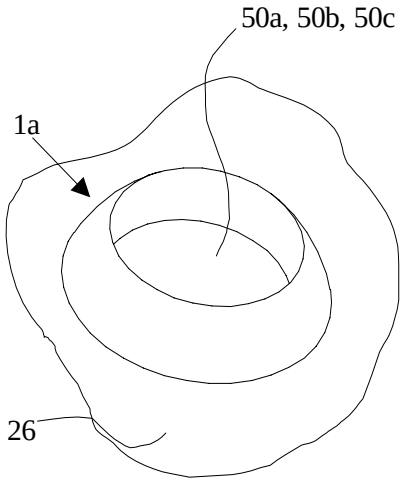


FIG. 2

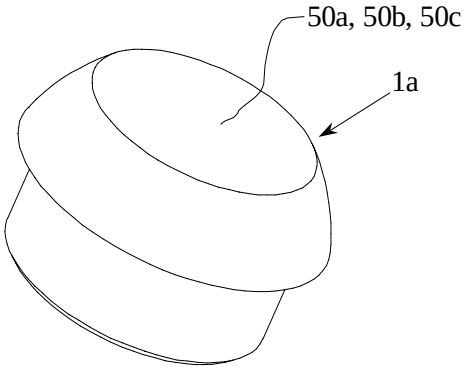


FIG. 3

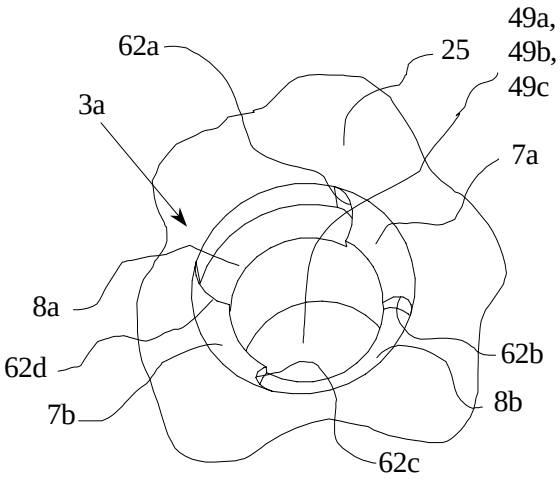


FIG. 4

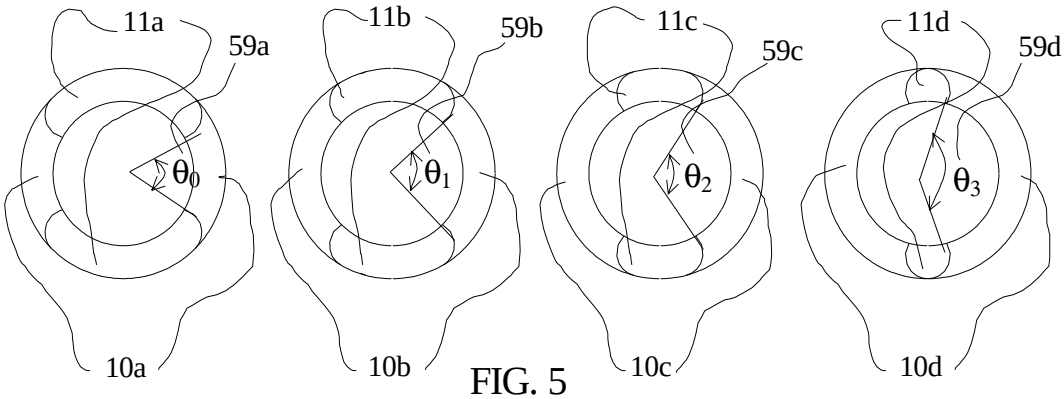


FIG. 5

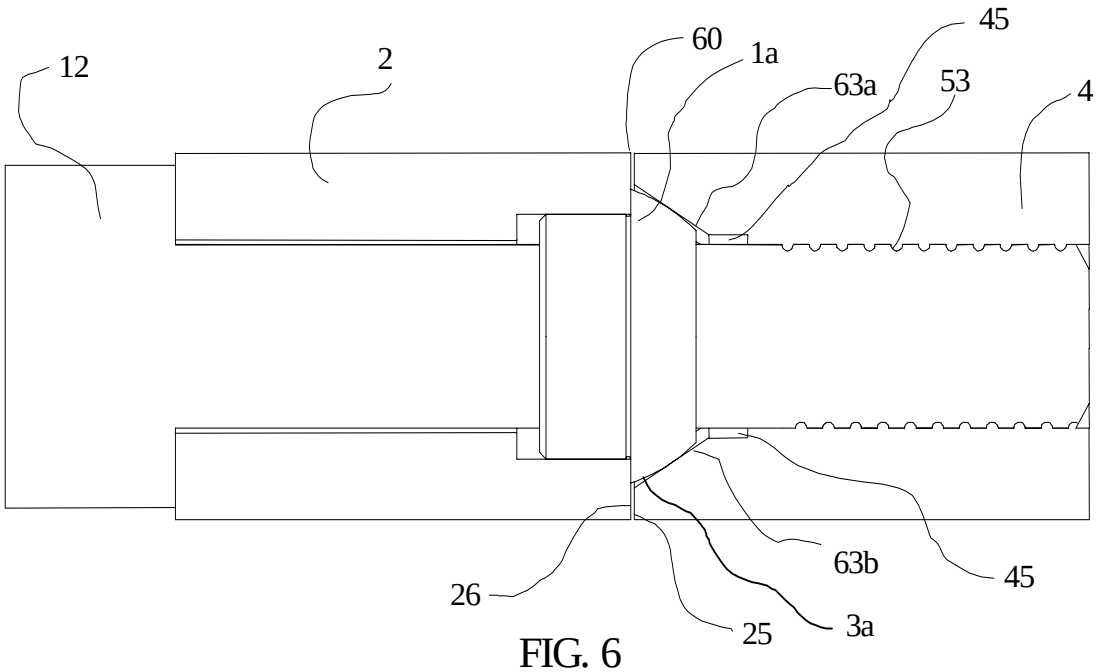


FIG. 6

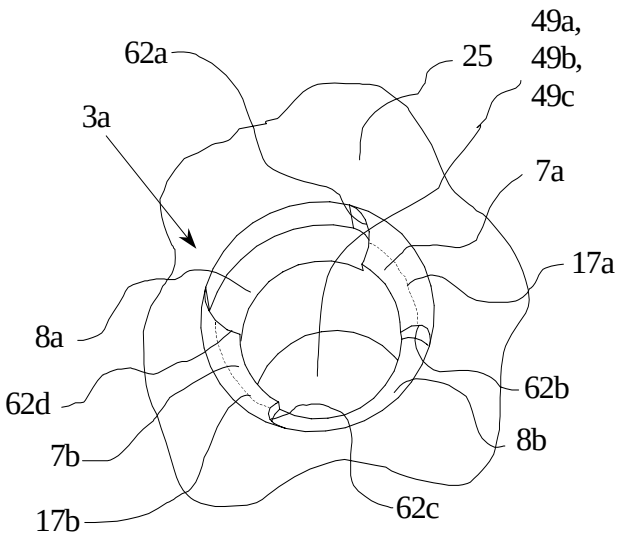


FIG. 7

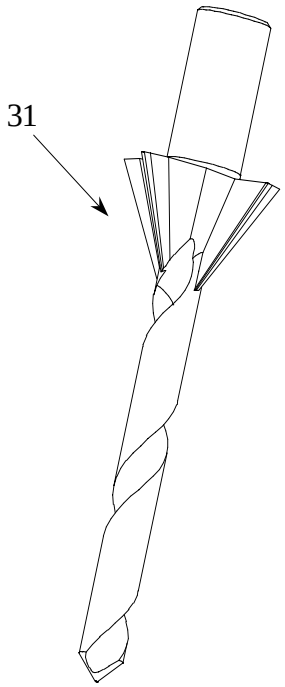


FIG. 8

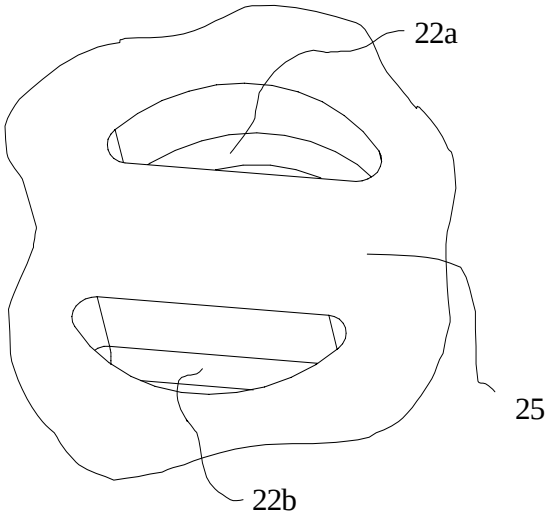


FIG. 9

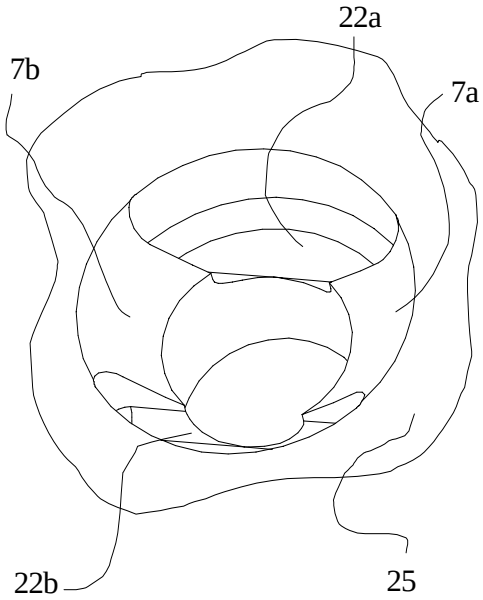


FIG. 10

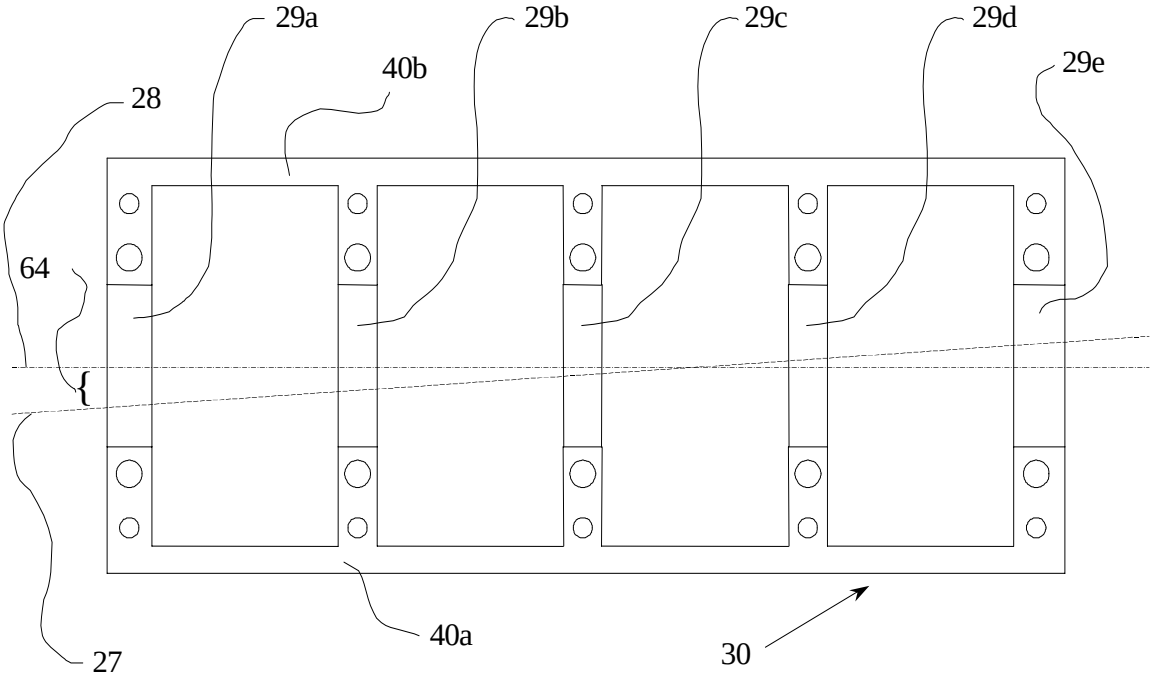


FIG. 11

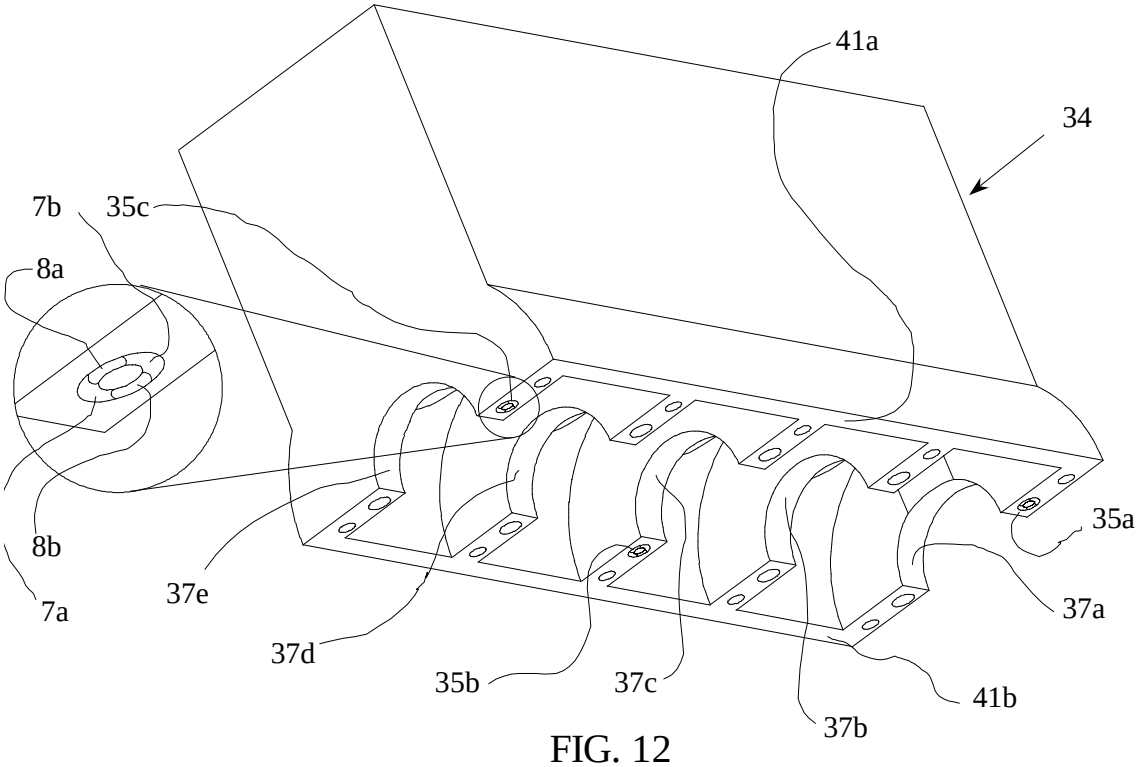

41a
34
7b
35c
8a
8b
7a
37e
37d
35b
37c
37b
41b
37a
35a

FIG. 12

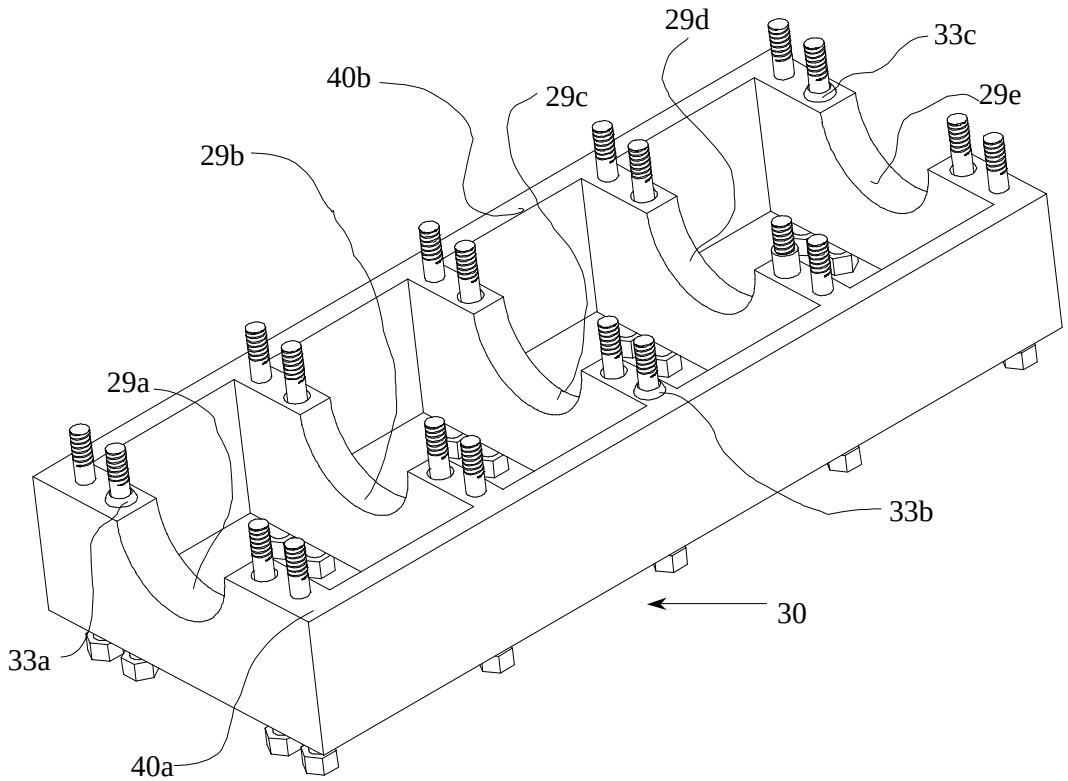

29d
33c
40b
29c
29e
29b
29a
33b
30
33a
40a

FIG. 13

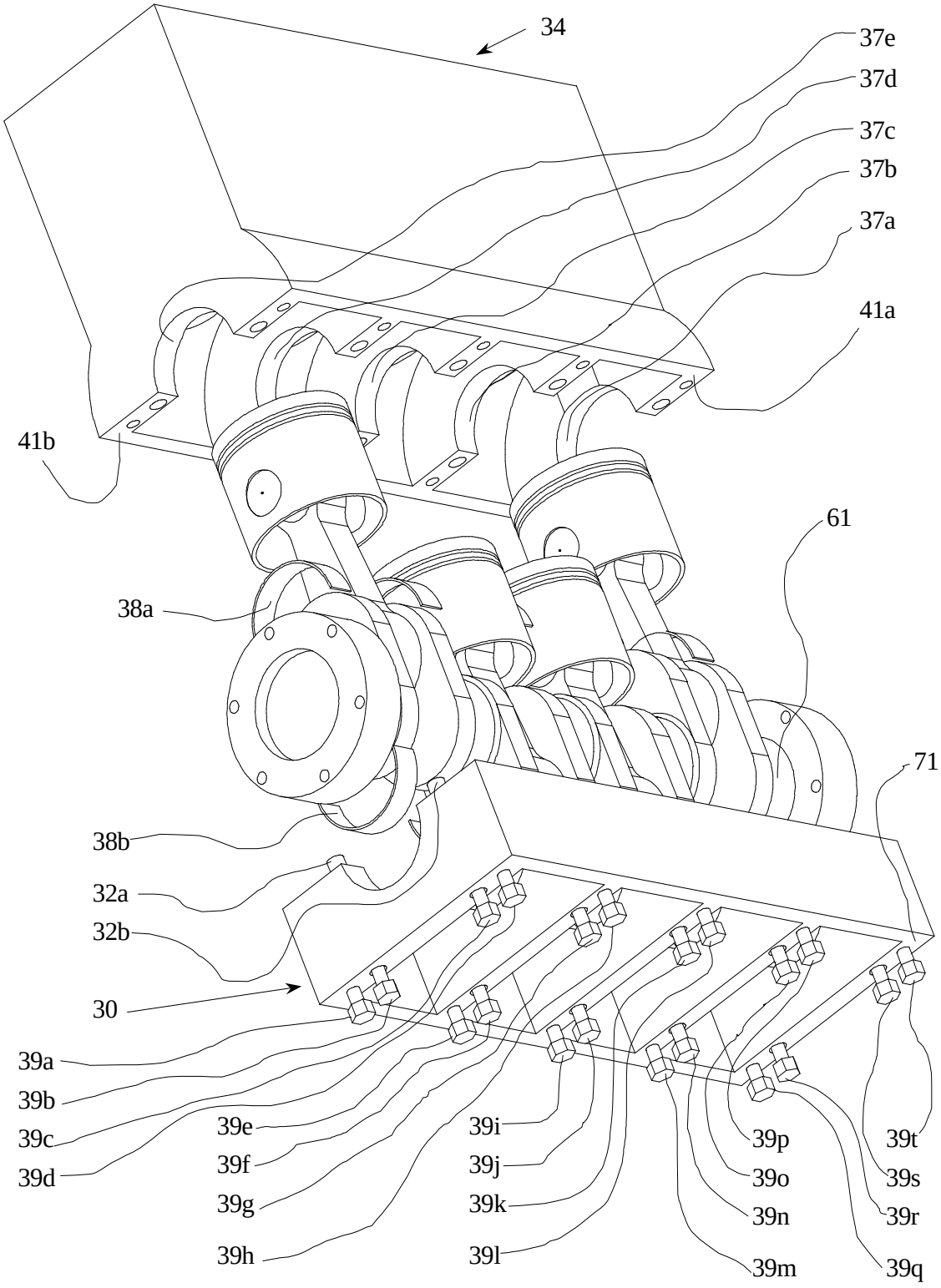

34
37e
37d
37c
37b
37a
41a
41b
61
38a
71
38b
32a
32b
30
39a
39b
39c
39d
39e
39f
39g
39h
39i
39j
39k
39l
39p
39o
39n
39m
39t
39s
39r
39q

FIG. 14

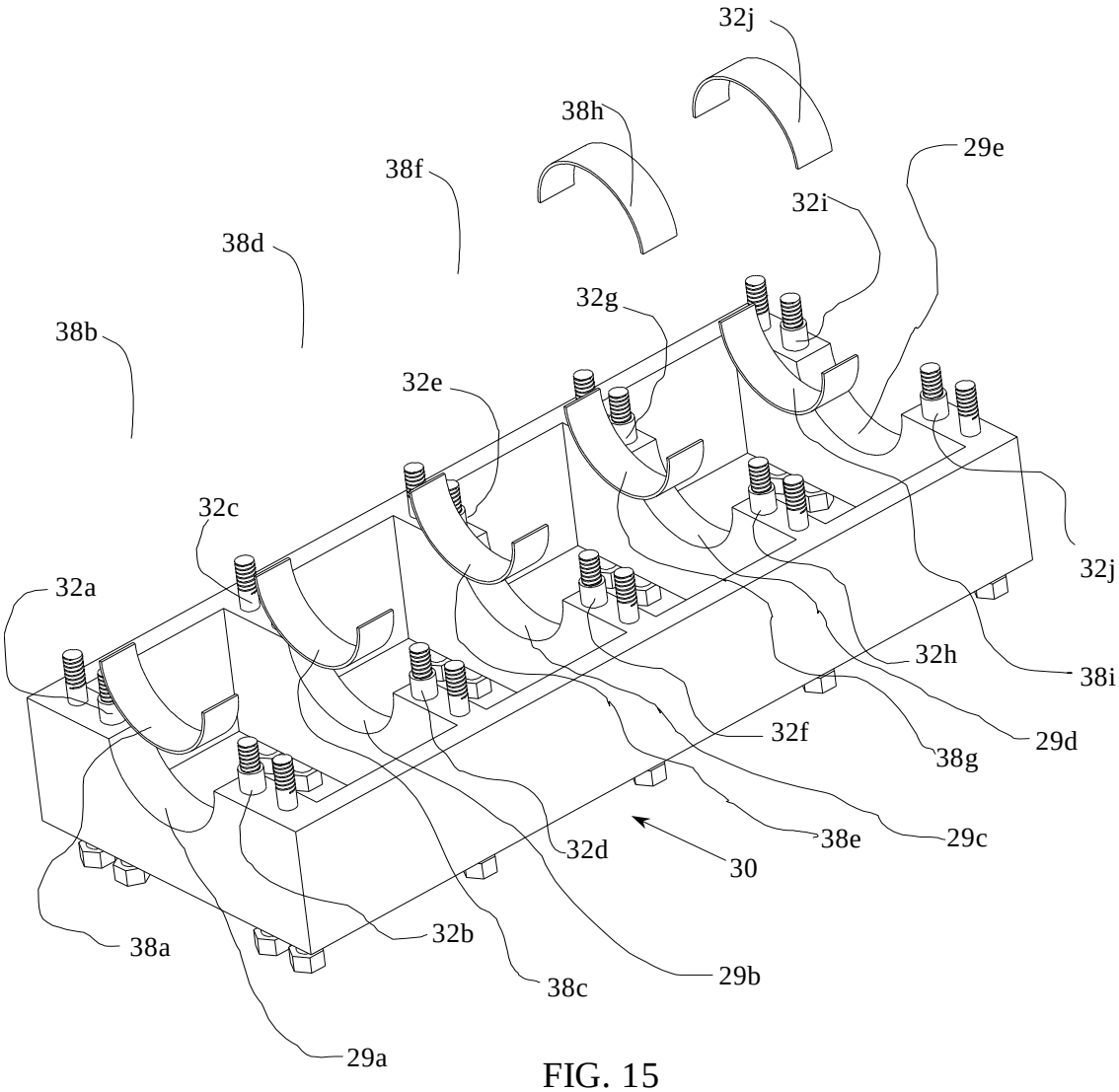

32j
38h
29e
38f
32i
38d
32g
38b
32e
32c
32j
32a
32h
38i
29d
32f
38g
38e
29c
32d
30
38a
32b
38c
29b
29a

FIG. 15

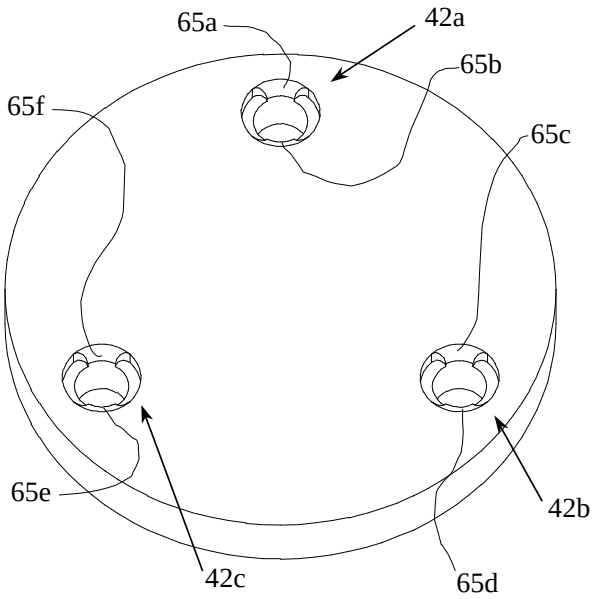


FIG. 16

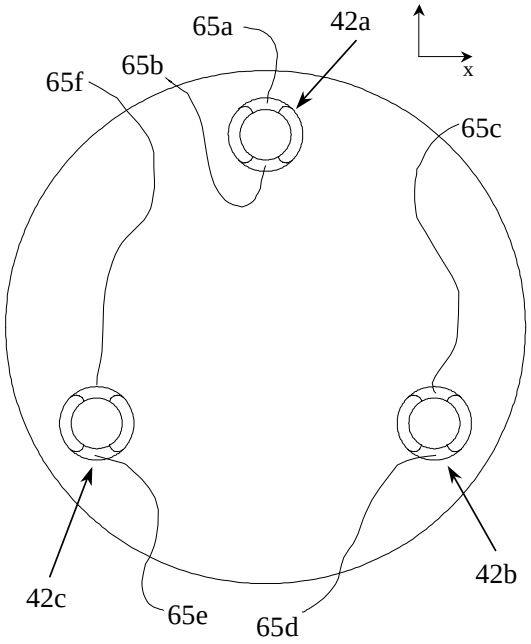


FIG. 17

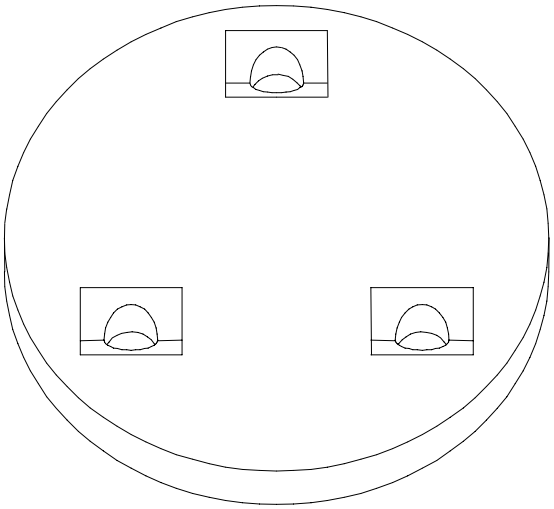


FIG. 18

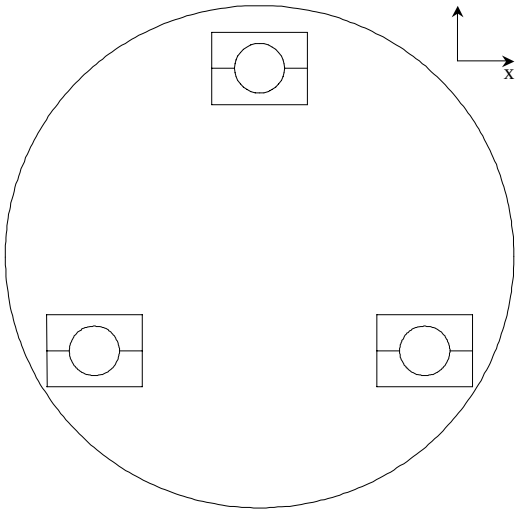


FIG. 19

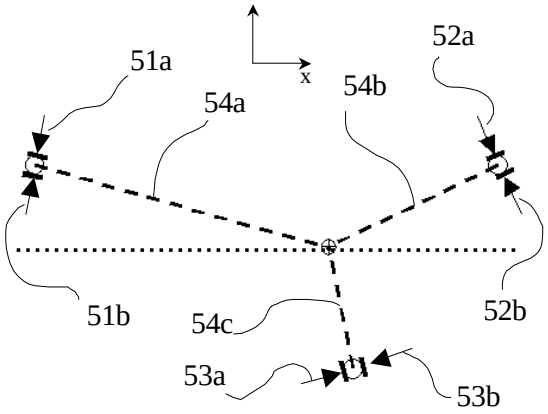


FIG. 20

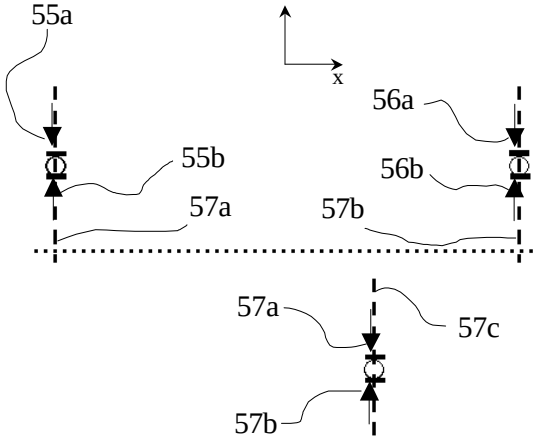


FIG. 21

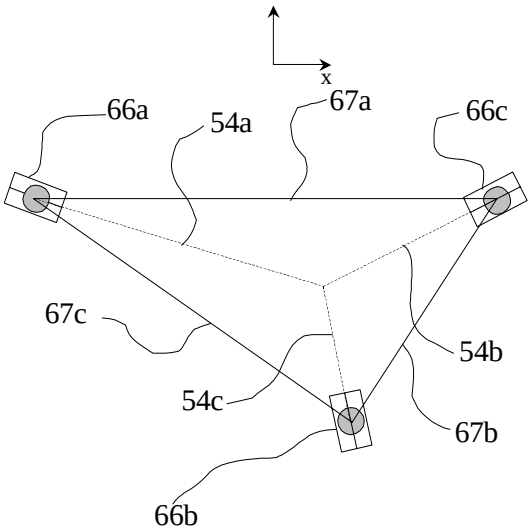


FIG. 22

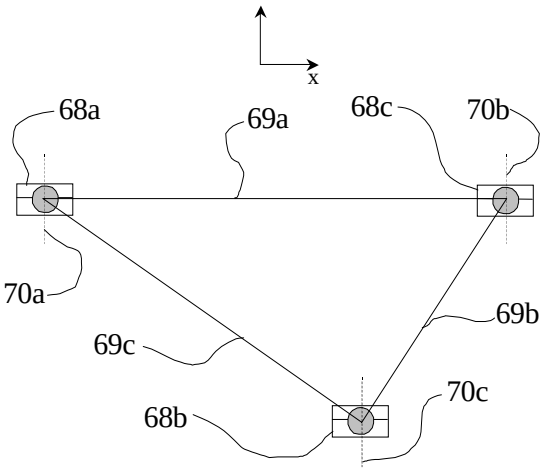


FIG. 23

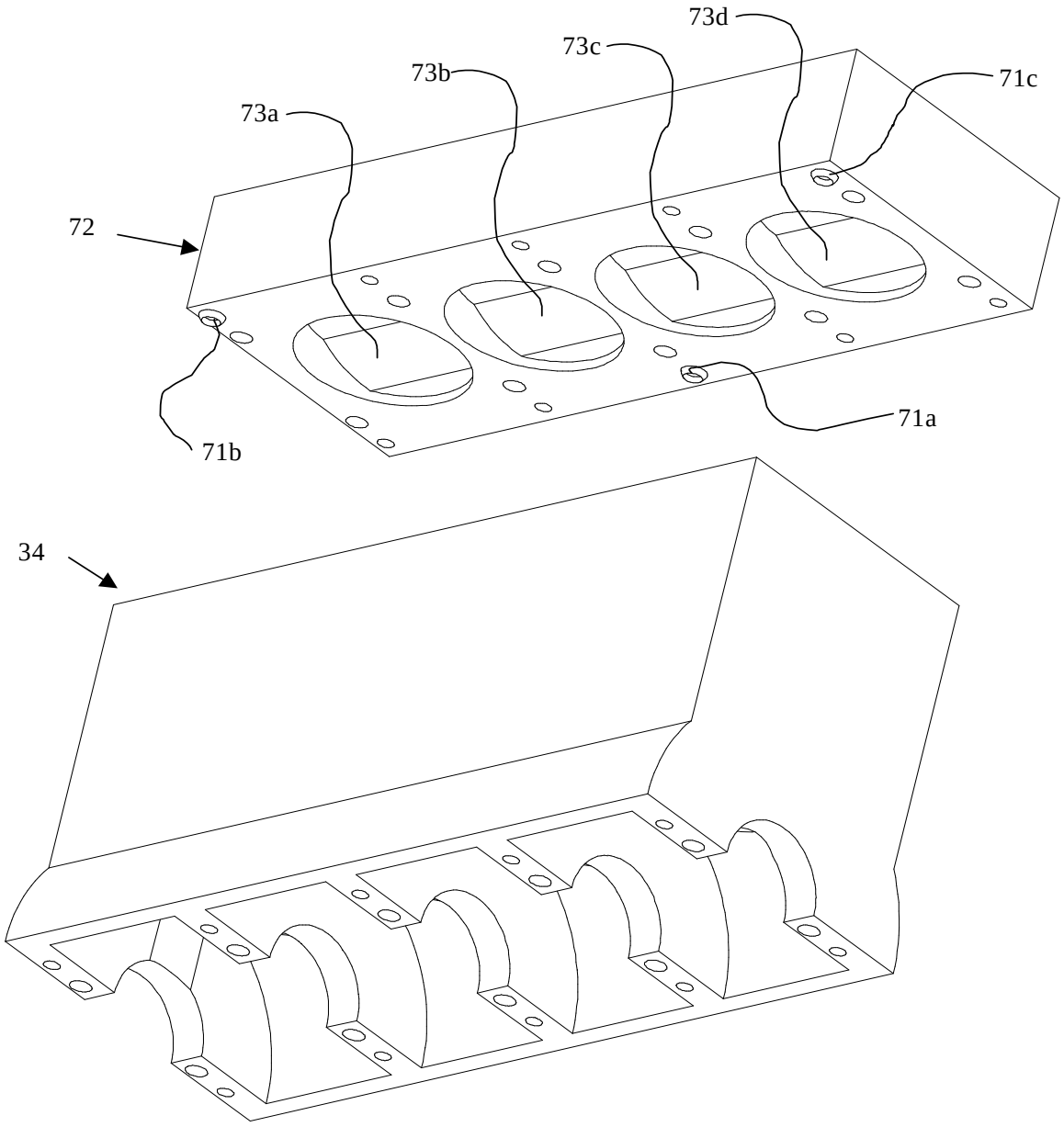


FIG. 24

Appendix F

DERIVATION OF SINUSOIDAL NORMAL DISPLACEMENTS

The QKC stiffness model allows the user to estimate the stiffness of the coupling in any of the six degrees of freedom. This appendix covers the derivation for imposed displacement equations which were implemented in the MathCad model (Appendix B).

F.1 Review of Distances of Approach

The details of converting imposed displacements in six degrees of freedom into components in functions $\delta_r(\theta_r)$ and $\delta_z(\theta_r)$ is fairly involved geometrically and mathematically. It is not necessary to understand this conversion before using the tool in Appendix B, however, they have been included here for those seeking understanding. We begin where Section 3.2.3 left off.

Imposed radial (δ_r) and axial (δ_z) distances of approach can be broken into their components in a Conical coordinate system. With the help of Figure F.1, one can determine these displacement as:

$$\delta_n = -\delta_r \cos(\theta_c) + \delta_z \sin(\theta_c) \tag{F.1}$$

$$\delta_l = \delta_r \sin(\theta_c) + \delta_z \cos(\theta_c) \tag{F.2}$$

When we consider that both δ_r and δ_z can be functions of θ_r, these equations become:

$$\delta_n(\theta_r) = -\delta_r(\theta_r) \cos(\theta_c) + \delta_z(\theta_r) \sin(\theta_c) \tag{F.3}$$

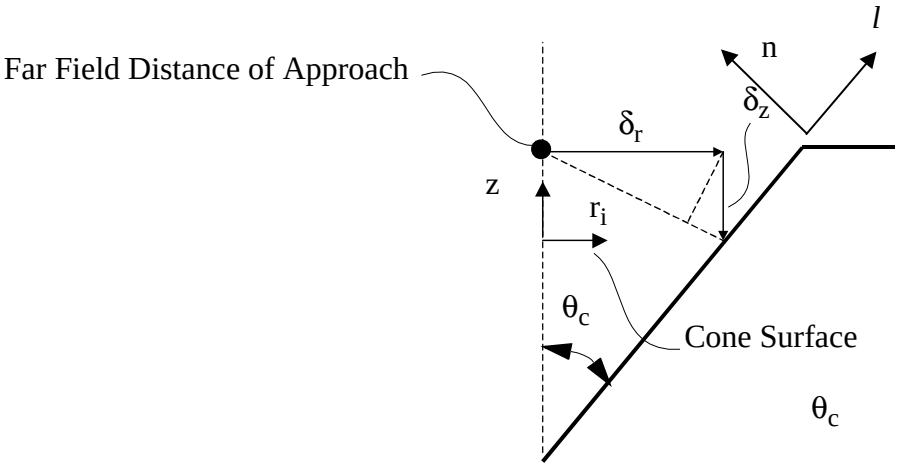


Figure F.1 Decomposition of Radial and Axial Movements to Conical Coordinates

$$\delta_l(\theta_r) = \delta_r(\theta_r)\sin(\theta_c) + \delta_z(\theta_r)\cos(\theta_c) \tag{F.4}$$

The task then is to determine the components δ_r and δ_z as functions of the radial angle, θ_r. Fortunately, it is simpler to do all calculations in terms of r, θ, and z coordinates because the distances of approach are a combination of various error motions which can (with clever manipulation) be easily described in terms of r, z, and θ_r. This will be made apparent in subsequent sections, but Table F.1 gives a preview of these relationships and the nature of their components.

TABLE F.1 Error Motion Affects on Normal and Lateral Distances of Approach

		Affect on δ_n and δ_l	
Error Motion	**Sub-Component(s)**	**Sinusoidal Component**	**Constant Component**
δ_{rcc}	δ_{xcc} and δ_{ycc}	X	
δ_{zcc}	δ_{zcc}		X
ε_{xy}	ε_x and ε_y	X	X
ε_z	ε_z	X	

In the following sections, the derivations of the relationships are provided for individual joints. They are then combined into a general formula for determining the resultant contact force for a joint. These resultant forces can then be summed over the three joints.

F.2 Components Due to δ_{rcc}

F.2.1 Magnitude

The relative movement between a contactor axis and target axis (parallel to the plane of mating) has components δ_{xcc} and δ_{ycc}. These components are combined into a common vector, δ_{rcc}. As this vector is parallel to the plane of mating, it has no components in the *z* direction.

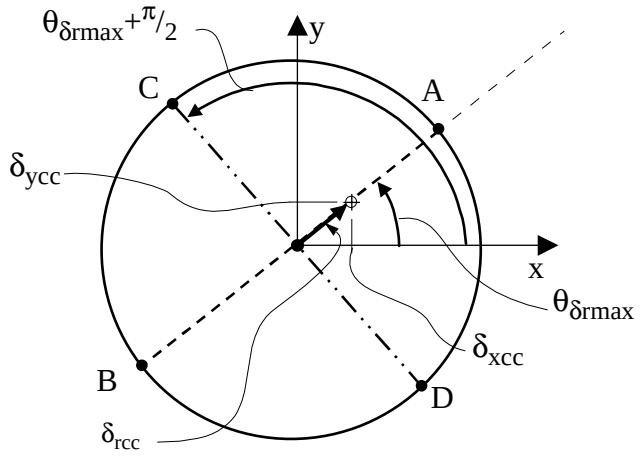


Figure F.2 Radial Displacement of Axisphere Center Relative To Cone Axis of Symmetry

It is easy for the user to understand and mathematically simpler for us to represent this and subsequent sinusoidal relations in terms of a maximum magnitude (equivalent to amplitude of the sinusoidal function) and direction the magnitude is applied. In this case, we choose to specify the magnitude of the maximum displacement as, Δr, and the direction of this displacement, $\theta_{\delta rmax}$ (specified from the *x* axis). The distance of approach between far field points in the contactor and target is a function of Δr and $\theta_{\delta rmax}$ and varies with θ_r.

F.2.2 Direction

Using Figure F.2 as an example, if we take a cross section along the line $\overline{AB}$, the maximum distance of approach will occur in the direction of A ($\theta_{\delta rmax}$), the minimum in the direction of B ($\theta_{\delta rmax} + \pi$). In a cross section along $\overline{CD}$ ($\theta_{\delta rmax} + {}^{\pi}/_{2}$ or $\theta_{\delta rmax} + {}^{3\pi}/_{2}$), the distance of approach will be zero. The radial component of the distance of approach can then be represented as:

$$\delta_r(\theta_r) = \delta_{rmax} \cdot \cos(\theta_{\delta rmax} - \theta_r) = \Delta r \cdot \cos(\theta_{\delta rmax} - \theta_r) \qquad \text{(F.5)}$$

Again using Figure F.2 as an example, $\theta_{\delta rmax} = 45$ degrees. As a check for understanding, the results of equation F.5 (as applied to Figure F.2) have been presented in Table F.2 for comparison with our qualitative discussion.

TABLE F.2 Tabulated Relation Between θ_r and $\delta_r(\theta_r)$

θ_r	θ_r In Context of Figure F.2	$\delta_r(\theta_r)$
$\theta_{\delta rmax}$	45^o	Δr
$\theta_{\delta rmax} + {}^{\pi}/_{2}$	135^o	0
$\theta_{\delta rmax} + \pi$	225^o	$-\Delta r$
$\theta_{\delta rmax} + {}^{3\pi}/_{2}$	315^o	0

Equation F.5 can then be substituted into the $\delta_r(\theta_r)$ portion of F.3.

F.3 Components Due to ε_{xy}

Before we continue, it is best to explain a generic form we will use for calculating components of errors due to imposed rotations.

F.3.1 Calculating Errors Due To Rotation

We consider the two components of error due to rotations as shown in Figure F.3. Provided the rotation is small (less than 5^o), the secondary component of the error will be less

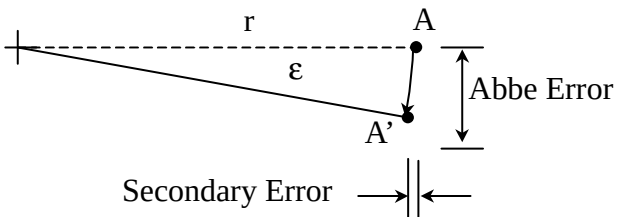


Figure F.3 Abbe Error Due To Rotation. (Rotation Vector Points Out Of Page)

than 5% of the Abbe error. Since we are dealing with very small error motions (micro-radians), the remainder of this discussion assumes this condition is satisfied.

Given ε as the rotation vector and *r* as the vector from the point of rotation to the location where an Abbe error is desired, the error can then be estimated using equation F.6.

$$\vec{\delta} = \vec{\varepsilon} \times \vec{r} \tag{F.6}$$

F.3.2 Decomposition of Rotational Errors

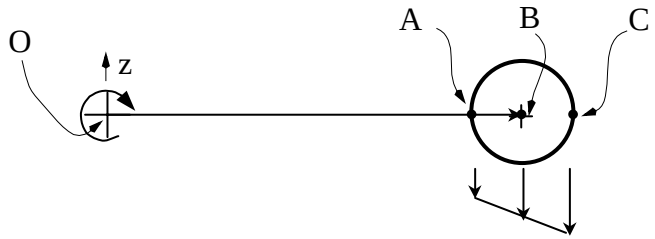


Figure F.4 Model For Decomposition of Rotation Abbe Error

Consider a ball which is rotated about point *O*. The rotation vector points into the page and the position vector (*r*) is the vector from *O* to the center of the ball. We will consider the displacement of three points (*A*, *B*, and *C*) in a cross section normal to the rotation vector. The displacement of B can be calculated using F.6.

$$\vec{\delta}_B = \vec{\varepsilon} \times \vec{r} \tag{F.7}$$

The displacements of points A and C could be done likewise, but upon inspection one can see that they can be expressed as a combination of the displacement at B and the product of the ball radius (R) and magnitude of the rotation (ε).

$$\delta_A = \vec{\delta}_B \bullet \hat{k} + (R \cdot \varepsilon) \tag{F.8}$$

$$\delta_C = \vec{\delta}_B \bullet \hat{k} - (R \cdot \varepsilon) \tag{F.9}$$

Here we have taken the dot product of equation F.7 with the unit vector in the k direction (direction of Abbe error) to make this a scalar equation. This amounts to plucking the z component of the displacement from the vector and using it in the calculation.

Equations F.8 and F.9 then become:

$$\delta_A = \varepsilon \cdot r + (R \cdot \varepsilon) \tag{F.10}$$

$$\delta_C = \varepsilon \cdot r - (R \cdot \varepsilon) \tag{F.11}$$

We began with the plane perpendicular to the rotation vector, as this will always contain the maximum distance of approach (for use in a sinusoidal equation). To describe the displacement in planes which are not perpendicular to the rotation vector, a modification must be applied to the second term in equations F.10 or F.11. The general equation for all cross sections then becomes (for δ_c),

$$\delta = (\varepsilon \cdot r) + (R \cdot \varepsilon \cdot \cos(\Lambda)) \tag{F.12}$$

Here Λ is the angle between the perpendicular plane and the new plane of interest.

F.3.3 Applying Decomposition of Rotational Errors to QKCs

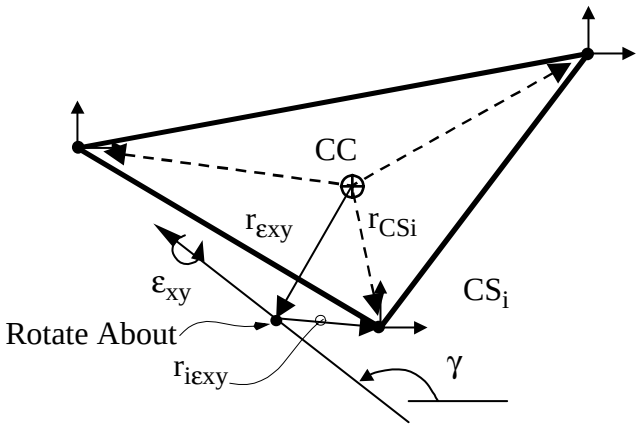


Figure F.5 Model For Calculating the Affects of ε_{xy}

Figure F.5 shows the model used for calculating the affect of ε_{xy} on QKCs. In addition to the geometry of the coupling, this model requires the magnitude ($|\varepsilon_{xy}|$) and direction (γ) of the rotation vector. Alternatively, one could define ε_x and ε_y then calculate ε_{xy} and γ using equations F.13 and F.14. It makes no difference which method is used, but the reader should notice the tool in Appendix B is set up to receive input for ε_{xy} and γ.

$$\gamma = \operatorname{atan2}(\varepsilon_x, \varepsilon_y) \tag{F.13}$$

$$\left|\varepsilon_{xy}\right| = (\varepsilon_x^2 + \varepsilon_y^2)^{1/2} \tag{F.14}$$

The position (relative to the coupling center) about which the rotation occurs ($r_{\varepsilon xy}$) is also needed. Given $r_{\varepsilon xy}$, one can find $r_{i\varepsilon xy}$ for each joint i. Following the reasoning of the previous section and using the variables described in Figure F.5, one can calculate the distance of approach for contact at each joint.

$$\delta_z(\theta_r) = \overrightarrow{\varepsilon_{xy}} \times \overrightarrow{r_{i\varepsilon xy}} \cdot \hat{k} + R_c \cdot \varepsilon_{xy} \cdot \cos(\theta_r - \theta_{\delta z \varepsilon xymax}) \tag{F.15}$$

Here $\theta_{\delta z \varepsilon xymax}$ is the direction at which the maximum distance of approach occurs. By default, this direction is $\gamma + \pi/2$. Again, θ_r is the angle measured from the x axis. Equation

F.15 can then be substituted in to the δ_z component of the general distance of approach equation, F.3.

F.4 Components Due to ε_z

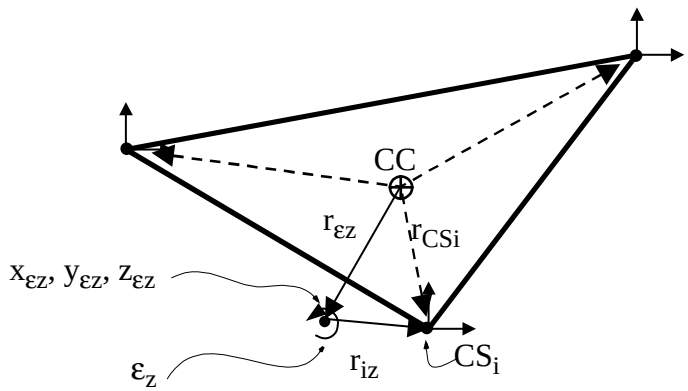


Figure F.6 Model For Calculating the Affects of ε_z

Calculating the distance of approach due to ε_z is more straight forward than that due to ε_{xy}. Figure F.6 shows the model used for calculating the affect of ε_z on QKCs. In addition to the geometry of the coupling, this model requires the magnitude ($|\varepsilon_z|$) of the rotation and the position about which the rotation occurs. It also requires the direction of maximum distance of approach. We will find this first.

We start with the form of equation F.6 expressed in terms of our model for the affects of ε_z. This gives the maximum distance of approach in the *r* direction as,

$$\vec{\delta}_{ri} = \vec{\varepsilon}_z \times \vec{r}_{iz} = \vec{\varepsilon}_z \times (\overrightarrow{r_{CSi}} - \vec{r}_{\varepsilon z}) \tag{F.16}$$

Where i denotes which joint is under consideration. The direction of the maximum distance of approach can found from the components of the vector δ_{ri}. This is simplified in equation F.17.

$$\theta_{\delta r max i \varepsilon z} = \operatorname{atan2}[(X_{CSi} - X_{\varepsilon z}), (Y_{\varepsilon z} - Y_{CSi})] \tag{F.17}$$

Or alternatively calculated as,

$$\theta_{\delta rmaxi\varepsilon z} = \operatorname{atan2}(\delta_{rmaxi\varepsilon z_X}, \delta_{rmaxi\varepsilon z_Y}) \tag{F.18}$$

The radial distance of approach for one joint can then be calculated knowing the magnitude and direction of the maximum distance of approach.

$$\delta_{rmaxi\varepsilon z} = \vec{\varepsilon_z} \times (\overrightarrow{r_{csi}} - \overrightarrow{r_{\varepsilon z}}) \cdot \hat{k} \cdot \cos(\theta_r - \theta_{\delta rmaxi\varepsilon z}) \tag{F.19}$$

F.5 General Distance of Approach Equation

The results of the preceeding equations are combined in a general equation (F.20) for the distance of approach in the n direction (see following page). This equation is used in Appendix B.

$$\delta_{ni}(\theta_r) = -[\delta_{rcc}\cos(\theta_r - \theta_{\delta rmaxi}) + \left|\vec{\varepsilon_z} \times (\overrightarrow{r_{csi}} - \overrightarrow{r_{\varepsilon z}})\right| \cos(\theta_r - \theta_{\delta rmaxi\varepsilon z})]\cos(\theta_c) + [\delta_{zcc} - \left|\overrightarrow{\varepsilon_{xy}}\right|(R_s\cos(\theta_c) + O_{SRr})\sin(\theta_r - \gamma) + \vec{k} \cdot \overrightarrow{\varepsilon_{xy}} \times (\overrightarrow{r_{csi}} - \overrightarrow{r_{\varepsilon xy}})]\sin(\theta_c) \quad \text{(F.20)}$$

Appendix G

PROOF FOR CONSTANT PLANE STRAIN ASSUMPTION

The QKC stiffness model assumes that the data provided from the FEA input is for constant plane strain. The following proof uses scaling arguments to develop the criteria for determining if the assumption of constant plane strain is valid.

G.1 Introduction to the Analysis

The use of axisymmetric elements in an FEA analysis assumes that the strain in the direction of the radial angle is constant. In QKCs, this is not necessarily true, as the distance of approach varies sinusoidally about the axis of symmetry. For instance, if we place a sphere in a cone and press the sphere into the cone along the cone's axis of symmetry, then the strain at all cross sections through the axis will be identical. However, we are imposing motions, i.e. δ_r, which result in varying amounts of strain about the contact arc. The task then, is to develop a criteria, which relates the geometry of the coupling elements and the imposed displacements to an acceptable amount of error. We will begin by expressing the analytic goal and reasoning used to reach it.

G.2 Goal and Reasoning Behind the Analysis

This analysis uses scaling arguments to justify our assumption of near constant strain with θ_r. We will use cylindrical coordinates which greatly simplify the analysis. In scaling the

following equations, we determine order of magnitude estimates for various quantities using characteristic dimensions of the coupling. These are provided in Table G.1.

TABLE G.1 Order of Magnitude Scaling Quantities

Quantity	**Varies As:**	**Order of Magnitude Estimate**
u_r	--->	δ_r
r	--->	Rc
$\Delta\theta_r$	--->	2π
$\left(\frac{1}{r}\right)$	--->	$\frac{1}{R_c}$
$\frac{\partial}{\partial\theta_r}\left(\frac{1}{r}\right)$	--->	$\left(\frac{1}{2\pi}\right)\left[\left(\frac{1}{R_c+\delta_r}\right)-\left(\frac{1}{R_c-\delta_r}\right)\right]$
$\frac{\partial}{\partial\theta_r}(u_{\theta r})$	--->	$2\delta_r$
$\frac{\partial^2}{\partial\theta_r^2}(u_\theta)$	--->	$\frac{2\delta_r}{2\pi}$
$\frac{\partial}{\partial\theta_r}(u_r)$	--->	$\frac{2\delta_r}{2\pi}$

The equation for strain in the direction of the radial angle is:

$$\varepsilon_{\theta r} = \frac{u_r}{r} + \frac{1}{r}\frac{\partial}{\partial\theta_r}(u_{\theta r}) \tag{G.1}$$

We wish for the variation in angular strain, $\Delta\varepsilon_{\theta r}$, to be small to the value of $\varepsilon_{\theta r}$. Mathematically, this is expressed as:

$$\frac{\Delta\varepsilon_{\theta r}}{\varepsilon_{\theta r}} \approx \frac{\frac{\partial\varepsilon_{\theta r}}{\partial\theta_r}\cdot\Delta\theta_r}{\varepsilon_{\theta r}} \ll 1 \tag{G.2}$$

Which says the ratio of the change in angular strain to the nominal value of angular strain should be much less than unity. We define the right most ratio in equation G.2 as the angular strain ratio.

G.3 Analysis For Estimating the Angular Strain Ratio

Taking the partial derivative of equation G.1 yields,

$$\frac{\partial \varepsilon_{\theta r}}{\partial \theta_r} = \frac{1}{r}\frac{\partial}{\partial \theta_r}(u_r) + u_r\frac{\partial}{\partial \theta_r}\left(\frac{1}{r}\right) + \frac{\partial}{\partial \theta_r}(u_{\theta r}) \cdot \frac{\partial}{\partial \theta_r}\left(\frac{1}{r}\right) + \frac{1}{r} \cdot \frac{\partial^2}{\partial \theta_r^2}\left(\frac{1}{r}\right) \tag{G.3}$$

Within equation G.3, the following term is equivalent to:

$$\frac{\partial u_{\theta r}}{\partial \theta_r} = \frac{\partial}{\partial \theta_r}(s) \tag{G.4}$$

Where *S* is the motion along the s direction. Through a scaling argument, one can obtain an order of magnitude estimate of the differential as follows:

$$\frac{\partial}{\partial \theta_r}(S) = \frac{\partial}{\partial \theta_r}(r \cdot \Delta\theta_r) = \frac{\partial}{\partial \theta_r}(r) \cdot \Delta\theta_r \sim \frac{(R_c + \delta_r) - (R_c - \delta_r)}{2\pi} \cdot 2\pi = 2 \cdot \delta_r \tag{G.5}$$

Where the scaled values have been chosen to provide the worst case, i.e. largest number, scenario. Using the values in Table G.1 and equation G.3, one can estimate the maximum variation in angular strain as:

$$\frac{\partial \varepsilon_{\theta r}}{\partial \theta_r} \sim \frac{2\delta_r}{2\pi} \cdot \frac{1}{R_c} + \frac{\delta_r}{2\pi} \cdot \left(\frac{1}{R_c + \delta_r} - \frac{1}{R_c - \delta_r}\right) + \frac{2\delta_r}{2\pi} \cdot \left(\frac{1}{R_c + \delta_r} - \frac{1}{R_c - \delta_r}\right) + \frac{2\delta_r}{2\pi} \cdot \frac{1}{R_c} \tag{G.6}$$

Equation G.6 can be simplified in terms of the radial distance of approach ratio, $\delta_r/_{Rc}$:

$$\frac{\partial \varepsilon_{\theta r}}{\partial \theta_r} \sim \frac{\delta_r}{R_c} \cdot \left(\frac{2}{\pi}\right) - \left(\frac{3}{\pi}\right)\frac{\left(\frac{\delta_r}{R_c}\right)^2}{1 - \left(\frac{\delta_r}{R_c}\right)^2} \tag{G.7}$$

By combining the results of equations G.2 and G.7, the angular strain ratio can be estimated as:

$$\frac{\frac{\partial \varepsilon_{\theta r}}{\partial \theta_r} \cdot \Delta\theta_r}{\varepsilon_{\theta r}} \sim \frac{4}{3} - \left(2 \cdot \frac{\left(\frac{\delta_r}{R_c}\right)}{1 - \left(\frac{\delta_r}{R_c}\right)^2} \right) \tag{G.8}$$

We wish the ratio on the left hand side to be much less than 1. With some rearrangement, equation G.8 is expressed as:

$$\frac{3}{2} \cdot \frac{\left(\frac{\delta_r}{R_c}\right)}{1 - \left(\frac{\delta_r}{R_c}\right)^2} \ll 1 \tag{G.9}$$

A plot of the equation G.7, provided in Figure G.1shows the relationship is approximately linear for small values of $\delta_r/_{Rc}$. It is common engineering practice to say that quantities

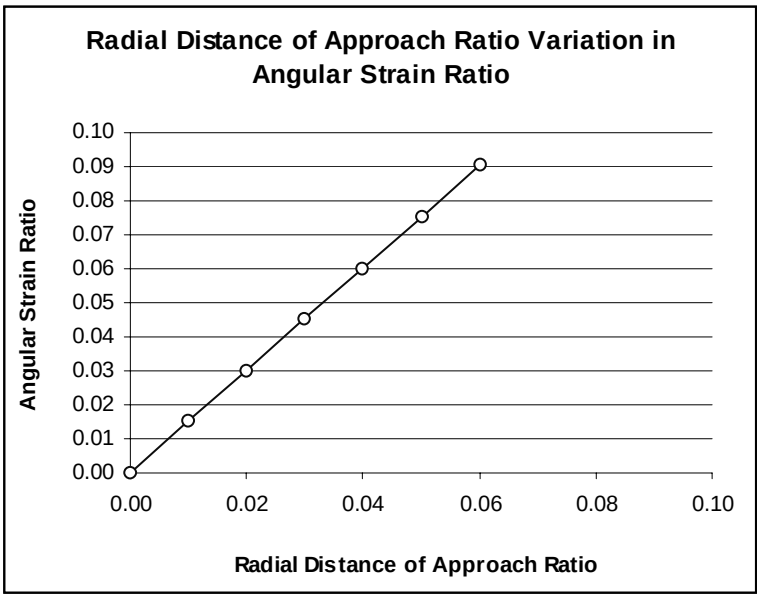


Figure G.1 Relation of Angular Strain and Radial Distance of Approach Ratios

which have less than X % effect on the total can be neglected. A common value for practical applications is X = 5 %, or 1 in 20 affect. From Figure G.1, one can see that this occurs at $\delta_r/_{Rc} = {}^3/_{100}$. In QKCs, this is not a difficult criteria to satisfy, as the ratio will be on the order of:

$$\left.\frac{\delta_r}{R_c}\right|_{QKC} \approx \frac{1 micron}{5 mm} \approx \frac{1}{5000} \tag{G.10}$$